Steerable Interstitial Needle for Cervical Brachytherapy

A Design and Validation Approach

Sander Streefkerk

Steerable Interstitial Needle for Cervical Brachytherapy

A Design and Validation Approach

by

Sander Streefkerk

in partial fulfilment of the requirements for the degree of

Master of Science

in BioMedical Engineering

at the Delft University of Technology,
to be defended publicly on Wednesday May 28, 2025 at 12:45

Faculty:	Mechanical Engineering
Student number:	4828658
Project Duration:	November, 2024 - May, 2025
Supervisor:	Prof. dr. J.J. van den Dobbelsteen

An electronic version of this thesis is available at http://repository.tudelft.nl/.

TUDelft

Abstract

Accurate needle placement is essential for effective cervical high dose-rate (HDR) brachytherapy in anatomically complex or asymmetric tumor regions. Conventional rigid obturators used with standard applicators, such as Elekta's Geneva and Venezia systems, lack the flexibility to reach off-axis targets, thereby limiting treatment precision. This study presents the development and validation of a manually operated steerable interstitial needle for gynecological brachytherapy. The device employs a compliant split-shaft mechanism that converts differential push-pull actuation into controlled tip deflection. Finite element analysis guided the selection of Grade 5 titanium and informed geometric optimization to balance flexibility with mechanical stability. A prototype was fabricated and integrated into a 3D-printed handheld actuation unit compatible with the Elekta Venezia applicator. Experimental evaluation in gelatin and silicone phantoms under computed tomography (CT) imaging demonstrated tip deflections of up to 33.0 mm with the Flexible Implant Tube 6F and up to 18.5 mm with the ProGuide 6F at an insertion depth of 80 mm. Placement accuracy remained within ± 5 mm in over 95% of the trials. These results validate the steerable needle concept and highlight its potential to improve maneuverability during clinical brachytherapy.

Clinical Relevance

In addition to enabling curved trajectories, this work introduces a novel approach to adaptive needle placement that responds to anatomical variability during the procedure. The manual actuation mechanism allows for real-time corrections without relying on complex robotic systems, making it suitable for implementation in both high- and low-resource clinical settings. Moreover, proven compatibility with standard applicator systems (Elekta Venezia) supports integration into current treatment protocols without significant procedural changes. This positions the steerable needle as a viable solution for extending interstitial coverage in patients with large or asymmetric tumors, where conventional linear insertions often require additional needles or custom planning. By enabling more precise needle placement that maximizes tumor coverage while sparing adjacent healthy tissue, the approach could improve dose distribution and reduce exposure to organs at risk (OARs). This, in turn, can reduce radiation toxicity, minimize treatment-related side effects, and ultimately lead to improved patient outcomes.

Keywords

Steerable needle, Gynecological brachytherapy, HDR brachytherapy, Cervical cancer, Interstitial needle, Minimally invasive.

Contents

List of Figures

List of Tables

Nomenclature

Abbreviations

Abbreviation	Definition
ANOVA	Analysis of Variance
CAD	Computer-Aided Design
CNC	Computer Numerical Control
CT	Computed Tomography
EDM	Electric Discharge Machine
FDM	Fused Deposition Modelling
FEA	Finite Element Analysis
HDR	High Dose-Rate
HPV	Human Papillomavirus
MRI	Magnetic Resonance Imaging
PLA	Polylactic Acid
SLA	Stereolithography
SMA	Shape Memory Alloy
US	Ultrasound
UV	Ultraviolet
SPSS	Statistical Package for the Social Sciences
3D	Three-Dimensional

Symbols and Parameters

Symbol	Definition
M	Mean (average) value of a data set
SD	Standard deviation, a measure of data dispersion
n	Sample size or number of observations
F	F-statistic in ANOVA, ratio of variance estimates
p	p-value, used in hypothesis testing to determine significance
η^2	Partial eta-squared, effect size indicator in ANOVA
R^2	Coefficient of determination, indicates proportion of variance explained
Δx	Lateral tip deflection in x-direction (axial plane)
Δz	Vertical deviation in z-direction (Error Z)
L	Insertion depth of the needle
σ_{vM}	von Mises stress, used in mechanical stress analysis
δ_{tip}	Tip displacement or deflection
θ	Bending angle of the needle

1

Introduction

1.1. Background

Cervical cancer is one of the most common malignancies in women worldwide. In 2020, an estimated 604,127 new cases and 341,831 deaths were reported worldwide, with a disproportionate burden in low- and middle-income countries [1, 59]. Persistent infection with high-risk human papillomavirus (HPV) types is the leading cause of cervical cancer, often leading to progressive invasion of the cervix and adjacent pelvic structures [9]. While early-stage cervical cancer is typically curable, advanced stages pose significant treatment challenges due to the anatomical complexity of the pelvic region and the need for high-precision radiation delivery [65].

The cervix is the lower, cylindrical part of the uterus that connects the uterine cavity to the vaginal canal. It is approximately 2,5 to 3,5 centimeters in length and consists primarily of dense connective tissue and smooth muscle fibers [77]. The cervix plays a key role in reproductive function, maintaining pregnancy, and dilating during childbirth. Its structure is divided into two regions: the ectocervix, which is lined with stratified squamous epithelium, and the endocervical canal, which is lined with columnar epithelium [47]. An overview of cervical cancer and its location within the female reproductive system is shown in Figure 1.1.

High dose-rate (HDR) brachytherapy is a
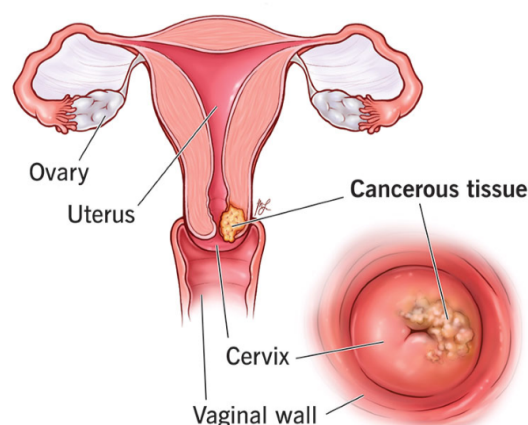
Figure 1.1: Illustration of cervical cancer showing cancerous tissue on the cervix and its anatomical context. Image source: Cleveland Clinic `https://my.clevelandclinic.org/health/diseases/12216-cervical-cancer` [10].

critical component of curative treatment and involves placing a radioactive source in or near the tumor to deliver a high dose of radiation while minimizing exposure to surrounding organs, such as the bladder and rectum [67]. This is typically achieved by intracavitary or combined intracavitary and interstitial insertions using applicator systems such as the Elekta Geneva and Venezia that guide the needle along fixed, linear trajectories [60].

Accurate placement of interstitial needles is essential to ensure optimal dose distribution and effective tumor coverage. This process is typically guided by imaging modalities such as ultrasound, computed tomography (CT), or magnetic resonance imaging (MRI). However,

the effectiveness of these standard techniques is limited when targeting large, asymmetric, or deeply infiltrating tumors. In such cases, standard needle trajectories may not provide adequate access to off-axis tumor regions, and deviations from the planned trajectory may result in underdosing or unintended irradiation of healthy tissue [66, 69].

Needle insertion in the pelvic region requires consideration of nearby critical structures such as the bladder, rectum, and pelvic sidewall [75]. Insertion is typically accomplished by applying axial force. If this force exceeds the critical load of the needle, buckling may occur, causing lateral deflection of the needle shaft [20]. This loss of control increases the risk of damage to surrounding tissue and can compromise the accuracy of needle placement [71]. In addition, tissue deformation and motion caused by needle-tissue interaction can make it difficult to reach the target location in a single attempt, often requiring repositioning and increasing the risk of complications [39].

To address these limitations, there is a growing need for improved needle maneuverability. A manually actuated steerable needle can improve directional control during insertion and allow the physician to navigate around anatomical obstacles [68]. Such a device has the potential to improve clinical outcomes by enabling more accurate source placement, reducing the number of insertion attempts, and minimizing tissue damage [39]. This research aims to develop and evaluate a steerable interstitial needle that is compatible with existing brachytherapy applicators and provides an intuitive and effective solution for complex clinical scenarios.

1.2. Steerable Needles

Steerable needles are designed primarily to bend or deflect within soft tissue, where their ability to adjust trajectory during insertion offers significant advantages. They allow clinicians to adjust the needle path in real time, which is particularly beneficial in procedures involving organs such as the liver, prostate, or cervix, where tissue deformation or anatomical complexity can hinder accurate placement.

Several needle steering strategies have been developed, including asymmetric bevel-tip designs, shape memory alloy (SMA) actuation systems, tendon- or cable-operated mechanisms, and flexible shaft architectures [33, 39, 71]. Each of these approaches has specific advantages and limitations in terms of achievable curvature, mechanical complexity, and responsiveness to user input. A more detailed review of potential steering mechanisms, such as ball joint configurations, compliant structures, and hinge-based systems, is provided in Appendix C.

Material selection also plays a critical role in the design and performance of steerable needles. Stainless steel or tungsten alloys offer biocompatibility and strength, but limited flexibility. In contrast, nitinol, a nickel-titanium shape memory alloy, provides superelasticity, corrosion resistance, and the ability to undergo large deformations without permanent damage [40, 58].

Modern steerable needles are often paired with imaging guidance, such as ultrasound, CT, or MRI, to enable real-time monitoring of the needle trajectory [62]. However, despite promising research, the clinical adoption of steerable needles remains limited due to challenges in mechanical reliability, imaging compatibility, intuitive user interfaces, sterilization compatibility, and overall cost-effectiveness [22, 33].

1.3. Problem Statement

Brachytherapy has proven highly effective in treating cervical cancer, but precise needle guidance within the intricate pelvic anatomy remains a challenge. While ultrasound imaging is frequently used for real-time visualization, distinguishing the needle tip from surrounding
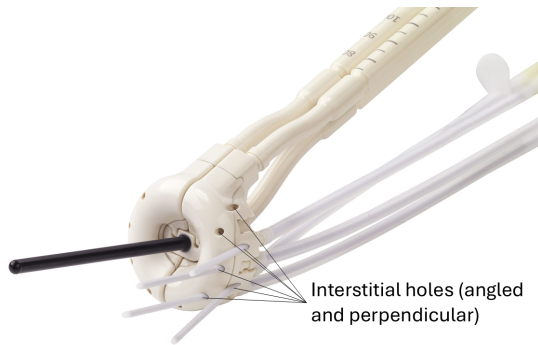
Figure 1.2: Elekta Venezia applicator with both angled and perpendicular interstitial holes for needle insertion. These allow for multidirectional placement but still pose limitations when navigating to off-axis or irregularly shaped tumors. Image source: Elekta `https://www.elekta.com/products/brachytherapy/venezia/` [18].

soft tissues is difficult due to limited resolution [65, 75]. MRI and CT offer higher spatial resolution but are generally impractical for continuous intraoperative monitoring. As a result, most clinicians rely heavily on ultrasound for real-time guidance during needle placement.

In cases involving asymmetric or parametrial tumor extensions, fixed-geometry applicators may not allow optimal needle placement, leading to underdosing of tumor margins and increased radiation exposure to surrounding healthy tissues. Although the Elekta Venezia system includes angled channels to extend access, both Venezia and Geneva remain limited by their fixed trajectories, which may prevent accurate targeting of off-axis regions (see Figure 1.2; Appendix A) [23].

As mentioned above, when applicators or needles cannot be placed accurately, dose distributions can become suboptimal, increasing radiation exposure to adjacent organs such as the bladder and rectum [60, 66]. Frequent repositioning also prolongs procedures, increases patient discomfort, and increases the likelihood of placement errors [33].

Manual steerable needles offer a promising alternative by allowing clinicians to dynamically control the path of the needle while receiving direct tactile feedback. Compared to robotic approaches, manual actuation can provide a

more practical and cost-effective solution without adding excessive complexity to the clinical workflow. However, developing such a device requires overcoming challenges in mechanical design, force transmission, imaging visibility, biocompatibility, and integration with standard applicator systems.

1.4. Goal of the Research

While recent advancements in steerable needle technology demonstrate significant potential to enhance source placement accuracy in brachytherapy procedures [39, 71], key challenges remain. Imaging limitations, anatomical complexity, and soft tissue deformation continue to hinder precise needle navigation and alignment [60, 67].

The main objective of this research is:

To develop and experimentally validate a manually actuated steerable interstitial needle that works seamlessly with established brachytherapy applicators (such as the Elekta Geneva and Venezia systems) and enhances the precision of needle placement in complex or hard-to-reach tumor regions.

This goal is supported by several sub-objectives:

- **Design and Integration:** develop a robust steering mechanism capable of smooth, controlled curvature within soft tissue, while maintaining compatibility with standard applicator-catheter assemblies.
- **Material Selection and Fabrication:** select materials that provide an optimal balance of flexibility, stiffness, biocompatibility and sterilizability.
- **Imaging and Navigation:** ensure that the steerable needle is clearly visible in clinical imaging modalities, to allow accurate navigation in future applications.
- **Evaluation and Validation:** experimentally assess the performance of the prototype in tissue-mimicking phantoms, comparing

it with conventional ProGuide obturators in terms of curvature and placement accuracy.

This project introduces a manually actuated steering mechanism that prioritizes intuitive use and direct compatibility with clinical brachytherapy systems. The scope of this project was limited to in vitro validation using tissue-mimicking phantoms and does not include in vivo testing or integration into full clinical workflows.

By addressing these objectives, the developed steerable needle has the potential to improve local tumor coverage, reduce radiation exposure to healthy tissues, and streamline cervical brachytherapy procedures. Ultimately, this work contributes to the development of more accessible and precise cancer treatment technologies.

1.5. Structure of the Report

The structure of this report is organized to reflect the progression from design requirements to experimental validation.

Chapter 2 introduces the clinical and technical requirements that guided the design of the steerable needle. Chapter 3 describes the conceptualization and mechanical design of the device. Chapter 4 details the material selection, fabrication processes and mechanical analysis, including finite element simulations. Chapter 5 presents results of the experimental evaluation in gelatin and silicone phantoms using CT imaging. Finally, Chapter 6 discusses the findings in the context of clinical application, identifies limitations, and outlines directions for future work, before concluding the thesis in Chapter 7.

2

Requirements

2.1. Must-Have Requirements

The must-have requirements define the essential functional and safety criteria that the steerable needle must satisfy for clinical applicability. These requirements are important to make sure the device can be used in a clinical setting and fits within existing brachytherapy systems.

1. **Dimensional compatibility:** a maximum outer diameter of 1.35 millimeters shall ensure compatibility with 6F ProGuide catheters (see Appendix A).

2. **Ultrasound visibility:** the device shall be clearly visible under ultrasound (US) imaging during brachytherapy procedures without producing image artifacts that obscure anatomical features or device boundaries under standard US settings.

3. **Manual control:** one-handed manual steering shall be enabled through integrated controls.

4. **Deflection performance:** at an insertion depth of 50 millimeters, the tip shall achieve a minimum lateral deflection of 20 mm in a soft-tissue phantom with stiffness comparable to cervical tissue.

5. **Targeting accuracy:** the planned target location shall be reached within a maximum positional deviation of ±5 millimeters in any direction in at least 95% of insertions under identical operating conditions in simulated cervical tissue.

6. **Structural integrity:** no visible buckling or permanent deformation shall occur when the device is inserted through Elekta Venezia and Geneva gynecological applicators into clinically representative phantom material under standard conditions.

7. **Degrees of freedom:** the design shall allow translation along the longitudinal axis, rotation about that axis, and adjustable curvature in a single plane.

8. **Sterilization compatibility:** all materials shall be compatible with standard steam sterilization at 130 °C. If this is not feasible, the design shall allow for alternative methods such as gamma irradiation at 25 kGy or hydrogen peroxide plasma sterilization.

9. **Biocompatibility:** all materials used shall comply with ISO 10993-1 standards for biocompatibility in the intended clinical application.

2.2. Nice-to-Have Features

These optional features are not essential for core functionality, but can improve clinical usability, adaptability, and manufacturability.

1. **Manufacturing compliance:** the device should be manufactured using validated and standardized processes in compliance with ISO 13485 to support consistent production and quality control.

2. **MRI visibility:** the device should be visible on magnetic resonance imaging (MRI) without introducing significant susceptibility artifacts in the region of interest.

2.3. Preconditions

The following preconditions define the boundary conditions to ensure that the design aligns with current clinical standards, technical capabilities, and safety requirements.

1. **Applicator compatibility:** the guiding tubes and template holes of the Elekta Venezia and Elekta Geneva gynecological applicators shall accommodate ProGuide 6F catheters (see Appendix A).

2. **Source flexibility:** the Flexisource high dose-rate (HDR) source shall not cause kinking of the catheter at a minimum bending radius of 10 millimeters.

3

Design

3.1. Layout

This chapter describes the design of a steerable interstitial needle for HDR cervical brachytherapy, emphasizing precision, compatibility, and single-handed manual control. An overview of the complete assembly, including the actuation unit and needle components, is shown in Figure 3.1. The design features a split-shaft mechanism in which the needle is longitudinally divided along most of its length, with the distal tip forming a continuous segment to ensure controlled curvature under differential actuation. The compliance of this region enables controlled deflection through differential actuation, where pushing one beam forward while retracting the other induces bending due to the asymmetric force distribution. This principle closely mirrors a four-bar linkage, in which linear forces applied to a segmented rod system result in a predictable angular deflection [43]. In this design, however, the pivot-like behavior is integrated within the material's elastic deformation, eliminating the need for separate mechanical joints [25].

The proposed needle shares fundamental similarities with loop-shaped steerable mechanisms, such as the Active Sheath developed in prior work (Yamada et al. [73]). The active sheath utilizes a looped flexible stylet within a fluororesin cannula, where push-pull actuation of the proximal ends allows bending

in controlled directions. In particular, a variation of this mechanism, stylet (B) in their study, incorporated an inhomogeneous thickness profile at the tip to facilitate a "virtual articulated joint", thereby enhancing its bending capabilities. Experimental validation in agar-based phantoms demonstrated significant lateral deflection with predictable path-following capabilities [73]. Compared to conventional ProGuide obturators, made of tungsten, the looped mechanisms exhibited superior curvature control. However, one limitation observed in these designs was the necessity of a separate sheath to house the flexible stylet, which introduces an additional interface that may affect the consistency of the actuation.

Another similar design was inspired by the elasticity-based kinematic modeling explored in another of Yamada's papers on closed elastica mechanisms [72]. These models describe how an elastic arm enclosed in a flexible sheath deforms under tension and compression, effectively mimicking a tendon-driven mechanism while avoiding the friction losses of cable routing. Finite element analyses confirmed that the bending profiles obtained with these elastic systems closely matched predictions derived from continuum mechanics models, further validating the feasibility of using such principles for steerable needle applications. However, a challenge observed in the elastic arm was the need for
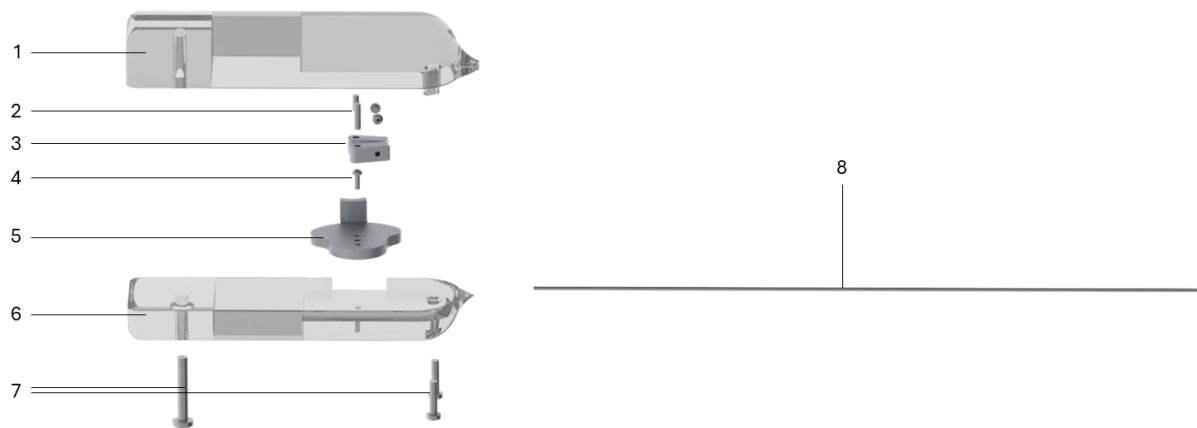
Figure 3.1: Exploded view of the actuation unit and steerable needle, showing the top cover (1), pins and screws (2), mounting blocks (3), pin (4), rotation wheel (5), bottom cover (6), screws (7), and steerable needle (8).

precise pretensioning to achieve optimal bending [72]. In contrast, the split-shaft design inherently balances structural stiffness through its geometry and does not require additional tuning of internal stress distributions (see Chapter 4).

The steering interface for the proposed needle is manually actuated, providing a tactile and intuitive control method for clinicians. Unlike the robotic-assisted needle insertion methods explored in other works, such as Yamada's robotic manipulator-driven tests, the current design prioritizes physician manual input and feedback [72]. Although robotic actuation can improve precision, manual control remains more practical for widespread use due to its simplicity and cost-effectiveness [73].

The key performance requirements of the present steerable needle focus primarily on achieving sufficient tip deflection, maintaining positional accuracy, and ensuring mechanical robustness while adhering to strict dimensional constraints. The outer diameter of the device must not exceed 1.35 mm to ensure compatibility with standard Elekta Geneva and Elekta Venezia applicators, but it shall generate a lateral deflection of at least 20 mm at an insertion depth of 50 mm. Additionally, the structure must resist buckling under insertion forces while providing translation along its longitudinal axis, rotation about that axis, and adjustable curvature in a

single plane containing the axis. The split-shaft configuration localizes compliance near the tip, enabling significant curvature while preserving axial rigidity for insertion stability.

It should be emphasized that this chapter and the broader thesis primarily focus on the underlying steering mechanism of the needle. Although manual actuation by the clinician and the transmission of forces along the shaft are taken into account, they are considered only in a broad sense. The main emphasis lies in analyzing and refining the geometry and elastic properties that enable precise directional control, thereby illustrating how the split-shaft concept provides reliable and intuitive steering without delving extensively into alternative actuation methods or complex transmission architectures. By confining all structural deformations to a single continuous material domain, the design further improves the predictability of deflection behavior, reducing mechanical interfaces that could introduce unwanted variability [74].

Further discussion of alternative design iterations and detailed comparisons with state-of-the-art control mechanisms are provided in Appendices B and C. Appendix B outlines the concept development process, breaking the design down into sub-functions with different potential solutions, while Appendix C provides an in-depth analysis of different

steering mechanisms, transmissions, and control units. Together, these sections explain the reasoning behind the final design selection and demonstrate how specific dimensions, material choices, and actuation techniques were optimized to achieve the required performance for gynecological HDR brachytherapy.

3.2. Steering Mechanism

The steerable needle is an example of a sophisticated compliant mechanism that combines the inherent flexibility of materials with a strategically engineered geometry to enable precise directional control in minimally invasive procedures. As described in Section 3.1 and illustrated in Figures 3.2 and 3.3, the needle is divided along most of its length into two flexible beams that remain connected only at the distal tip, forming a significant cutout that serves as the crucial flexure region. This design facilitates steering without relying on traditional mechanical joints, which can be prone to wear and complex to manufacture on such a miniature scale [28]. As stated in Section 3.1, the clinician's manual actuation applies differential forces through the split-shaft mechanism, advancing one beam while retracting the other, to translate the rotational input into predictable elastic bending of the distal tip. The elongated slot near the tip is key to defining the compliance of the bending region, directly influencing both the precision of the steering and the curvature limits [73]. As a result, uneven loading within the flexure region causes the needle tip to deflect toward the side that receives the push force. The deflection magnitude is directly proportional to the applied push-pull forces and the mechanical properties of the needle material.

A similar principle was presented in previous work (van de Berg et al. [6]), which used a pseudo-rigid body (PRB) diagram to illustrate the interplay between internal and external forces in a multi-segment steerable needle design. In their framework, an internal load (F_{int}) is applied by
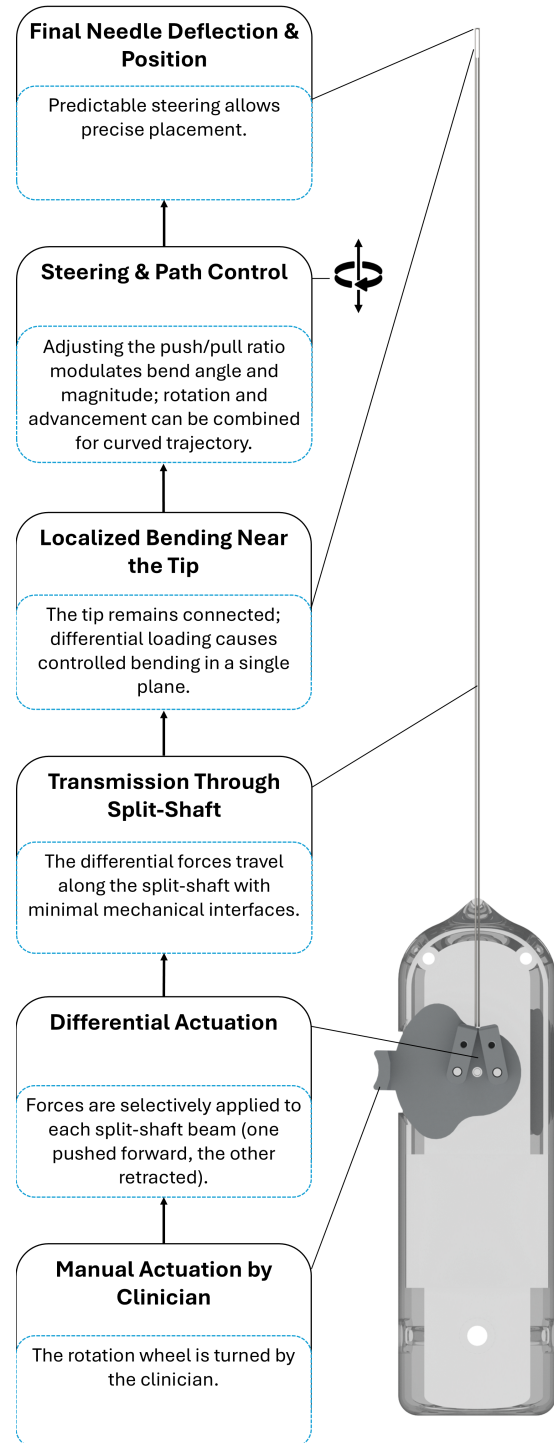
Figure 3.2: Conceptual schematic of the differentially actuated, steerable needle system illustrating how manual input translates into localized bending and precise tip deflection.

the user at the proximal end (through a lever and transmission wheel), translating one or more stylet segments relative to the outer cannula. This translation drives the distal tip articulation.

Any external load (F_{ext}) acting on the needle tip is transmitted along the shaft, but due to its very short moment arm, it generates minimal torque. As a result, the force does not significantly alter the direction of the proximal steering mechanism and instead causes only a small elastic deflection. By modeling the cannula guidance as roller supports, the PRB diagram shows that the distal tip articulation remains well defined and stable under typical loading conditions. Consequently, even if the needle encounters significant external resistance, the manual interface at the proximal end experiences negligible rotation due to the efficient constraint of the design of off-axis forces. Adopting a similar approach in the present steerable needle ensures that internal actuation forces dominate the deflection behavior, while external loads primarily induce elastic bending rather than disrupting the steering input.

The compliant mechanism operates on the principle of elastic deformation, where the material undergoes bending without yielding or permanent deformation. This behavior is critical to ensure that the needle can be repeatedly steered without compromising its structural integrity. Materials such as stainless steel, titanium alloys or superelastic alloys such as nitinol are typically selected for their high fatigue resistance and ability to sustain numerous cycles of bending and straightening without failure [36, 57]. The precise engineering of the slot geometry, its length and width, is paramount to balance flexibility with the necessary rigidity to penetrate tissue effectively. Increasing the length and width of the slot enhances compliance and steering, but must be carefully balanced to prevent loss of structural integrity during insertion.

The design considerations for such a compliant and steerable needle are numerous. Material selection is critical, as the chosen material must be not only sufficiently flexible, but also biocompatible and fatigue resistant. Computational modeling and finite element analysis are often employed during the design
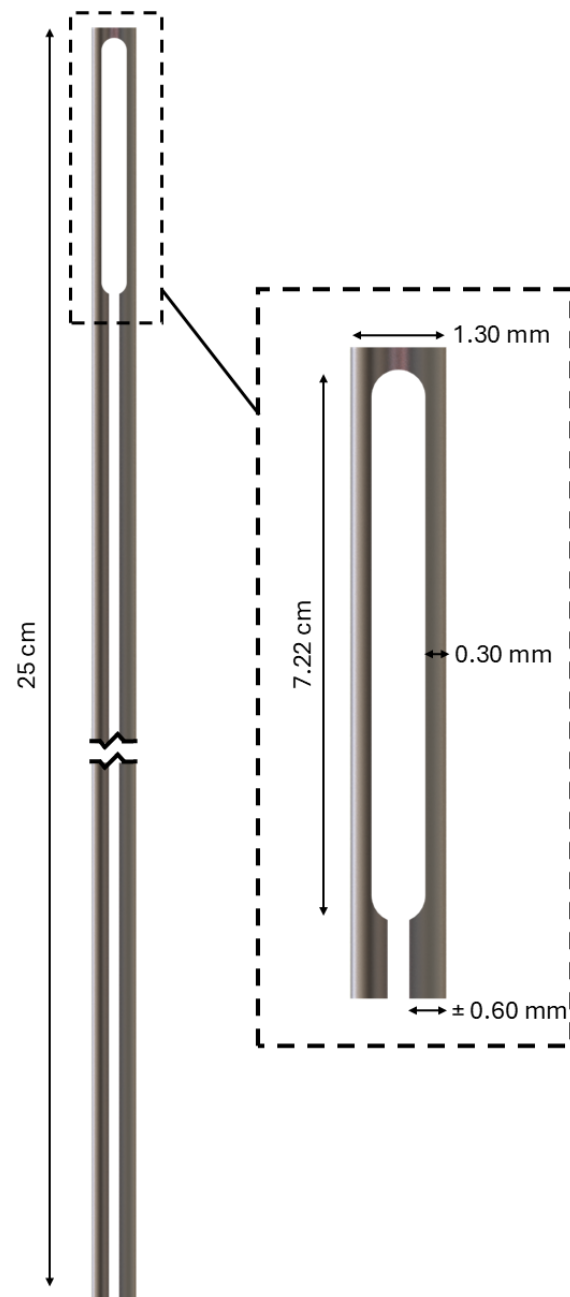
Figure 3.3: Dimensional schematic of the steerable needle, highlighting the elongated slot near the tip used for differential actuation.

phase to predict the mechanical behavior of the needle under various loading conditions, ensuring that the elastic deformation remains within safe limits to prevent permanent bending or failure. Figure 3.4 illustrates the complete assembly of the steerable needle housed within the handpiece. The internal differential actuator

is enclosed within a compact grip, allowing intuitive manual control of the bending behavior of the needle.

+208 mm

132 mm

40 mm
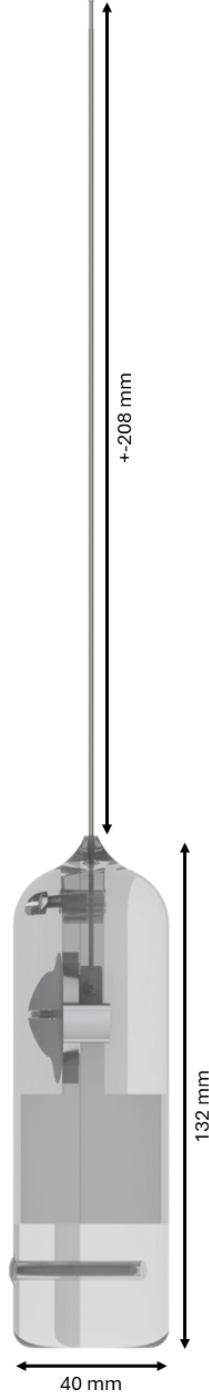
Figure 3.4: Side view of the fully assembled handpiece, showing the internal differential actuator and the attached steerable needle.

Actuation mechanisms must be precise and responsive to allow accurate control over the trajectory of the needle. This typically involves the integration of mechanical actuators or external manipulation tools capable of applying the necessary differential forces to the needle's beams. The steering motion should remain smooth and predictable, avoiding abrupt deflections that could lead to excessive tissue stress or unintended needle behavior.

3.2.1. Mechanical Characterization

The longitudinally split-shaft mechanism increases the rotational degrees of freedom (DOFs) from zero in a conventional rigid needle to two in the steerable design. This added freedom of movement, essential for precise steering in HDR brachytherapy, reduces the sectional moment of inertia by approximately 21% compared to a standard ProGuide obturator. As a result, both the bending and axial stiffness of the needle are affected.

The resistance of the needle to bending is characterized by its flexural rigidity, defined as the product of the material's Young's modulus (E) and the second moment of inertia (I) of its cross section:

$$\text{Flexural rigidity} = E \times I, \qquad (3.1)$$

For the steerable needle, the reduced moment of inertia due to the longitudinal slot results in a flexural rigidity of approximately $22 \times 10^{-3}\,\text{N} \cdot \text{m}^2$, where $E = 200$ GPa (AISI 301 see Section 4.1) and $I = 0.11\,\text{mm}^4$. This lower flexural rigidity facilitates controlled bending under differential actuation forces. However, if it becomes too low, the needle may deflect excessively or unpredictably during insertion.

The needle's ability to resist axial compression and avoid buckling is described by its axial rigidity, given by

$$\text{Axial rigidity} = E \times A, \qquad (3.2)$$

where A is the cross-sectional area. In the steerable design, the effective cross-sectional area is reduced from 1.432 mm^2 in a standard

rigid needle to 0.46 mm^2, representing a reduction of approximately 68%, mainly due to the incorporation of the longitudinal slot. This decrease is due in part to the smaller needle diameter of 1.3 mm compared to the 1.35 mm typically used in the rigid straight design due to supplier constraints. Such a substantial reduction in area results in lower axial rigidity and makes the needle more compliant. Although increased compliance is crucial for steering, the needle must also retain enough axial strength to resist buckling under compressive forces during insertion. Understanding and quantifying these mechanical properties is essential for predicting the needle's behavior under clinical conditions, since flexural stiffness controls the needle's bending response to differential actuation forces and ensures accurate steering along complex anatomical trajectories, while axial stiffness is critical for maintaining structural integrity during insertion.

3.3. Control Mechanism

Rotating the handpiece about its longitudinal axis allows the user to change the plane of curvature, enabling directional steering in any 2D plane. The steering mechanism of the split-shaft needle is based on the principle of differential actuation. To test this concept effectively, a simple handpiece was developed to transmit user input into the required differential motion. The handpiece incorporates a semicircular rotation wheel and two clamp blocks, both sized and positioned to provide an intuitive single-handed interface suitable for both left- and right-handed users. The clamp blocks are designed with matching slots that hold the beams firmly, preventing any lateral play. The rotation wheel and clamp blocks are mechanically linked via pins. Turning the wheel advances one beam while retracting the other by an equivalent amount. This direct coupling ensures that the longitudinal displacement of each beam exactly matches the rotation of the wheel, minimizing
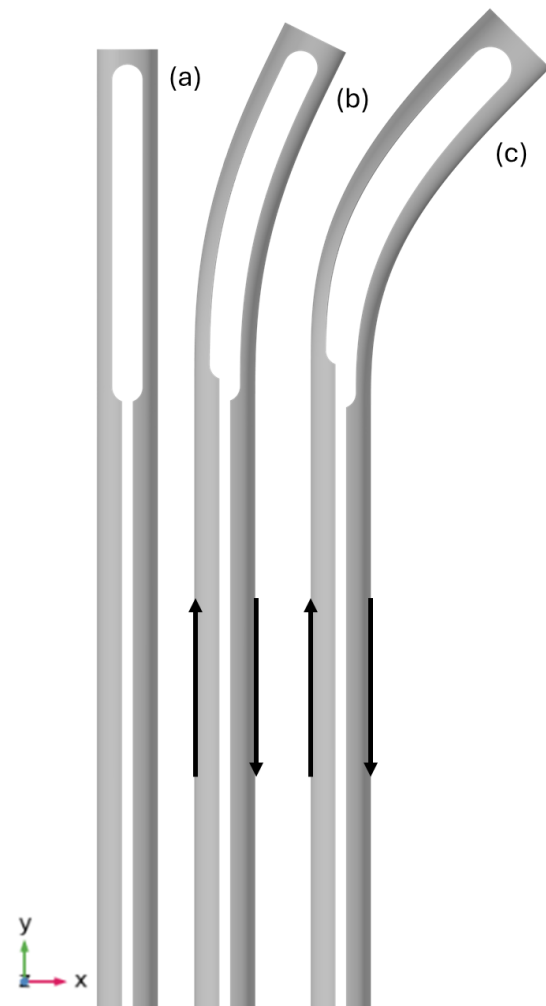
Figure 3.5: Progressive bending states of the steerable needle under varying differential actuation: (a) no deflection, (b) partial bend, and (c) maximum curvature.

backlash and maintaining control accuracy.

The core functionality of the handpiece lies in the ability to make fine adjustments to the axial offset. Small rotations of the wheel by the clinician result in proportionally small changes in the axial position of the beams, which, in turn, generate correspondingly minor bends at the tip. The transmission converts the rotation into translation, after which the needle provides the deflection. The amount of translation can be adjusted by repositioning the clamping blocks, with the maximum displacement determined using COMSOL Multiphysics® simulations (see Chapter 4). This relationship between wheel rotation and deflection provides a granular level of control over the needle trajectory. In practical

use, the clinician can rotate the wheel slowly, monitoring how the tip moves in real time. The effect of differential actuation on needle bending is illustrated in Figure 3.5, where the needle transitions from an unbent state (a) to a partially bent configuration (b) and finally to its maximum curvature (c). In this model, the medial surfaces of the legs are subjected to a roller constraint, which emphasizes the tip's bending behavior. This progression shows how small changes in differential motion lead to gradual curvature adjustments, allowing controlled directional guidance. If a sharper bend is needed, the user simply continues to turn the wheel until the desired curvature is reached. Once the beams are returned to parallel alignment, the needle resumes a straight form. The elastic design of the needle supports repeated bending and straightening cycles, making it suitable for multiple insertions or reorientations during a single procedure.

As described in Section 3.1, the minimalist handpiece incorporates a provision for free rotation of the entire assembly on its longitudinal axis, as seen in Figure 3.2. Figure 3.6 illustrates the bending behavior of the steerable needle when housed within a ProGuide 6F catheter, highlighting the feasibility of controlling curvature even when the needle is enclosed within a guiding sheath. Further testing is required to determine if the needle can achieve the required angular range with the ProGuide 6F catheter to meet the design requirement, *the steerable needle shall be capable of achieving a minimum tip deflection of 20 millimeters at an insertion depth of 50 millimeters in tissue*, see Chapter 5 for the relevant experiments. By twisting the handle, the user changes the plane in which the needle deflects, allowing the needle to curve in any arbitrary direction. This rotation does not introduce additional complexity into the actuation mechanism because the beams remain aligned with the rotation wheel and clamp blocks, ensuring that the same differential push-pull action consistently produces a bend

in the same relative direction regardless of the orientation of the handpiece. Furthermore, the uncluttered design provides direct tactile feedback, allowing the operator to feel resistance when encountering denser tissues and adjust push-pull forces accordingly to avoid excessive bending or unintended deflections, while the rigid grip of the clamp blocks ensures that external loads on the distal tip do not induce independent motion of the beams.
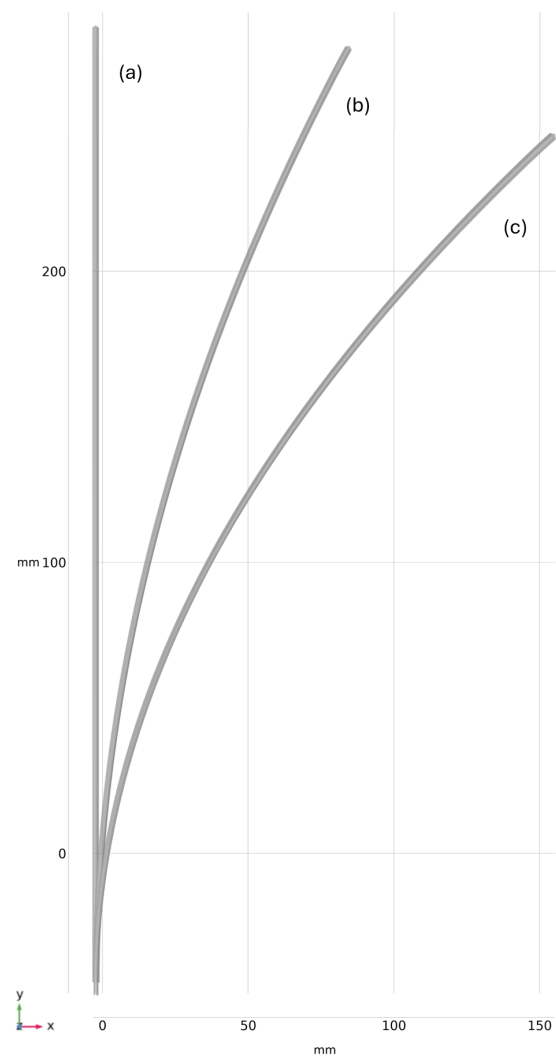
Figure 3.6: The steerable needle housed within a catheter is shown in three bending states: (a) no curvature, (b) moderate curvature, and (c) maximum curvature.

All control inputs are transmitted through straightforward mechanical interactions: the rotation of the wheel directly sets the beam offset, which in turn defines the needle's bend. This avoids mechanical complexity and minimizes

frictional losses, allowing immediate response to user input without the need for gears or cables. This streamlined configuration simplifies testing and demonstrates that appropriate steering can be achieved with minimal components.

3.4. Integration of Components

The steerable needle assembly is formed by combining three principal subsystems: the split-shaft needle itself, the actuation mechanism, and the handpiece housing. Each subsystem must meet strict geometric and functional constraints to ensure that the final device is compact and reliable. Integration of the steerable needle with the actuation unit requires precise alignment of its mechanical components. As shown earlier in Figure 3.1, the actuation mechanism highlights key elements such as the clamp blocks (3), the rotation wheel (5), and the split shaft needle (8). Note that the handpiece is divided into two parts (1 and 6), with separation occurring along the frontal plane at the cutout for the rotation wheel knob, thereby facilitating easy assembly and disassembly. The arrangement of these components ensures accurate force transmission while maintaining a compact and ergonomically efficient configuration suitable for clinical manipulation.

A key consideration in integrating the split-shaft needle with the handpiece is the precise alignment of the two beams of the needle where they pass through the clamp block. These beams must remain parallel for most of their length to allow clean differential actuation without introducing lateral stress or twisting. The clamp block includes matching slots or recesses to preserve parallel alignment, ensuring that axial motion in one beam is mirrored by equal and opposite motion in the other. The beams are fastened with screws on their medial sides within the clamp blocks, and tight tolerances in this area prevent off-axis shifting, thereby ensuring consistent bending performance.

Another important challenge is to ensure that the steering mechanism remains accessible and user-friendly while protecting internal components from potential damage during handling. The rotation wheel provides a simple user interface for advancing or retracting one beam relative to the other, but it also needs to be robustly mounted so that it remains concentric with the beams and can be operated with minimal friction. The design addresses this by positioning the wheel just behind the center plane in a way that balances ease of manual operation with a secure attachment to the clamp block via pins and another pin to the handpiece. This configuration maintains a direct actuation path, minimizing the likelihood of misalignment and preserving the tight mechanical coupling needed for precise steering.

Where the split-shaft needle exits the handpiece, it is essential that the beams are able to move freely without being obstructed. To ensure this, the housing around the exit point is trimmed to avoid any interference with the relative motion of the needle shafts. Material selection plays a critical role in ensuring the durability and mechanical performance of the steerable needle system. The clamp blocks and rotation wheel must be made of materials that can securely hold the needle's beams while minimizing friction and wear at their contact interfaces [2].

A coaxially introduced catheter can be placed over the needle, which requires that the external diameter of the assembly remain small enough to fit inside the catheter tube. To ensure proper function, the slot in the needle shaft must be positioned and dimensioned so that it does not obstruct the catheter from sliding smoothly over it.

Although the handpiece is primarily intended for testing, its assembly allows easy cleaning during gelatin-based experiments, with potential adaptations for clinical sterilization in future iterations. Figure 3.7 provides a front view of the actuation unit, showing critical elements such as the clamping blocks (3), the rotation

user's perception of how much force is actually applied at the tip, undermining one of the key advantages of a direct-actuated system. In contrast, any looseness in the connections would introduce backlash, decreasing the steering precision. Precise machining and careful fastening ensure that the design supports both secure assembly and sensitive tactile feedback, ensuring that the needle's differential actuation remains responsive and controllable even under the varying forces encountered in clinical use.

Figure 3.7: Front view of the steerable needle's actuation unit, showing: (1) steerable needle, (2) screw hole, (3) block to clamp the needle, (4) screw to clamp the needle, (5) pin to mount the rotation wheel, (6) pin to mount the block, (7) knob of the rotation wheel, (8) rotation wheel, (9) bottom part of the grip, and (10) screw hole.

wheel (8), and the input point for manual rotation (7). The alignment of these components ensures that the differential forces applied to the beams are transferred effectively, preserving precise control over tip deflection. The relatively simple geometry of the handpiece allows for disassembly, cleaning, and reassembly without specialized tooling.

Finally, achieving a secure but low friction interface at each junction is essential to maintain tactile feedback from the needle. Excess friction within the handpiece could distort the

4

Prototyping

4.1. Finite Element Analysis

This section provides a comprehensive overview of the finite element analysis (FEA) carried out on the steerable needle prototype. Three-dimensional models of the needle and catheter assembly were developed in SolidWorks® 2023 (Dassault Systèmes, Vélizy-Villacoublay, France) to reflect a clinically relevant configuration. These models were then imported into COMSOL Multiphysics®, where rigorous finite element simulations were performed to evaluate stress distributions, deformation behavior, and potential failure modes under clinical loading scenarios.

The simulation framework includes static analyses to study the effects of differential actuation forces applied to the needle structure. The material properties were carefully assigned on the basis of experimental data and the published literature. Material properties were defined based on published literature and prior experimental data to ensure physiological realism in simulation. In our model, the needle is defined using AISI 301 stainless steel as research by Martijn de Vries on a similar steerable needle for prostate brachytherapy showed that this material provides the required balance between strength and flexibility [12]. The catheter component was modeled using polyoxymethylene (POM), as this is the material used in commercial ProGuide 6F catheters [69].

The simulation results help determine whether the steerable needle can withstand the mechanical forces applied during actuation and manipulation while remaining within acceptable deformation and stress limits. The actual performance during phantom insertion will be examined later in Chapter 5 Testing and Validation. These finite element simulations serve as an early indicator of the feasibility of the design, and the insights gained from these analyses guide further design refinements and advance to prototype fabrication.

4.1.1. Needle Only

This subsection presents a detailed finite element analysis of the needle component in isolation, aimed at evaluating the inherent bending performance and structural response of the split-shaft needle design without the added complexity of catheter interactions. An extremely fine free tetrahedral mesh, consisting of 905.137 elements, was used to discretize the needle. This high-resolution meshing ensures that localized stress concentrations and subtle deformation patterns, particularly in the split region where bending occurs, are accurately captured.

To simulate differential actuation forces, one of the proximal segments of the needle (see Figure 3.3) was fixed to simulate a clamped boundary condition, while a prescribed displacement of 1

mm was applied at the proximal part of the other leg. This controlled displacement is intended to induce bending in the distal part of the needle, allowing us to assess its ability to deform predictably and maintain its structural integrity under the applied load. A roller constraint was applied at the medial (flat) part of the split beams of the needle, as this was done to isolate and evaluate the theoretical maximum displacement of the tip only.

The simulation results indicate a maximum von Mises stress of 322 MPa. This value demonstrates that, under the prescribed displacement, the design of the needle remains well below the yield strength of 964 MPa for stainless steel AISI 301 (see Table 4.1). The insights gained from this analysis serve as a critical benchmark for further design refinements, ensuring that the needle alone possesses the necessary mechanical robustness before incorporating additional components such as a catheter.

Table 4.1: Material properties used in COMSOL Multiphysics simulations (sourced from Granta EduPack 2024 R2).

Material	Young's Modulus (GPa)	Yield Strength (MPa)
AISI 301 Stainless Steel	197	964
POM (Polyoxymethylene)	3	64

4.1.2. Needle-Catheter Configuration

Cutout Length

This subsection examines in detail the mechanical behavior of the integrated needle–catheter assembly under bending conditions. In this analysis, as described in Section 4.1.1, the proximal end of one beam of the split needle is rigidly fixed at its bottom end, while the proximal end of the other beam is subjected to a prescribed displacement of 1 mm. The catheter is also fixed at its proximal bottom end. The length of the split-shaft steerable needle is 296.0 mm. The catheter length, following the ProGuide 6F cervical
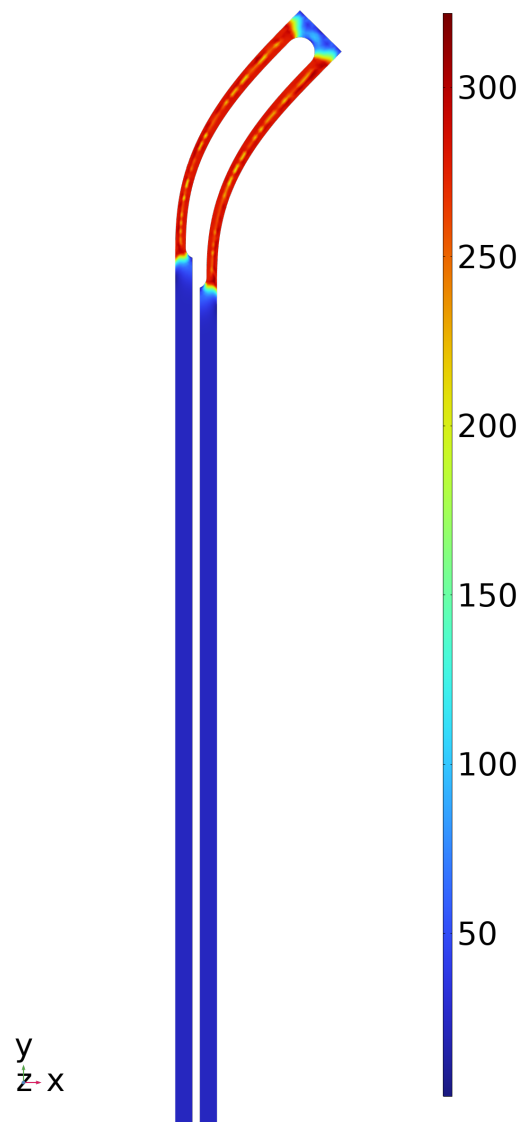
Figure 4.1: Finite element simulation of the needle without a catheter, showing a maximum von Mises stress of 321.975 MPa.

brachytherapy catheters, is 294.0 mm [16]. This arrangement allows us to simulate the bending behavior of the needle in a clinically relevant configuration, where the catheter does not restrict the movement of the needle throughout its length but provides a defined stopping point at its tip. The entire assembly is discretized using an extra-fine free tetrahedral mesh comprising 98,720 elements.

A similar steerable needle concept was described previously (see Yamada et al. [73]);

they employed a needle stylet with an outer diameter of 0.9 mm and a slot length of 5.0 mm, which yielded a slot-to-diameter ratio of approximately 5.56. When applying the same ratio to our needle, which has a diameter of 1.3 mm, the recommended corresponding slot length is about 7.2 mm. The close correspondence in these proportions reinforces the idea that maintaining a similar ratio is beneficial in achieving the desired bending performance while maintaining stress levels within acceptable limits.

Three configurations were analyzed by varying only the slot length, keeping other parameters constant on the needle. In the first configuration, the slot length is 5.0 mm. The edge thickness was kept at 0.3 mm. As seen in Table 4.2, the simulation produces a maximum von Mises stress of 648 MPa and a maximum displacement of 157.6 mm. In the second configuration, the slot length is increased to 7.2 mm. Figure 4.2 and Table 4.2 show that the maximum stress decreases to 586 MPa, while the maximum displacement remains nearly identical at 157.5 mm. In the third configuration, the slot length is extended to 9.0 mm. As shown in Table 4.2, this arrangement results in an increased maximum von Mises stress of 703 MPa along with a higher maximum displacement of 166.7 mm.

Table 4.2: Effect of slot length on maximum von Mises stress and tip displacement in needle–catheter assemblies.

	5.0 mm	7.2 mm	9.0 mm
Max. von Mises Stress (MPa)	648	586	703
Max. Displacement (mm)	157.6	157.5	166.7

A detailed comparison of these configurations, as summarized in Table 4.2, revealed that the length of the slot is a critical design parameter that influences the bending behavior of the needle. The configuration with a 7.2 mm slot exhibits a more favorable stress distribution compared with the 5.0 mm configuration while maintaining effective bending performance. In contrast, the 9.0 mm slot configuration, despite providing a greater displacement, induces

significantly higher stress levels that may compromise structural integrity under clinical loading conditions.

Slot lengths in the region of 7.2 mm were also tested with a variation of 0.01 mm. Up to $\pm$ one millimeter was explored in this region to see if an even better slot value could be identified. Among these, a slot length of 7.22 mm consistently produced the lowest maximum von Mises stress while maintaining a high deflection-to-stress ratio, confirming it as the optimal choice within the tested range.

Figure 4.2 clearly illustrates the stress distribution and displacement pattern for the 7.22 mm slot configuration. All figures from the FEA analysis can be found in Appendix E. These simulation results provide critical information on stress concentrations, allowing targeted refinements of the slot geometry while confirming that the design achieves the intended bending performance while maintaining structural integrity.

Edge Thickness

In the previous subsection on *length cutout*, the 7.22 mm slot length was identified as an optimal configuration to balance stress and displacement. Building on this, the influence of varying the *edge thickness* on the mechanical behavior of the steerable needle is now examined. Figure 4.3 shows a top view of the split-shaft steerable needle, highlighting the cutout region evaluated in this analysis. Edge thickness is a critical design parameter that affects the bending region compliance, thus affecting both the steering accuracy and the overall structural robustness of the needle.

In this analysis, three edge thicknesses were evaluated: 0.275 mm, 0.300 mm (the baseline established in the previous section) and 0.325 mm. Table 4.3 summarizes the simulation results, where all tests were performed with the slot length fixed at 7.22 mm. The results show that reducing the edge thickness to 0.275 mm significantly increases the maximum von
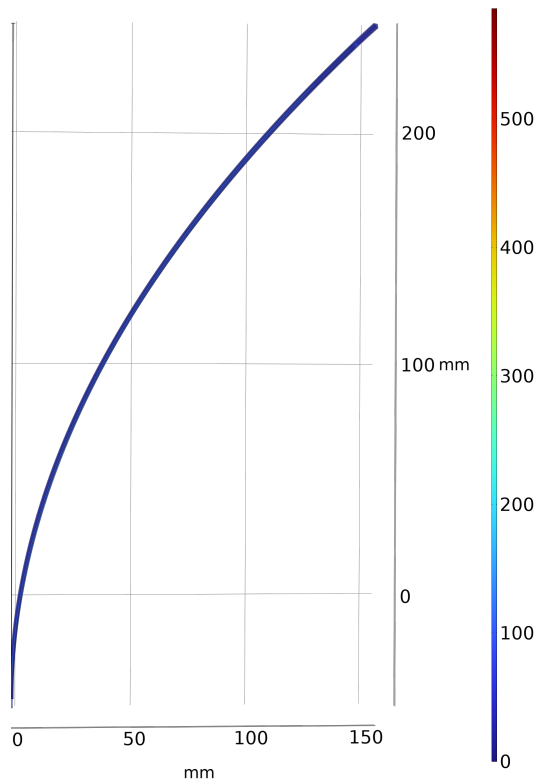
Figure 4.2: Simulation output of the needle–catheter assembly with a 7.22 mm slot and 0.3 mm edge thickness. Maximum von Mises stress is 585.900 MPa with 157.50 mm displacement, indicating a favorable balance between stress and flexibility.

Mises stress to 973 MPa, while the maximum displacement is reduced to 139.3 mm. In contrast, the 0.300 mm configuration exhibits a lower maximum stress of 586 MPa and a displacement of 157.5 mm. The configuration with an edge thickness of 0.325 mm shows an intermediate stress value of 1048 MPa, with a slightly higher displacement of 159.0 mm.

Table 4.3: Effect of edge thickness on maximum von Mises stress and tip displacement (slot length fixed at 7.22 mm).

	0.275 mm	0.300 mm	0.325 mm
Max. von Mises Stress (MPa)	973	586	1048
Max. Displacement (mm)	139.3	157.5	159.0

The higher stress observed at 0.275 mm suggests that a thinner edge concentrates loads more intensely, potentially leading to premature fatigue or failure, despite offering less displacement. In contrast, the thicker edge

of 0.325 mm provides a greater displacement, indicative of increased flexibility, but at the cost of a higher peak stress than the 0.300 mm edge thickness configuration.

The relative edge thickness of the present design can be compared to that of a previously reported steerable needle (Yamada et al. [73]). In their work, the edge of the loop-shaped stylet had a thickness of 0.225 mm for a needle with an outer diameter of 0.9 mm, which yielded an edge-to-diameter ratio of 0.25. In our design, using a needle with an outer diameter of 1.3 mm, the baseline edge thickness of 0.300 mm corresponds to a ratio of approximately 0.23, whereas an edge thickness of 0.325 mm yields a ratio of 0.25. Although the 0.325 mm edge thickness results in an edge-to-diameter ratio comparable to a previously reported design [73], the higher stress observed in our simulation indicates that this ratio does not directly translate to optimal performance for our needle geometry.

The trial and error testing process revealed that although several edge thickness values near 0.325 mm were considered, the 0.300 mm configuration exhibited the most optimal balance between stress reduction and sufficient displacement. The combination of lower peak stress and acceptable flexibility makes this configuration the most suitable to prevent fracture while still achieving precise needle steering.

These findings support the design principles in Chapter 3, emphasizing controlled elastic deformation and mechanical robustness for effective needle control. By systematically adjusting slot length and edge thickness, the design achieves a well-calibrated trade-off between flexibility and structural integrity, allowing the needle to bend as intended without exceeding material stress thresholds. In addition, the finite element analysis performed in section 4.1 and extended here served as a rigorous quantitative framework for evaluating these design variables. It allowed systematic exploration of critical parameters
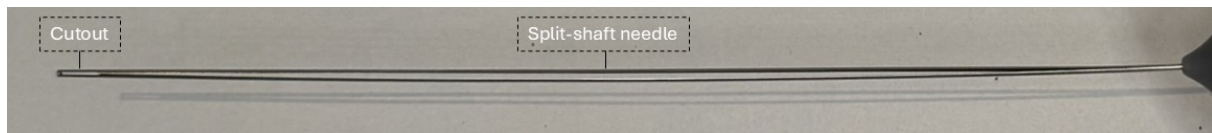
Figure 4.3: Top view of the split-shaft steerable needle without catheter.

under simulated conditions, providing deeper insight into how geometric changes affect needle performance.

4.2. Material Selection

Material selection is critical to balance flexibility, stiffness, biocompatibility, and imaging compatibility in steerable needle devices. The material must withstand repeated bending without undergoing permanent deformation while still providing sufficient rigidity for controlled steering. It also needs to be biocompatible and capable of being sterilized, as described in Chapter 2. In addition, the material shall be compatible with standard steam sterilization at 130°C (or alternative methods such as gamma irradiation at 25 kGy or hydrogen peroxide plasma sterilization if steam sterilization is not possible), conform to ISO 10993-1 biocompatibility standards, and be clearly visible under ultrasound imaging during brachytherapy procedures without introducing significant image artifacts. For a comparative overview of candidate materials and their properties, including ultrasound visibility, see Table 4.4.

ProGuide obturators for cervical interstitial brachytherapy are manufactured from tungsten alloy CMW 3000. This high-density material is selected for its robust mechanical properties and inherent echogenicity, ensuring reliable performance during tissue insertion [17, 26]. Additionally, tungsten alloy needles exhibit inherent echogenicity, improving ultrasound visibility, as demonstrated in Table 4.4. However, their high stiffness and relatively low elasticity can pose challenges for steerable applications, as bending may induce plastic deformation [40].

Nitinol, also known as NiTi, is frequently used in biopsy needles, guidewires, and surgical instruments used with robotic assistance due to its shape memory effect and exceptional fatigue resistance [15]. Its ability to undergo large elastic deformations without becoming permanently deformed has made it the standard material for flexible medical applications. However, for our specific needle, where a virtual articulated joint deflects the needle, the yield strength of nitinol may be insufficient to handle the resulting stresses. When the needle bends at the virtual joint, excessive stress concentrations could lead to material failure, making nitinol an unlikely candidate for this application [55].

For bending applications in steerable needles, AISI 301 stainless steel is a strong candidate due to its high yield strength and work hardening capability [46]. Although AISI 302 is a common stainless steel known for its excellent formability and good corrosion resistance, it generally has a lower yield strength and a lower Young's modulus compared to AISI 301. This means that AISI 302 is more prone to plastic deformation and may not provide the same level of stiffness, which is critical to preventing uncontrolled deflection during steering [4]. In contrast, the superior strength and stiffness of AISI 301, combined with its ability to endure repeated bending cycles without permanent deformation, makes it the preferred material for a steerable needle [24]. Its extensive use in springs further demonstrates its aptitude for elastic recovery, and its high natural echogenicity (as shown in Table 4.4) supports its use in imaging, making AISI 301 a fitting choice for precision and durability in clinical applications [63].

Ti-6Al-4V, also known as Grade 5 titanium, shows great promise for steerable needle applications because it combines strength,

Table 4.4: Comparison of candidate materials for steerable needle applications (properties from Granta EduPack 2024 R2).

Material	Young's Modulus (GPa)	Yield Strength (MPa)	Biocompatibility	Ultrasound Visibility
Nitinol (Ni-Ti)	41-75	324-472	Yes	Low (Can be enhanced with coatings or surface texturing)
Stainless Steel (AISI 301)	193-200	887-1040	Yes	High (Naturally echogenic)
Stainless Steel (AISI 302)	189-197	205-310	Yes	High (Naturally echogenic)
Titanium Alloy (Ti-6Al-4V)	110-119	786-910	Yes	Moderate (Lower than stainless steel, but sufficient for clinical use)
Tungsten Alloy (CMW 3000)	310-360	545-670	Yes	High (Naturally echogenic)

flexibility, and biocompatibility [21]. Compared to stainless steel, its lower Young's modulus provides greater flexibility while still providing sufficient rigidity for controlled steering [19]. Stainless steel tends to suffer permanent deformation under bending, while Ti-6Al-4V resists plastic deformation more effectively, making it better suited for applications that require precise bending without excessive stiffness. In addition, Grade 5 titanium offers a favorable balance between flexibility and strength. Its relatively high yield strength helps resist permanent deformation during steering, while its lower stiffness compared to stainless steel allows controlled bending [21]. Although beta titanium alloys offer even greater flexibility, their limited availability reduces their use in medical applications despite favorable mechanical properties [50]. Although its ultrasound visibility is considered moderate (see Table 4.4), Grade 5 titanium still provides sufficient echogenicity for clinical use [76]. For steerable needle designs, its flexibility, high yield strength, and biocompatibility make it a good and balanced material choice [19].

Based on these considerations and the data presented in Table 4.4, Grade 5 titanium was selected for the steerable needle prototype. Its lower stiffness compared to stainless steel enhances bendability while maintaining sufficient rigidity for controlled steering. The following section provides a detailed evaluation of how this alloy meets key requirements for sterilization, biocompatibility, and imaging.

4.3. Required Material Properties

4.3.1. Sterilization

Grade 5 titanium components are designed for compatibility with standard steam sterilization at 130 °C [5], fulfilling design Requirement 8 (see Chapter 2). Steam sterilization by autoclaving is preferred because it quickly and effectively kills pathogens without leaving chemical residues [56]. The high thermal stability and melting point of the alloy (1660 °C) ensure that repeated exposure to steam does not compromise its mechanical integrity. An additional benefit of autoclaving is the controlled thickening of the native titanium dioxide (TiO_2) surface layer. This passive film plays a critical role in preventing corrosion, improving long-term durability, and contributing to biocompatibility. The process slightly reinforces the oxide layer without affecting the surface characteristics important for clinical performance [21, 51].

4.3.2. Biocompatibility

Although no internal tests were performed in this study, the extensive literature confirms that Grade 5 titanium behaves in an inert manner within biological environments. Extensive in vitro and in vivo evaluations have demonstrated that the alloy maintains its stability without significant ion release, ensuring that any observed tissue response is primarily mechanical rather than chemical and confirming its safety for temporary biomedical use [70].

Grade 5 titanium has a long-standing history of use in medical implants approved by the Food and Drug Administration for both temporary and permanent applications, reflecting its strong clinical safety record and broad regulatory acceptance [61]. This proven track record is supported by its compliance with the biocompatibility criteria defined in requirement
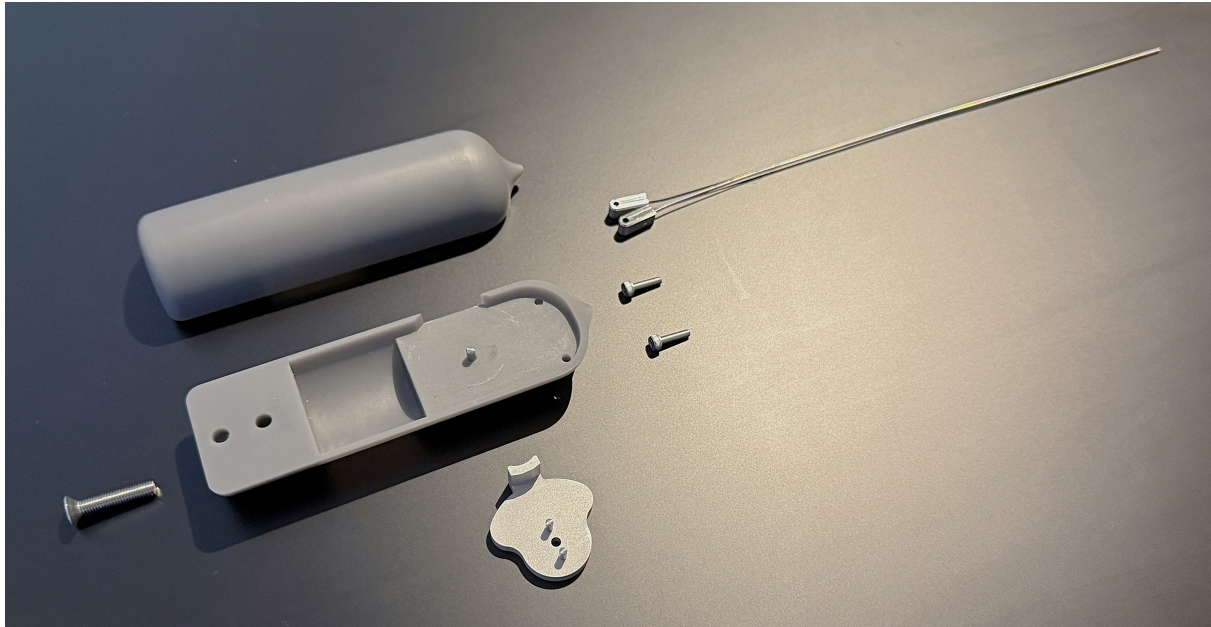
Figure 4.4: Exploded view of all the components of the steerable needle.

9, which includes adherence to international standards such as ISO 10993-5 for cytotoxicity and ISO 10993-10 for sensitization and irritation, alongside regulatory approval for clinical use (see Chapter 2) [70]. The naturally occurring titanium dioxide (TiO_2) layer on its surface, which is further enhanced by steam sterilization, effectively minimizes corrosion and limits the release of metal ions. This reduces the risk of cytotoxicity, allergic reactions, and tissue irritation during clinical procedures [8]. These biocompatibility characteristics make Grade 5 titanium a suitable choice fot the steerable brachytherapy needle.

4.3.3. Ultrasound Visibility

According to design requirement 2 (see Chapter 2), the steerable needle must be clearly visible on ultrasound imaging during brachytherapy procedures. Although in-house ultrasound tests were not performed in this study, previous research supports the suitability of Grade 5 titanium for ultrasound-guided applications.

Grade 5 titanium alloys, whether produced conventionally or through additive manufacturing, exhibit favorable acoustic properties that allow clear ultrasound imaging and effective tracking against soft tissues [34]. Titanium alloys with an oxide surface layer, similar to that naturally formed on Grade 5 titanium, have been shown to enhance the reflection of ultrasonic signals while minimizing artifacts, which is essential to preserve image clarity [41].

These studies confirm that Grade 5 titanium can produce a strong and stable ultrasound signal, offering a critical advantage over other materials such as stainless steel or nitinol, which tend to generate more acoustic distortion. As summarized in Table 4.4, Grade 5 titanium strikes a favorable balance between visibility and minimal image disruption, validating its selection to achieve reliable real-time needle guidance during brachytherapy.

4.4. Prototype Manufacturing

4.4.1. Steerable needle

Early form-finding and geometric feasibility were done by Fused Deposition Modelling (FDM) printing Polylactic Acid (PLA) models on a Creality Ender 3; see Appendix D for photos of these 3D printed prototypes. The steerable needle is manufactured using a Fanuc Robocut
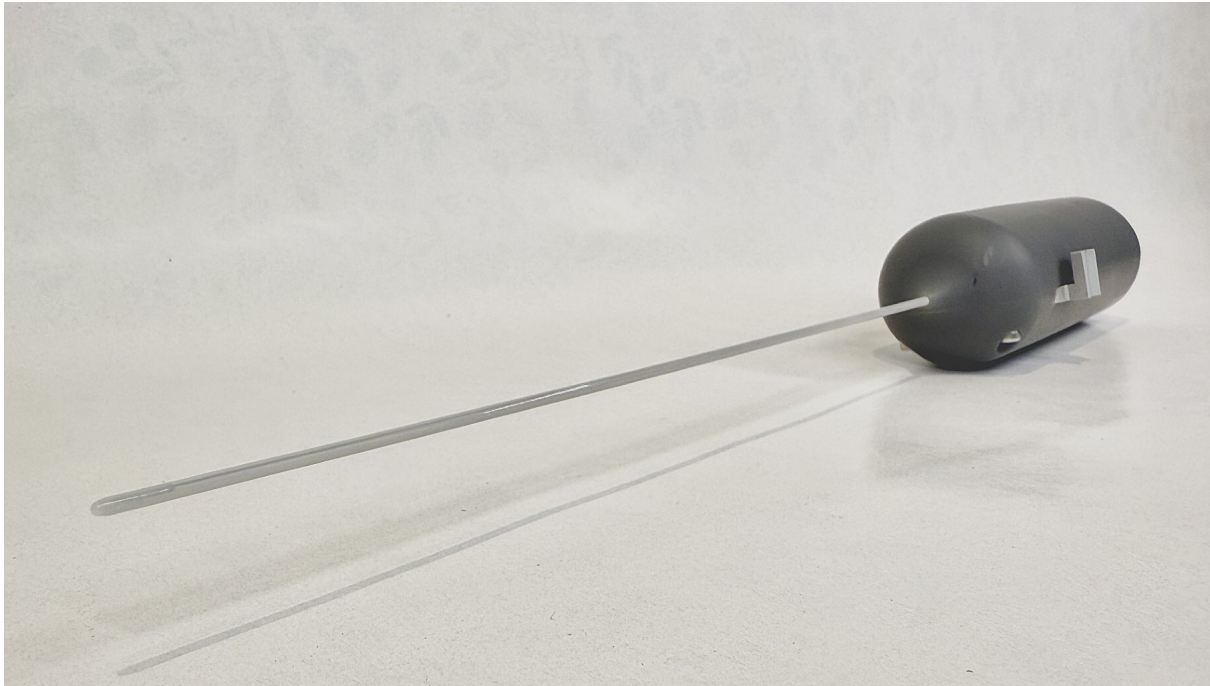
Figure 4.5: Photograph of the fully assembled steerable needle prototype, including handpiece, needle, and actuation mechanism.

160iS-WB electric discharge machine (EDM). The needle has a total length of 25.0 cm and a uniform outer diameter of 1.3 mm. During manufacturing, the needle is securely clamped in a custom-designed fixture, where it is positioned in a precisely machined slot and held in place by clamping plates. The EDM process precisely separates the shaft along its axis, extending to the distal slot of 7.22 mm, to form the compliant steering segment. In particular, the clamping plates that hold the needle are also machined by the EDM process. This precise computer-controlled process guarantees high dimensional accuracy and a clean finish, which are critical for achieving the intended mechanical properties of the needle and ensuring reliable performance under repeated bending cycles [48].

4.4.2. Handpiece

Figure 4.4 shows the components of the handpiece assembly. The handpiece is made as a two-piece structure using an stereolithography (SLA) printer (Formlabs 3L) with a build height of 0.5 mm. To ensure that all cylindrical features, such as the mounting interfaces, retain their precise shape and minimize the need for additional support structures, parts are printed orthogonally to the build plate. After printing, the components undergo post-processing, including cleaning and ultraviolet (UV) curing, to achieve a smooth finish. Then precise screw holes are drilled and tapped to secure the two parts. The final assembly includes a dedicated pin to mount the rotating wheel, a critical element to transmit the manual actuation input during testing.

4.4.3. Transmission Parts

The transmission components are machined using a Fehlmann P55 computer numerical control (CNC) machine. These parts include the rotation wheel and clamping blocks. The rotation wheel is precisely milled to convert the manual rotation input into the differential push-pull action required to steer the needle. Meanwhile, the clamping blocks are engineered with tight tolerances to securely hold the needle's split beams and ensure effective force transmission. The CNC machining process provides high

dimensional accuracy and a smooth surface finish, both of which are critical to the reliable performance of the transmission system [3].

Full assembly and part drawings for the handpiece, steerable needle, rotation disk and clamping blocks are provided in Appendix F.

4.5. Functionality Test

This section presents a preliminary functionality test to verify the operation of the steerable mechanism in an unloaded (non-phantom) setting. The assembled needle and handpiece were actuated manually using the rotation wheel to assess deflection response and consistency of curvature.

Figure 4.6: Steered configuration of the manually actuated prototype needle housed in a catheter, showing successful lateral deflection upon full actuation during bench testing.

The prototype was tested in both bare and catheter-enclosed configurations to evaluate the impact of the catheter (ProGuide 6F) on steering

behavior. In both sets of conditions, the rotation wheel produced a differential push–pull action on the two beam segments of the split-shaft design, resulting in a consistent lateral deflection of the needle tip. Figure 4.6 illustrates the needle in its steered state, confirming that the steering mechanism functions effectively and produces, as intended, a curvature at the needle tip.

The successful outcome of these tests verifies that the core steering mechanism is operational and establishes a solid foundation for subsequent experiments using tissue-mimicking phantoms.

These preliminary results confirmed the basic actuation principles, setting the stage for a detailed validation in tissue-mimicking phantom experiments, discussed in Chapter 5.

Testing and Validation

5.1. Goal of the Experiments

The primary objective of these experiments was to validate the functional performance of the steerable interstitial needle in accordance with the predefined design requirements (Chapter 2), particularly deflection capacity and targeting accuracy under simulated clinical conditions. In essence, the experiments aimed to demonstrate that the needle can achieve the precise lateral deflection and controlled curvature necessary for accurate targeting, ensuring a minimum tip deflection of 20 mm at an insertion depth of 50 mm while maintaining positional accuracy within ±5 mm.

Experiment 1 established a baseline by evaluating the steering behavior of the needle in a gelatin phantom using a template-guided insertion approach. Experiment 2 built on this by using CT imaging to capture full three-dimensional needle trajectories in a gelatin phantom, allowing for a direct comparison between the steerable needle and a conventional straight ProGuide obturator. Finally, Experiment 3 further challenged the system by testing it in a more demanding and realistic silicone phantom that includes a simulated tumor region, with various catheter configurations to explore the operational limits of the steering capability of the needle. Together, these experiments provide the quantitative evidence needed to bridge theoretical design specifications with practical in vitro performance, supporting the potential of the needle for clinical application. As a result, each experiment employs different measurement methods and evaluation metrics tailored to its specific objectives and experimental design.

5.2. Experiment 1 - Template-Guided Phantom Needle Steering

This experiment evaluates a steerable brachytherapy needle using a custom template that mimics a gynecological applicator. Two insertion procedures are compared using the same template, 10 wt% porcine gelatin phantom [49], using the same needle design paired with either a ProGuide 6F or Flexible Implant Tube 6F catheter. In the first procedure, the needle is advanced 5 cm in a linear path through the template, then steered for an additional 5 cm to achieve a total depth of 10 cm. In the second procedure, the steering is activated immediately upon insertion and the needle is continuously steered until a depth of 5 cm is reached.

5.2.1. Materials and Methods

A 10 wt% porcine gelatin phantom (Dr. Oetker) was used as a soft-tissue surrogate to replicate the mechanical behavior of cervical tissue for gynecological brachytherapy simulation. The gelatin solution was poured into a PMMA
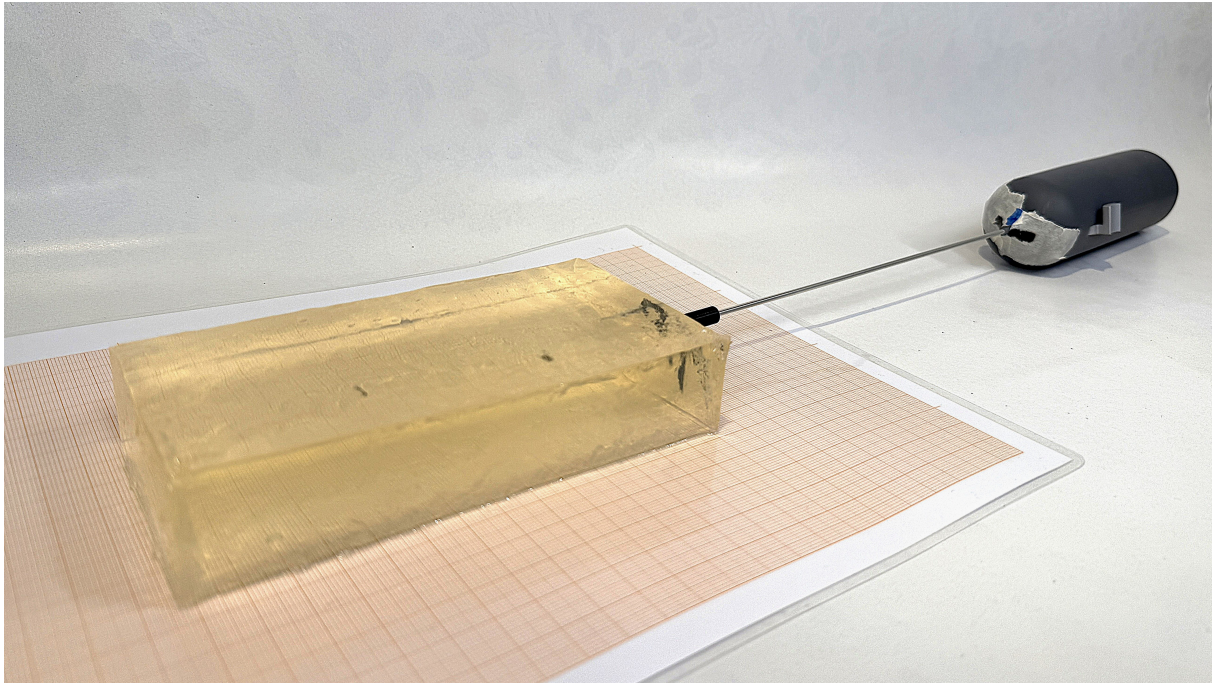
Figure 5.1: Experimental setup for Experiment 1: steerable needle inserted into a gelatin phantom.

container with internal dimensions of 270 mm x 150 mm x 90 mm, cooled and then solidified at 4 °C. Once fully set, the phantom was carefully removed and cut to dimensions of 140 mm × 70 mm × 30 mm (length × width × height). External target marks were applied at the 5 cm and 10 cm insertion depths, and a millimeter grid was placed beneath the phantom to facilitate accurate top-down visualization of the needle trajectory; see Figure 5.2. In this setup, the x-axis represents the insertion depth, the y-axis captures the lateral deflection, and variations along the z-axis (height) are not considered.

A custom template with a 2.15 mm inner diameter replicating the channel of an Elekta gynecological applicator provided initial guidance for the steerable needle. The needle, which serves as the inner component, was tested using a ProGuide 6F catheter or a Flexible Implant Tube 6F catheter. The ProGuide 6F is a clinically used semi-rigid brachytherapy catheter made of polyoxymethylene (POM), while the Flexible Implant Tube is a highly flexible guiding catheter made from polytetrafluoroethylene (PTFE), designed to offer minimal bending resistance.

Top-down photographs were taken after each insertion to document lateral needle deflection.

5.2.2. Experimental Procedure

To rigorously assess needle steering performance in an in vitro gelatin phantom, the following procedure was implemented under controlled conditions to ensure reproducibility and enable precise quantitative analysis of the needle deflection and curvature.

1. **Positioning:** the gelatin block is placed on a millimeter grid so that the grid is clearly visible for subsequent deflection measurements. The custom template is then aligned on the phantom surface to guide the needle as it enters.

2. **Needle Loading:** the steerable needle, which serves as the inner component of the selected 6F catheter, is carefully loaded to ensure that it fits properly through the template.

3. **Insertion:**

   • **Method A:** the needle is advanced 5 cm through the template without

| (a) | (b) | (c) |
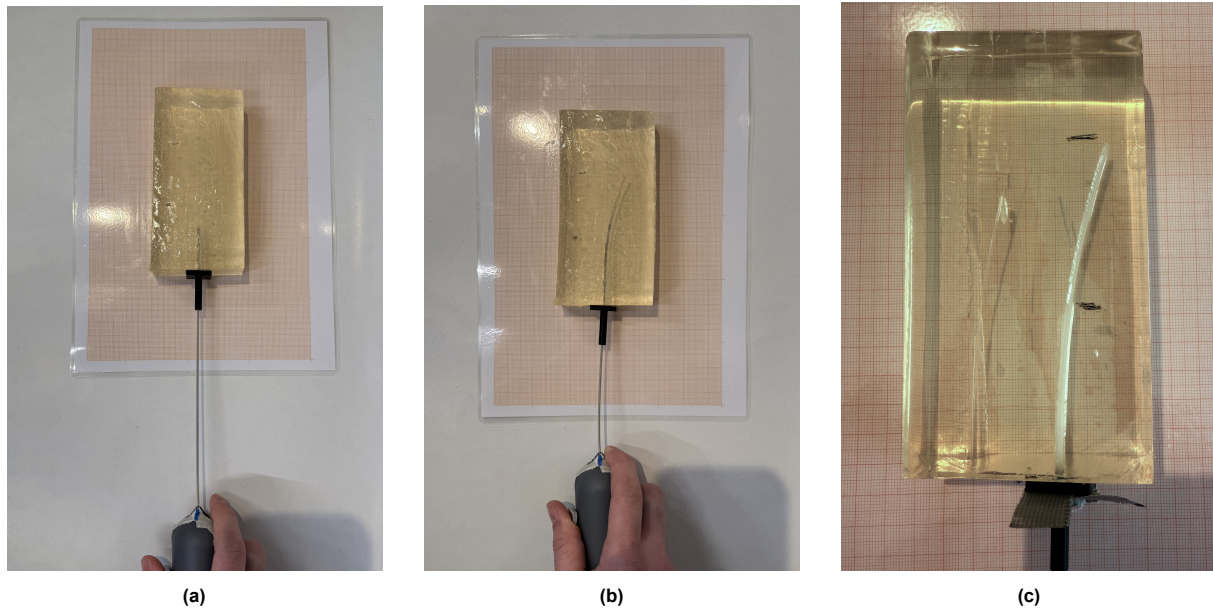
Figure 5.2: Top-down views from Experiment 1: (a) Initial needle insertion; (b) needle deflection after steering; (c) close-up of the steerable needle curvature.

activating the steering mechanism, maintaining a straight, linear path. Once the needle tip reaches a depth of 5 cm, the steering mechanism is maximally activated, and the needle is advanced an additional 5 cm, achieving a total insertion depth of 10 cm. The resulting bending is visually monitored from above.

- **Method B:** using the same template, maximum steering is activated immediately after insertion. The needle is continuously steered as it is inserted until a depth of 5 cm is reached, with the steering movement being observed in real time from above.

4. **Documentation of Deflection:** upon reaching the target depth (5 cm or 10 cm), the needle is held in place while a top-down image is taken. The millimeter grid under the phantom is clearly visible in the image to allow accurate image-based measurement of lateral deflection.

5. **Withdrawal and Cleaning:** the needle and catheter are carefully removed from the phantom. Any residual gelatin is rinsed off with water and cleaned with alcohol. The phantom is then repositioned or rotated to expose a fresh insertion site, and the process is repeated for subsequent trials.

Multiple repetitions (see Table 5.1) were performed to gather robust data on deflection and steering accuracy. All trials were completed on the same day under consistent environmental conditions.

5.2.3. Post-Processing and Analysis

The top-down photographs captured immediately after each insertion were analyzed using ImageJ. The images were first calibrated using the millimeter grid visible beneath the phantom to establish an accurate scale. Deflection measurements were then determined at the specific insertion depths (both 5 cm and 10 cm for Method A and 5 cm for Method B) by quantifying the lateral displacement of the needle tip from the expected straight trajectory. These measurements provide quantitative data on the steering performance of the needle and are used for subsequent statistical analysis.

Table 5.1: Mean (M), standard deviation (SD), and sample size (n) of lateral deflection (mm) by catheter type and insertion depth (n = 7 per group).

Catheter Type	10 cm Insertion	5 cm Insertion	Total (All Depths)
ProGuide 6F	n = 7, M = 15.30, SD = 3.24	n = 7, M = 10.91, SD = 1.87	n = 14, M = 13.10, SD = 3.42
Flexible Implant Tube 6F	n = 7, M = 26.61, SD = 3.47	n = 7, M = 18.09, SD = 1.51	n = 14, M = 22.35, SD = 5.12
Total per Depth	n = 14, M = 20.96, SD = 6.70	n = 14, M = 14.50, SD = 4.07	n = 28, M = 17.73, SD = 6.36
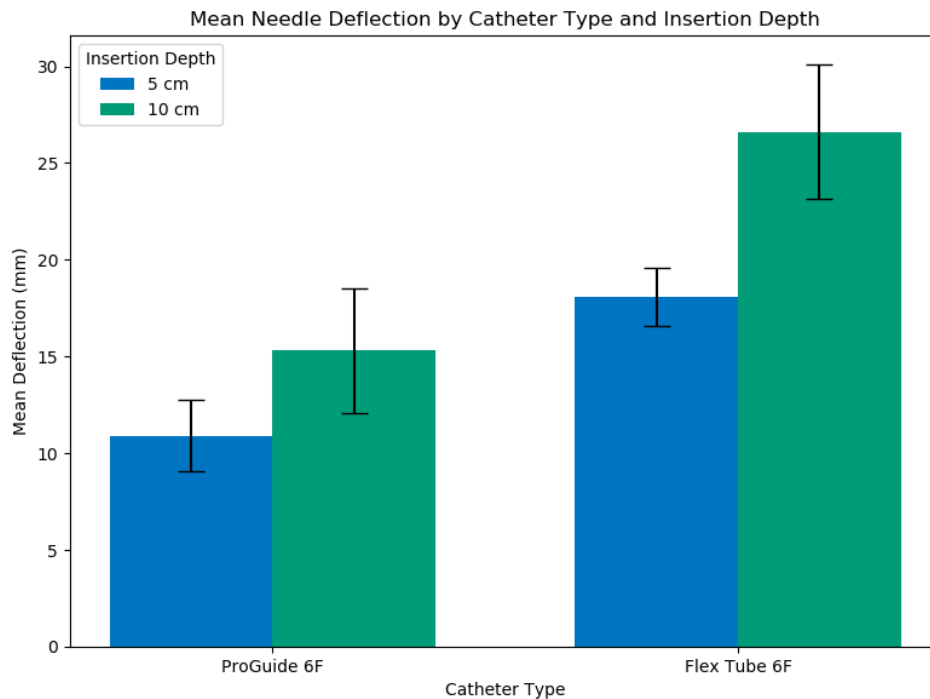
Figure 5.3: Mean needle tip deflection by catheter type and insertion depth (error bars indicate ±1 SD).

5.2.4. Experimental Results

The deflection data for each experimental condition were analyzed using IBM SPSS Statistics 29. Descriptive statistics were first calculated, followed by assumption testing and a two-way analysis of variance (ANOVA). The normality of the deflection measurements was evaluated using the Shapiro-Wilk test, as well as visual inspection of Q–Q plots and histograms. All p-values of the Shapiro-Wilk tests were above 0.05, and the Q–Q plots showed approximately linear distributions, indicating that the data were normally distributed and suitable for parametric analysis (see Appendix G for full SPSS output).

Then a two-way ANOVA was performed to examine the effects of catheter type and insertion depth on needle deflection. The two independent variables were catheter type

(ProGuide 6F versus Flexible Implant Tube 6F) and insertion depth (5 cm versus 10 cm), with seven measurements per group (n = 28 total).

As shown in Table 5.1 and Figure 5.3, the highest mean deflection was observed for the Flexible Implant Tube 6F catheter at the insertion depth of 10 cm (M = 26.61 mm), while the lowest was recorded for the ProGuide 6F catheter at 5 cm (M = 10.91 mm).

Table 5.2 presents the results of the two-way ANOVA. In addition to statistical significance, the effect sizes were reported using a partial eta squared (η^2), which quantifies the proportion of variance explained by each factor in the model. The analysis revealed a statistically significant main effect of catheter type, $F(1, 24) = 84.447$, $p < 0.001$, partial $\eta^2 = 0.779$, indicating that catheter design had a large effect on deflection. A significant main effect was also found for

insertion depth, $F(1, 24) = 41.223$, $p < 0.001$, partial $\eta^2 = 0.632$.

These results confirm that both catheter flexibility and insertion depth independently influence the amount of tip deflection.

Source	df	F	p-value	Partial η^2
Catheter Type	1, 24	84.447	< 0.001	0.779
Insertion Depth	1, 24	41.223	< 0.001	0.632
Error	24	–	–	–

Table 5.2: Two-way ANOVA results for needle tip deflection.

The model explained a substantial proportion of the variance in deflection, with $R^2 = 0.844$. This value indicates that approximately 84.4% of the variability in deflection can be attributed to the catheter type and insertion depth.

To further explore these relationships, the point-biserial Pearson correlations were calculated by coding catheter type (ProGuide 6F = 0, Flexible Implant Tube 6F = 1) and insertion depth (5 cm = 0, 10 cm = 1) as binary variables. The correlation between deflection and catheter type was strong and positive ($r \approx 0.73$, $p < 0.001$), indicating that the use of the Flexible Implant Tube 6F catheter was associated with higher deflection. The correlation between deflection and insertion depth was moderate ($r \approx 0.51$, $p = 0.005$), indicating that deeper insertions contributed to greater tip deflection.

In summary, the data indicate that catheter type and insertion depth both significantly influence needle tip deflection.

5.3. Experiment 2 – CT Evaluation of Needle Steering in a Gelatin Phantom

Unlike Experiment 1, which relied on top-down photographs to measure lateral deflection in a 2D plane, Experiment 2 utilized computed tomography (CT) imaging to capture the full 3D trajectory of the needle. This enabled a more comprehensive assessment of steering performance, including both lateral deflection and deviation in the Z-direction (Error Z).

Additionally, Experiment 2 introduced a direct comparison between the steerable needle and a conventional rigid ProGuide obturator, both inserted through a custom 3D printed template into a gelatin phantom. By using CT-based reconstruction, the experiment minimized measurement variability and provided consistent analysis of needle behavior under standardized conditions.

5.3.1. Materials and Methods

To simulate a realistic gynecological setup, a 3D-printed needle template was developed that replicates the geometry and functional layout of a standard gynecological applicator. This template featured an inner channel diameter of 2.15 mm and a length of 8 mm, consistent with the channel dimensions used in clinical applicators [16]. The template was designed with nine equally spaced holes arranged in a straight row, allowing the precise alignment of multiple insertions. Each hole served as an entry channel to ensure that all needles were inserted from a consistent starting position and orientation, thereby standardizing the trajectory plane under experimental conditions. The template was used in combination with a 10 wt% porcine gelatin phantom [49], prepared in the same way as in Experiment 1.

To maintain initial alignment and prevent any off-axis twisting, a 3D printed handpiece holder was used during the early phase of insertion. This ensured that all deflections occurred within a single, well-defined plane and that any curvature observed was the result of intentional steering rather than unintended torsion or deviation.

Imaging was performed using a Siemens SOMATOM CT scanner. After the insertions, the phantom was scanned at high resolution (1 mm) to capture the full 3D needle trajectory within the gelatin. CT scans allowed reconstruction of the lateral deflection of the needle in the XY plane and its vertical deviation along the Z axis (Error Z), which had not been measurable in the 2D analysis of Experiment 1. All insertions

(a) **(b)**
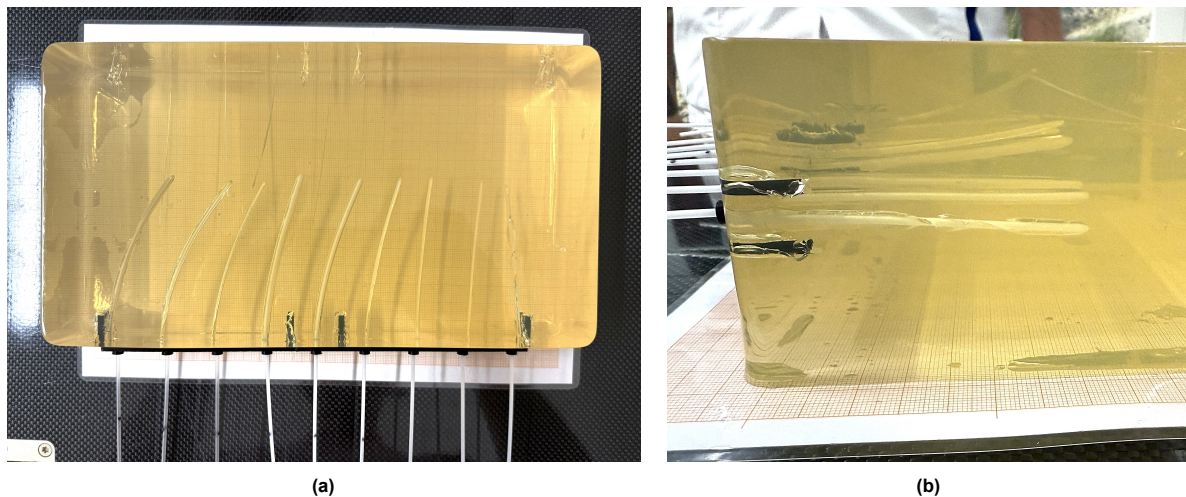
Figure 5.4: Experiment 2 setup: (a) needle insertion into gelatin phantom; (b) steerable needle deflection after actuation.

and scans were performed under consistent environmental conditions to minimize variability.

5.3.2. Experimental Procedure

The complete procedure used to evaluate the steering of the needle in 3D is outlined below.

1. **Template Setup:** the 3D-printed needle template was placed on the long side of the gelatin phantom out of the PMMA container and aligned to ensure perpendicular needle insertion. One of the nine available template holes was used for each test to ensure consistent starting geometry and avoid interference between insertions.

2. **Needle Loading and Stabilization:** the needle (either steerable or the conventional ProGuide obturator) was inserted through the selected template hole. A 3D-printed handpiece holder was used to stabilize the needle shaft during insertion.

3. **Insertion:** all needles were inserted to a depth of 8 cm. For steerable needles, the steering mechanism was maximally activated immediately after insertion. ProGuide obturators were inserted without steering.

4. **Needle Withdrawal:** the needle was carefully removed from the catheter. The catheter remained in place within the

phantom to preserve the track.

5. **CT Imaging:** the phantom was scanned using a Siemens SOMATOM CT scanner. This captured the complete three-dimensional trajectory of the needle inside the phantom.

Each needle-catheter combination (steerable-ProGuide 6F, steerable-flexible implant tube 6F, and ProGuide obturator-ProGuide 6F) was tested three times, resulting in a total of 9 insertions. All trials were performed under identical environmental conditions on the same day.

5.3.3. Post-Processing and Analysis

CT scans acquired after each insertion were imported into 3D Slicer (version 5.6.2) for post-processing and analysis. The needle trajectories were visualized in 3D and manually segmented using the built-in software tools. For each insertion, the following metrics were extracted.

- **Tip deflection:** the lateral deviation of the needle tip from the expected straight trajectory in the axial plane (x-y).

- **Error Z:** the vertical displacement of the needle tip from the original horizontal insertion plane (z-axis), used to assess out-of-plane deviation.

Table 5.3: Mean (M), Standard Deviation (SD), and Sample Size (n) of needle tip deflection and Error Z (in mm) for each experimental condition.

Needle Type	Catheter Type	n	Depth (cm)	Deflection (M $\pm$ SD)	Error Z (M $\pm$ SD)
Steerable	ProGuide 6F	3	5	12.88 ± 0.75	-0.26 ± 1.62
Steerable	ProGuide 6F	3	8	18.46 ± 3.50	1.31 ± 1.12
Steerable	Flexible Implant Tube 6F	3	5	19.00 ± 2.11	5.95 ± 1.97
Steerable	Flexible Implant Tube 6F	3	8	32.99 ± 6.16	8.86 ± 10.36
Obturator	ProGuide 6F	3	5	2.82 ± 0.49	6.50 ± 2.17
Obturator	ProGuide 6F	3	8	5.94 ± 0.71	6.50 ± 1.56
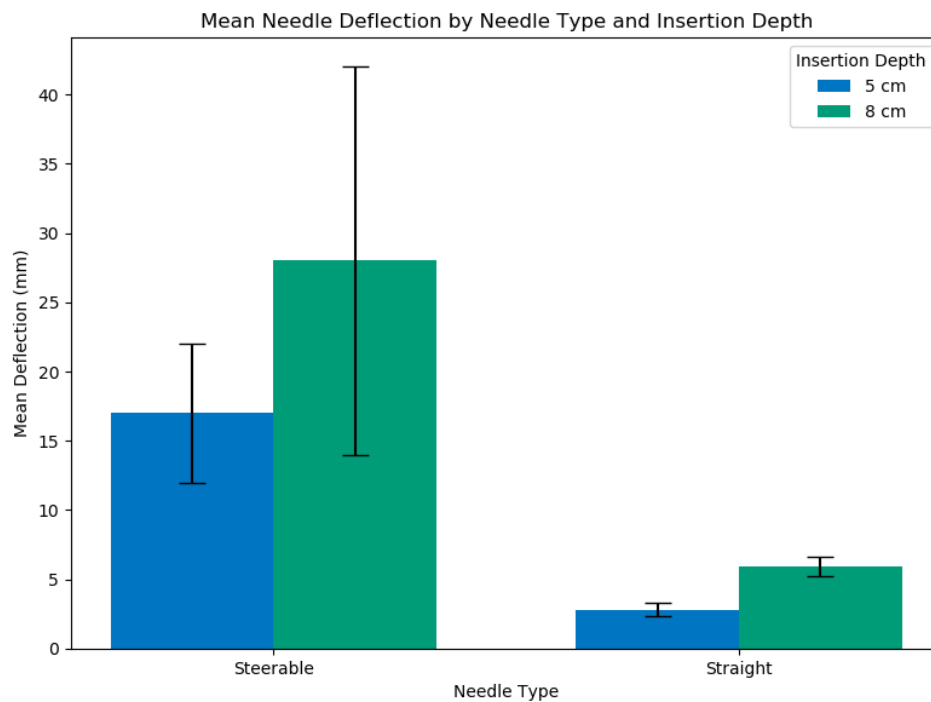
Figure 5.5: Mean needle tip deflection across experimental conditions based on CT analysis (error bars represent ±1 SD).

To maintain consistency, the starting point of each trajectory was aligned with the base of the guiding template, and the final tip position was marked manually using anatomical landmarks within the phantom. The resulting measurements were exported from Slicer and organized in a structured dataset for statistical analysis.

5.3.4. Experimental Results

CT-based needle trajectory measurements were analyzed to compare the performance of the steerable needle and the obturator in terms of tip deflection and vertical deviation (Error Z). A three-way analysis of variance (ANOVA) was performed using IBM SPSS Statistics

v29 to examine the effects of needle type (steerable versus straight obturator), catheter type (ProGuide 6F versus Flexible Implant Tube 6F), and depth of insertion (5 cm versus 8 cm) on lateral deflection. All insertions were performed to a depth of 5 cm and 8 cm, with three catheters per condition, resulting in a total of 18 insertions. The normality of the data was verified using the Shapiro-Wilk test and Q-Q plots. The full SPSS output for Experiment 2 is provided in Appendix H.

As shown in Table 5.3 and Figure 5.5, the highest mean deflection was observed for the steerable needle with the Flexible Implant Tube 6F at 8 cm insertion depth (M = 32.99 mm), while the lowest was recorded for the ProGuide

obturator at 5 cm (M = 2.82 mm). The out-of-plane deviation (Error Z) was observed in all trials and increased with insertion depth.

Table 5.4 presents the results of the three-way ANOVA. In addition to statistical significance, the effect sizes were reported using partial eta squared (η^2), which quantifies the proportion of variance explained by each factor in the model. The analysis revealed a statistically significant main effect of needle type, $F(1, 12) = 41.034$, $p < 0.001$, partial $\eta^2 = 0.774$, indicating that needle design had a large effect on the outcome. A significant main effect was also found for catheter type, $F(1, 12) = 34.295$, $p < 0.001$, partial $\eta^2 = 0.741$, as well as for insertion depth, $F(1, 12) = 28.344$, $p < 0.001$, partial $\eta^2 = 0.703$.

Table 5.4: Three-way ANOVA results for needle tip deflection based on CT analysis.

Source	df	F	*p*-value	Partial η^2
Needle Type	1, 12	41.034	< 0.001	0.774
Catheter Type	1, 12	34.295	< 0.001	0.741
Insertion Depth	1, 12	28.344	< 0.001	0.703
Error	12	–	–	–

In general, CT-based evaluation confirmed that the steerable needle achieved substantially greater lateral deflection compared to the conventional ProGuide obturator under all tested conditions. The increase in insertion depth and the use of a more flexible catheter each further enhanced deflection, supported by the significant main effects (see Table 5.4). Vertical deviations (Error Z) were generally minimal for the steerable needle used with the ProGuide 6F catheter, but increased with catheter flexibility and insertion depth. The model explained a very large proportion of the variance in deflection, with $R^2 = 0.940$, indicating that 94.0% of the variability in deflection can be attributed to the type of needle, the type of catheter, the insertion depth and their interactions. Overall, the steerable needle achieved lateral deflections approximately 10 to 27 mm greater than the conventional ProGuide obturator at both 5 cm and 8 cm insertion depths, confirming a substantial mechanical advantage under all

conditions tested.

5.4. Experiment 3 – CT Evaluation of Needle Steering in a Silicone Phantom (Pilot Study)

Based on the findings of the gelatin phantom study, Experiment 3 aimed to further evaluate the steering performance of the novel needle design under more clinically realistic conditions. A pilot study was conducted using a silicone phantom that replicates cervical tissue, including a denser tumor-like region on the left side. Initially, both a Flexible Implant Tube 6F catheter and a ProGuide 6F catheter were tested in combination with the steerable needle. However, the configuration using the Flexible Implant Tube 6F proved nearly non-functional due to its excessive flexibility, resulting in inadequate tissue penetration. Therefore, this experiment focused on comparing the performance of the steerable needle using the ProGuide 6F catheter with that of a conventional ProGuide obturator using the same catheter. CT imaging was used to reconstruct the needle trajectories in three dimensions, allowing quantification of lateral deflection and steering angle. The objective of this experiment was to demonstrate that the steerable needle design provides significant clinical advantages for cervical brachytherapy by enabling enhanced lateral targeting.

5.4.1. Materials and Methods

A custom silicone phantom was used for the experimental evaluation. This phantom was originally developed and characterized by Kanhai in her master's thesis at TU Delft [27], where it was designed to replicate the anatomical geometry and mechanical properties of cervical and surrounding pelvic tissues. The phantom includes a denser, tumor-shaped region on the left side to simulate clinically relevant challenges in needle steering, such as off-axis tumor

targeting and variation in tissue stiffness.

The phantom was cast at TU Delft's Phantom Lab and used without modifications for the current study.

To replicate clinical practice, an Elekta Venezia applicator was used to guide needle insertions. The applicator was placed against the anterior surface of the phantom, mimicking standard gynecological placement during cervical brachytherapy procedures.

The configurations tested in this experiment were as follows:

- **Steerable Needle with ProGuide 6F:** the steerable needle was inserted using a ProGuide 6F catheter.
- **ProGuide Obturator with ProGuide 6F:** a standard ProGuide obturator was inserted with a ProGuide 6F catheter.

For the ProGuide obturator configuration, flexible guide tubes were attached to the Venezia applicator in accordance with Elekta's clinical protocol. In contrast, the steerable needle did not use these tubes due to incompatibility with its reduced overall length, which made engagement impossible.

After all insertions were completed, the phantom was scanned using a Siemens SOMATOM CT scanner. Volumetric scans were acquired with a slice resolution of 1 mm to capture the complete three-dimensional needle trajectories. These CT images were used for accurate reconstruction and quantification of the following metrics: lateral tip deflection and steering angle relative to the needle shaft.

Initial testing included an additional configuration using the steerable needle in combination with the Flexible Implant Tube 6F catheter. However, these preliminary tests showed that this configuration was not feasible due to excessive flexibility of the catheter resulting in insufficient penetration of the phantom material. Therefore, this configuration was excluded from the main experiment. The two remaining configurations, steerable needle with

ProGuide 6F and standard ProGuide obturator with ProGuide 6F, were able to successfully penetrate the phantom, although both required high insertion forces.

5.4.2. Experimental Procedure and Observations

The complete procedure used to evaluate the steerable and straight needle configurations in the silicone phantom is outlined below.

1. **Applicator Preparation:** a thin layer of lubricant was applied to the Elekta Venezia applicator to minimize friction between the catheters and the phantom surface. The applicator was then aligned with the anterior surface of the silicone phantom to replicate clinical placement.

2. **Channel Selection:** only the perpendicular (non-angled) channels of the applicator were used to ensure that the needle trajectories remained within the boundaries of the phantom during insertion and to allow direct comparison against standard linear (perpendicular) insertion paths.

3. **Needle Insertion:**

   - the steerable needle with ProGuide 6F catheter was inserted through channels B and D on the left and right sides, respectively (see Appendix A).
   - the standard ProGuide obturator with ProGuide 6F catheter was inserted through channels F on both the left and right sides (see Appendix A).

   Each needle was manually inserted through its assigned channel and withdrawn before the next insertion to prevent phantom deformation and maintain consistent test conditions.

4. **CT Imaging:** after all insertions were completed, the phantom was transferred to a Siemens SOMATOM CT scanner. Volumetric scans were acquired at 1 mm slice resolution to capture the

full three-dimensional trajectories of the needles within the phantom.

5. **Trajectory Analysis:** the resulting CT data were used to reconstruct each needle trajectory and evaluate steering metrics, including lateral tip deflection and angular deviation in the XY plane.

The two experimental configurations were evaluated under identical environmental conditions on the same day.
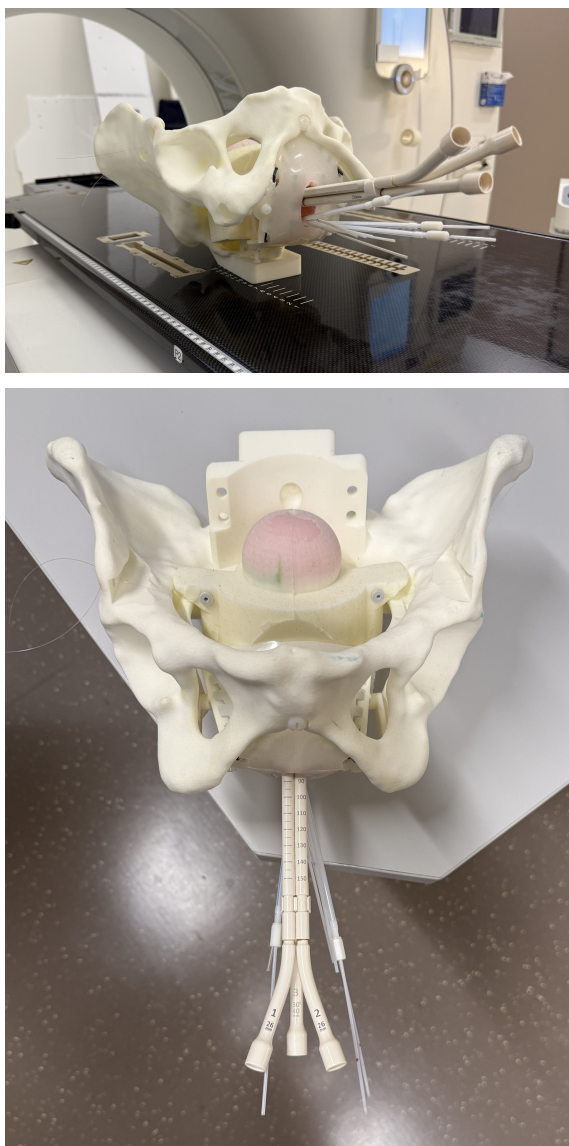
Figure 5.6: Experiment 3 setup: perspective and top view of the silicone phantom with applicator and catheters in place.

5.4.3. Post-Processing and Analysis

The CT scan data were imported into 3D Slicer (version 5.6.2) for quantitative analysis of the needle trajectories. For each needle, an ideal straight insertion path was defined by extending a line from the exit point of the applicator channel along the intended axis. The actual needle trajectory was then compared to this reference line. The maximum lateral deflection was determined as the greatest perpendicular distance between the needle trajectory and the ideal insertion axis. In addition, the steering angle was calculated by measuring the angle between the tangent of the needle trajectory at the tip and the reference insertion line. All measurements were made using the 3D Slicer's built-in ruler and angle tools. The results were summarized as mean ± standard deviation for each configuration. Figure 5.7 shows the reconstructed needle trajectories for both the steerable needle and the ProGuide obturator, along with the corresponding steering angles.

5.4.4. Experimental Results

Table 5.5 summarizes the results of the CT-based analysis of needle trajectories in the silicone phantom. The steerable needle combined with the ProGuide 6F catheter demonstrated a mean lateral deflection of 12.7 ± 2.6 mm and a mean steering angle of 14.0 ± 2.4°, based on four insertions. In contrast, the ProGuide obturator configuration achieved a much smaller mean deflection of 1.46 ± 0.06 mm and a minimal steering angle of 1.5 ± 0.02°, based on two insertions. These findings suggest that the steerable design produced substantially greater lateral deflection than the ProGuide obturator. Although formal statistical significance testing was not feasible due to the small sample size (n = 4 for the steerable needle, n = 2 for the ProGuide obturator), the magnitude of the observed difference was assessed using Cohen's d. Cohen's d is a standardized measure of the effect size that
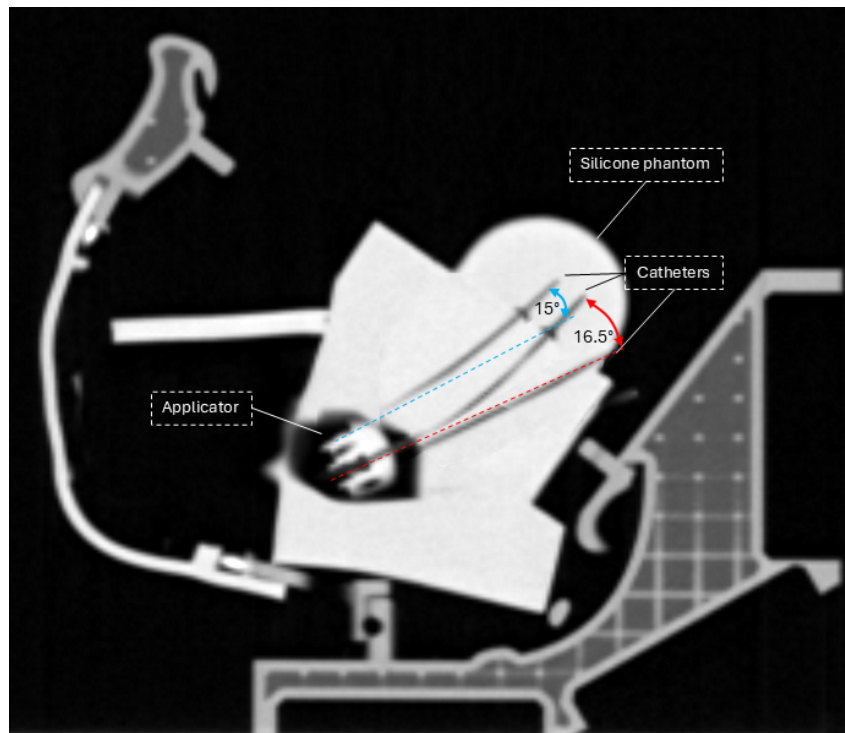
Figure 5.7: Composite sagittal CT images of the silicone phantom showing the three catheters on the left side of the applicator, with reconstructed needle trajectories. Steering angles for the steerable catheter are indicated by dashed lines and annotated with their corresponding values.

Table 5.5: Summary of insertion depth, lateral deflection, and steering angle (mean ± SD) for each needle configuration in Experiment 3.

Group	n	Mean Insertion Depth ± SD (mm)	Mean Deflection ± SD (mm)	Mean Steering Angle ± SD (°)
Steerable + ProGuide 6F	4	54.3 ± 2.5	12.7 ± 2.6	14.0 ± 2.4
ProGuide obturator + ProGuide 6F	2	54.2 ± 3.0	1.46 ± 0.06	1.5 ± 0.02

quantifies the difference between the means of two groups relative to their pooled standard deviation, with values greater than 0.8 generally interpreted as a large effect. In this study, the calculated effect size was approximately 5.05, reflecting an exceptionally large difference between the steerable needle configuration and the obturator configuration. In this pilot study, the steerable needle achieved mean lateral deflections approximately 11.2 mm greater than the straight ProGuide obturator, suggesting a potential advantage in steering performance under more clinically realistic conditions. These results suggest that the steerable needle enables meaningful steering even in higher-stiffness tissues, offering improved access to complex tumor geometries in anatomically constrained settings.

5.5. Evaluation of Design Requirements

This section systematically evaluates the degree to which the steerable needle prototype meets the predefined design requirements outlined in Chapter 2, based on the experimental results presented in Chapter 5.

5.5.1. Must-Have Requirements

1. **Maximum outer diameter of 1.35 mm**
   Achieved.
   The manufactured steerable needle has a measured outer diameter of 1.30 mm, satisfying the dimensional constraint for

compatibility with ProGuide 6F catheters (Section 3).

2. **Visibility under ultrasound imaging without significant artifacts**
Assumed achieved.

Although in-house ultrasound experiments were not performed, prior studies on Grade 5 titanium alloys confirm favorable ultrasound visibility with minimal artifacts [34, 41].

3. **Manual one-handed steering through integrated controls**
Achieved.

The handpiece design, incorporating a rotation wheel for differential actuation, enables intuitive one-handed control for both left- and right-handed users (Figure 3.4).

4. **Minimum tip deflection of 20 mm at 50 mm insertion depth**
Partially achieved.

In Experiment 1 (gelatin, 10% wt), the Flexible Implant Tube 6F configuration achieved a mean tip deflection of 18.09 mm at 5 cm insertion depth and 26.61 mm at 10 cm (Table 5.1). The ProGuide 6F configuration achieved 10.91 mm at 5 cm and 15.30 mm at 10 cm.

In Experiment 2 (CT-based gelatin evaluation), the Flexible Implant Tube 6F reached 19.00 mm at 5 cm and 32.99 mm at 8 cm, while the ProGuide 6F reached 12.88 mm at 5 cm and 18.46 mm at 8 cm (Table 5.3).

Based on extrapolated trends, the 20 mm deflection requirement was likely to be met using the Flexible Implant Tube 6F and may be nearly achieved with the ProGuide 6F catheter at comparable depths.

However, in the silicone phantom (Experiment 3), the steerable needle combined with the ProGuide 6F catheter achieved a mean lateral deflection of only 12.7 mm at approximately 54 mm insertion depth (Table 5.5), suggesting that the requirement was not yet met under higher-friction, tissue-like conditions rather than purely due to increased stiffness.

5. **Maximum positional deviation of ±5 mm in 95% of insertions**
Achieved in gelatin phantom.

Analysis of SPSS outputs (see Appendix G and Appendix H) for Experiments 1 and 2 showed that for the ProGuide 6F catheter configuration, 100% of lateral deviations remained within ±5 mm at 5 cm insertion depth, satisfying the requirement under controlled conditions. For the Flexible Implant Tube 6F catheter at greater depths, occasional deviations above 5 mm occurred, which correlates with its greater steering capability.

6. **No visible buckling or permanent deformation under clinical insertion conditions**
Achieved.

Throughout all insertions in gelatin and silicone phantoms, no visible buckling or permanent deformation of the steerable needle was observed, even under high insertion forces (Section 5).

7. **Translation, rotation, and adjustable curvature in a single plane**
Achieved.

The needle supports longitudinal translation, axial rotation of the handle, and controlled curvature adjustment through differential actuation of the split-shaft needle (Figures 3.5, 3.6).

8. **Compatibility with preferably steam sterilization at 130 °C**
Achieved.

The material Grade 5 titanium is fully compatible with steam sterilization at 130 °C, as detailed in Section 4.

9. **Biocompatibility according to ISO 10993-1 standards**
Achieved.

Grade 5 titanium is a clinically established

biocompatible material, conforming to ISO 10993-1 standards for temporary medical devices (Section 4).

5.5.2. Nice-to-Have Requirements

1. **Manufacturability according to ISO 13485 standards**
   Not evaluated.
   While the prototype was fabricated using high-precision EDM and CNC processes, no formal ISO 13485 process validation was performed, since the current project focused on functional prototyping.

2. **Visibility under MRI without compromising image quality**
   Not evaluated.
   No MRI visibility experiments were conducted within the scope of this work.

5.5.3. Preconditions

1. **Compatibility with 6F ProGuide catheters and template holes**
   Achieved.
   The steerable needle was successfully inserted through the standard 6F channels of the Elekta Venezia applicator (Section 5.4).

2. **No kinking of Flexisource HDR source at bending radii greater than 10 mm**
   Not directly evaluated. No HDR source was used during this study; however, given the measured steering angles and radii (Experiment 3, Figure 5.7), the minimum bending radii appear compatible.

6

Discussion

This chapter reviews the development, experimental validation, and clinical potential of the manually controlled steerable interstitial needle designed for gynecological brachytherapy. First, the key findings are summarized and interpreted in light of the research objectives (Chapter 1). These findings are then contextualized with reference to the relevant literature. The limitations of the study are discussed, followed by a critical analysis of its potential use and future research opportunities. The chapter concludes with a summary of the clinical relevance, identifying both benefits and remaining challenges of the proposed design.

6.1. Summary of Key Findings

The general objective of this work was **to create and experimentally test a manually controlled steerable interstitial needle that easily integrates into familiar brachytherapy applicators (such as Elekta Geneva and Venezia systems) and improves the precision of needle placement in anatomically challenging tumor regions** (Chapter 1). The experimental results presented in Chapter 5 confirm that the steerable needle met its primary functional goals under simulated clinical conditions.

The results indicate that the steerable needle of the proposed design provides larger lateral deflection compared to standard ProGuide

obturators. The gelatin phantom experiments demonstrated significantly greater tip deflections in visual 2D (Table 5.1) and CT 3D (Table 5.3) experiments. In a custom silicone phantom, the steerable needle achieved a mean steering angle of up to 14.0°, with a mean tip lateral deviation of 12.7 mm at a depth of approximately 54 mm (Table 5.5). These outcomes indicate that even in higher-friction, tissue-like environments, the needle maintains effective curvature, supporting its use in anatomically constrained cases.

This study validates the goal that differential actuation using a split-shaft compliant mechanism provides a feasible, effective, and practical method for manual real-time needle steering. These results contribute to the understanding of how manual steering can be integrated into HDR brachytherapy procedures to improve dose coverage and conformity in the treatment of complicated cervical cancer cases. Figure 6.1 illustrates how the steerable needle integrates with the Elekta Venezia applicator, maintaining compatibility with standard catheters while allowing lateral deflection through manual actuation.

Unlike ProGuide obturators that follow linear insertion paths, the steerable needle enables targeted access to off-axis or irregular tumor extensions that are otherwise difficult to reach. This makes it particularly valuable in clinical scenarios where anatomy or applicator constraints limit optimal needle positioning,
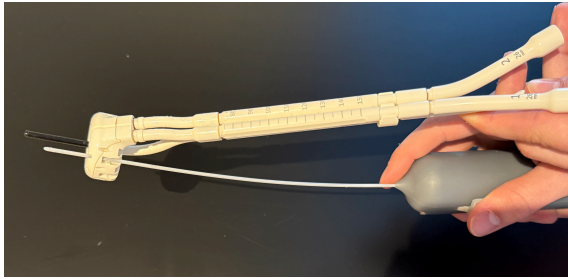
Figure 6.1: Steerable needle inserted into an Elekta Venezia applicator, demonstrating compatibility with standard clinical catheters and enabling lateral trajectory adjustment.

offering a more versatile solution within existing interstitial brachytherapy workflows.

6.2. Interpretations

The experimental data strongly support the basic design concepts of the manually controlled steerable needle, showing successful control of the trajectory in both ideal and clinically appropriate conditions. Across all experiments, the results demonstrate that active manual control of the needle trajectory via a split-shaft compliant mechanism is both feasible and effective. This distinction is especially important in the context of cervical tumors with lateral or asymmetric extension beyond the central axis [60]. Insertions with ProGuide obturators often fail to adequately reach irregular tumor regions, requiring the use of additional needles or custom applicator configurations to achieve sufficient coverage [44, 45]. The steerable design provides a flexible solution that can navigate within standard applicator channels and dynamically adjust the trajectory, potentially improving dose conformity without increasing procedural complexity.

In the gelatin phantom tests (Chapter 5), the findings verified two points of the main factors that affect steering performance: the flexibility of the outer catheter and the insertion depth. According to the goal, larger deflections were achieved when the steerable needle was coupled with the Flexible Implant Tube 6F compared to the default ProGuide 6F catheter. In particular,

the steerable needle achieved nearly double the tip deflection when paired with the more flexible catheter, approaching the design objective of 20 mm at a depth of 50 mm (Table 5.1). This finding supports the underlying design principle that reducing external constraints, such as catheter stiffness, allows the needle to achieve greater curvature.

This correlation was also directly visualized: more lateral displacement was caused by deeper insertions (Table 5.3), particularly when the steerable needle was inserted with the more flexible outer catheters. This is in line with theoretical predictions, as longer curved pathways will, by virtue of their length, result in a larger lateral deviation of the true path from the straight path.

Furthermore, a comparison of the steerable needle and the ProGuide obturator revealed that with standard ProGuide 6F catheters, the steerable needle was able to achieve considerable lateral displacement, while the ProGuide obturator remained nearly linear. This indicates that mechanical actuation created by the use of a compliant design produces a qualitatively distinct insertion characteristic compared to rigid needles, a finding of particular significance for its proposed clinical use.

Out-of-plane movement, measured in experiments using 3D CT, indicated that the needle generally retained its target planar steering, in particular when restrained by a stiff catheter like the ProGuide 6F. Minor vertical (Z-axis) displacements under steering using a Flexible Implant Tube 6F indicate that increased flexibility causes a minor loss of directional stability. However, these out-of-plane deviations were relatively small compared to lateral deflections and are consistent with previously reported behavior in steerable needle systems [39]. Measured tip deflections showed low variability, with standard deviations between 1.2 and 2.5 mm across all experimental conditions, demonstrating reproducible performance of the steering

mechanism.

The pilot study in a silicone tissue phantom (Section 5.4) served as a valuable reality check for needle steering in a more clinically representative environment. The steerable needle once again outperformed the ProGuide obturator, registering mean steering angles of approximately 14° and mean tip displacements of approximately 12.7 mm (Table 5.5). However, the magnitude of deflection was lower than in the gelatin experiments.Although this reduction might initially suggest that increased phantom stiffness was responsible, it is more likely attributable to higher insertional friction between the needle and the silicone material during insertion. This frictional resistance limited the achievable curvature, a finding that aligns with existing models of needle–tissue interaction where friction is a dominant factor in steering performance [39, 71].

Taken together, these interpretations indicate that while catheter stiffness and insertion depth are tunable parameters in the control of steering performance, the clinical utility of the steerable needle will depend on finding an optimal balance in the trade-off between steerability and mechanical stability [40, 71]. The results also demonstrate that controlled deflection is achievable with a manually actuated device that operates through existing applicators, consistent with initial design goals and extended findings from previous needle steering research [60, 67].

6.3. Implications

This research has a number of implications regarding the development and clinical translation of steerable needle technology, especially in the context of brachytherapy in the presence of complex tumor anatomy.

First, the effective deployment of a manually driven, split-shaft compliant mechanism demonstrates that high levels of steering are possible without the necessity of robot assistance. This contradicts the idea, expressed

in the prior literature on steerable needles [53, 71], that active steering inherently needs to utilize advanced mechatronic systems. In contrast, the findings demonstrate the clinical viability of compact, manually controlled systems, aligning with established priorities for simplicity and usability in HDR brachytherapy [60].

Secondly, this work expands knowledge beyond prior studies by showing that significant controlled deflections are possible even when using conventional clinical applicators, which are compatible with standard clinical catheters such as the ProGuide 6F (Appendix B). Compliant needle designs introduced in earlier work [72, 73], typically required custom or specialized outer sheaths. In contrast, the current design is compatible with existing catheter/applicator systems, reducing the need for additional components.

The results of the finite element analysis also support previous theoretical work on the critical role of slot geometry in achieving flexibility and durability in compliant designs [73]. By demonstrating that certain ratios of slot size to edge thickness must exist to prevent material failure but also allow adequate deflection (see Section 4.1.2 and 4.1.2), the present study supports these design principles and provides practical evidence for their use in the context of medical devices.

From a material point of view, Grade 5 titanium (Section 4) meets the accepted requirements for biocompatibility, sterilizability, and imaging compatibility, as documented in previous reports [21, 34]. This shows that material selection, while critical, can be effectively managed to achieve clinically applicable steerable devices.

Significantly, showing steering capabilities not only in homogeneous gelatin phantoms but also in a silicone phantom that mimics basic heterogeneity through the inclusion of a stiffer tumor-like region (Section 5.4), this work addresses a general weakness of previous studies [39]. It demonstrates that manually actuated steerable needles can maintain

functionality under more realistic and clinically relevant conditions, a step toward future clinical translation.

In general, this work presents new evidence that steerable needle systems can combine flexibility, robustness, and usability in a manual system, which holds a potential solution to improve the precision and effectiveness of brachytherapy treatment procedures. These results present both the practical implications for the design and the clinical potential of incorporating steerable technology into current treatment procedures.

6.4. Limitations

Although the findings of this study demonstrate the potential of the design of manually actuated steerable needles, several limitations must be acknowledged regarding experimental methods, prototype fabrication, and generalizability of the results.

The measurement process posed inherent uncertainties. In Experiment 1, lateral deflections were manually quantified using millimeter grids and ImageJ analysis, which introduced errors through limited spatial resolution and manual point selection. Furthermore, the 3D printed template used did not fully replicate the frictional and mechanical properties of the clinical (Elekta) applicators, which could affect the dynamics of needle insertion.

Manufacturing imperfections caused deviations from the ideal prototype design. During EDM machining, the needle developed a slight rotational twist (approximately 10–20°) relative to the intended curvature plane, leading to minor steering inaccuracies. This unintended twist could also have contributed to the out-of-plane deviations (error Z) observed during the experiments. Although the needle was designed for purely planar steering, some vertical displacement occurred, particularly at deeper insertions and when used with flexible catheter configurations. Although

these out-of-plane deviations were relatively small compared to lateral tip offsets, they highlight a limitation in precisely controlling the three-dimensional path of the needle and emphasize the sensitivity of steering behavior to fabrication tolerances. Furthermore, the differences between the physical prototype and simulation models, particularly the use of a 250 mm Grade 5 titanium shaft instead of a 294 mm AISI 301 stainless steel model, restrict the direct correlation between the predicted and experimental results, although both materials have comparable mechanical properties.

The experimental variability was also influenced by manual actuation. Differences in applied torque and tactile feedback among insertions introduced variability in the achieved curvature. Furthermore, some ProGuide 6F catheters had pre-existing curvature from prior use, possibly biasing the results. In Experiment 3, the shorter needle length prevented the use of flexible guiding tubes with the Elekta Venezia applicator, leading to a modified insertion method that bypassed the flexible guiding tubes typically used to constrain the initial trajectory. In the same experiment, the Flexible Implant Tube 6F configuration, although beneficial in maximizing deflection in soft gelatin, excessive flexibility compromised pushability and prevented successful advancement in denser media. This real-world constraint clarifies the practical trade-off between flexibility (to enable steering) and stiffness (to maintain penetration capability), which informs future design optimization efforts.

The sample sizes in Experiment 2 and 3 were limited, especially in Experiment 3, where only a small number of insertions were performed. This restriction constrained the statistical power and robustness of the conclusions, despite reporting effect size metrics to characterize observed differences. Additionally, repeated use during testing led to minor deformation near the proximal end of the needle, as shown in Figure 6.2. This deformation was likely caused

by localized stress concentrations near the rotation wheel and may have subtly influenced steering performance during later insertions.
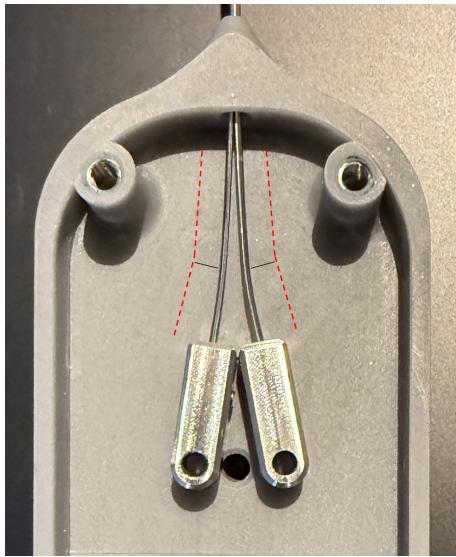
Figure 6.2: Minor bending observed at the proximal ends of the steerable needle after repeated use during testing, likely caused by localized stress near the rotation wheel.

The scope of imaging evaluation also presents a limitation. Although material selection was guided by the literature that demonstrated favorable ultrasound properties for Grade 5 titanium, no direct evaluations of imaging performance were performed under ultrasound or magnetic resonance guidance. As a result, potential imaging artifacts and the effectiveness of real-time needle tracking remain to be established in future studies under clinical imaging protocols.

Finally, the clinical applicability of the findings remains limited by the use of simplified phantom models. Although the silicone phantom included a region with increased stiffness to simulate a tumor, it does not fully replicate the viscoelastic behavior, perfusion, and anisotropic properties of living tissues. Moreover, additional clinical factors such as patient movement, dynamic tissue deformation, and anatomical variability could further influence the behavior of the steerable needle. However, the results of this study demonstrate the fundamental feasibility of the proposed design and identify key areas for

further optimization and clinical validation.

Despite these limitations, the study convincingly demonstrates the fundamental feasibility of the steerable needle design.

6.5. Future Recommendations

Building on the promising results of this study, several clear directions are proposed to accelerate the clinical translation of the manually actuated steerable needle.

Primarily, further refinement of the ergonomics of the handpiece and actuation mechanism is necessary. Mechanical coupling between the rotation wheel and actuator shaft could be improved to allow for more precise and intuitive steering with reduced proximal deformation. Future iterations should explore the integration of geared systems or mechanisms that offer mechanical advantage mechanisms to enhance force transmission while minimizing operator effort, ultimately increasing steering fidelity during clinical use.

In addition, a systematic exploration of the geometry parameters of the slot is essential to fully optimize needle performance. Varying slot length, width, and edge thickness would allow fine-tuning of the flexibility-to-strength balance, providing a robust design framework adaptable to different tissue environments and clinical requirements. Such a parametric study would directly support the customization of steerable needle designs for specific anatomical challenges.

Catheter compatibility is another critical area of advancement. Although Flexible Implant Tubes 6F improved deflection in soft tissue models, they had limited pushability in stiffer environments. This was not solely due to the increased stiffness of the phantom but also due to the elevated friction between the catheter and the surrounding material during insertion. In contrast, the standard ProGuide 6F catheter offers a better balance of flexibility and axial rigidity. This enables effective steering while maintaining

sufficient stiffness and reduced surface friction for smoother tissue penetration. Future work should focus on developing customized outer sheaths that optimize this balance further by combining moderate flexibility with enhanced pushability and low-friction characteristics to maximize steerability and procedural reliability in clinical settings.

Validation must extend beyond homogeneous phantoms. Testing in anatomically detailed, mechanically heterogeneous phantoms that simulate vascular structures, fibrotic tissues, and organ boundaries would better approximate clinical conditions. Following successful mechanical optimization, preclinical in vivo studies and early phase clinical trials should be conducted to evaluate the performance of the system under dynamic physiological conditions, including tissue perfusion and patient movement.

In addition, integration of real-time imaging and navigation is a critical next step. An explicit evaluation of the visibility of the steerable needle should be performed under live ultrasound, CT, or MRI guidance. Incorporating real-time imaging feedback could facilitate the development of image-guided manual steering protocols, further enhancing accuracy and safety during interventions.

Given the manual nature of actuation, future studies should also systematically assess operator variability and learning curves. Investigating steering performance among clinicians with varying levels of experience would inform refinements in device design and training protocols, ensuring reproducible results and facilitating clinical adoption.

Finally, dosimetric studies are essential to quantify the therapeutic impact of steerable technology. Simulations comparing dose distributions achieved with steerable versus straight needles should be conducted, with a focus on improvements in HR-CTV coverage and saving organs at risk. Demonstrating dosimetric advantages would provide compelling evidence to support clinical integration of the

steerable needle into standard brachytherapy workflows [44, 69].

6.6. Clinical Relevance

This study demonstrates that manually actuated steerable needles directly address a critical clinical challenge in interstitial brachytherapy: enabling accurate, targeted needle placement in anatomically complex or asymmetrical tumor regions that conventional linear instruments cannot effectively reach. By allowing active trajectory control while maintaining compatibility with standard brachytherapy procedures, the developed steerable needle addresses limitations associated with rigid ProGuide obturator insertions, particularly in targeting lateral tumor extensions while minimizing trauma to surrounding healthy tissues.

The compatibility of the prototype with existing brachytherapy catheter systems, such as the ProGuide 6F, ensures that the technology could be incorporated into current HDR brachytherapy procedures without requiring significant workflow changes or additional expensive equipment. Furthermore, the steerable needle offers significant added value when used with applicator systems that feature only linear, non-angled channels, such as the Elekta Geneva applicator. In these cases, the ability to actively steer the needle provides critical flexibility for reaching off-axis tumor regions that would otherwise be difficult or impossible to access through fixed geometries.

Lateral deflections of 10–15 mm in realistic phantom models suggest a meaningful expansion of the reachable high-risk clinical target volume (HR-CTV), potentially reducing the number of needles needed to achieve adequate dose conformity and improving dosimetric efficiency. Although the achieved deflections were slightly lower than the original 20 mm design target, they still represent a clinically significant improvement over conventional straight ProGuide obturator insertions performed

with standard catheters such as the ProGuide 6F. This has important clinical implications: it may improve HR-CTV coverage, reduce the number of interstitial needles required, and minimize the overall treatment burden for patients, particularly when used in rigid applicator systems such as Elekta Geneva.

In addition, the intuitive manual actuation mechanism maintains procedural familiarity and provides direct tactile feedback, allowing clinicians to retain full control over needle navigation without relying on complex robotic systems or requiring extensive retraining. Should future studies confirm improvements in dose delivery and clinical feasibility, manually steerable needles can improve the safety and effectiveness of brachytherapy for cervical cancer and other malignancies requiring precise interstitial placement.

Overall, the steerable needle addresses a key limitation in current interstitial brachytherapy by enabling accurate navigation to anatomically challenging tumor sites using standard applicator systems. The steerable needle may enable clinicians to more accurately target the tumor while requiring fewer needle insertions, thereby making the treatment more effective, less painful for the patient, and potentially safer overall.

7

Conclusion

This chapter presents the final conclusions based on the main findings, limitations, implications, and clinical relevance of the developed steerable needle system.

This study aimed to design, fabricate, and validate a manually actuated steerable interstitial needle that integrates seamlessly with standard brachytherapy applicators and enhances needle placement precision in anatomically complex tumor regions. A novel split-shaft compliant mechanism was designed and successfully demonstrated, maintaining compatibility with standard ProGuide 6F catheters.

The steerable needle consistently achieved significantly greater lateral deflection compared to the conventional ProGuide obturator in both gelatin and silicone phantom models. In gelatin phantoms, the combination of a steerable needle with a Flexible Implant Tube 6F yielded deflections approaching 20 millimeters, while pairing with the stiffer ProGuide 6F catheter produced deflections between 11 and 13 millimeters. In a stiffer silicone phantom, mean steering angles of approximately 14 degrees and lateral tip deviations of more than 12 millimeters were achieved.

These findings confirm that catheter stiffness and insertion depth are critical parameters that influence steering performance. The steerable needle offers particular added value for brachytherapy applicators with only linear, non-angled holes, such as the Elekta Geneva system, by enabling internal trajectory adjustment without requiring angled applicators.

Despite some limitations related to manual input variability and prototype constraints, the steerable needle demonstrated intuitive, reliable operation without buckling or permanent deformation. This work presents a promising design concept that merits further study for clinical implementation of cervical HDR brachytherapy.

With further optimization and clinical validation, this technology has the potential to transform cervical interstitial brachytherapy into a more precise, adaptable, and patient-tailored intervention.

References

[1] Marc Arbyn et al. "Estimates of incidence and mortality of cervical cancer in 2018: a worldwide analysis". In: *The Lancet Global Health* 8.2 (Feb. 2020), e191–e203. ISSN: 2214109X. DOI: `10.1016/S2214-109X(19)30482-6`.

[2] Micheal F.. Ashby. *Materials selection in mechanical design.* Butterworth-Heinemann, 1992, p. 502. ISBN: 0750643579.

[3] Temitayo M Azeez et al. "Measurement of Surface Roughness on a Transmission Shaft using CNC and Conventional Lathes Machining". In: *INTERNATIONAL JOURNAL OF SCIENTIFIC & TECHNOLOGY RESEARCH* 8.10 (2019). ISSN: 2277-8616. URL: `www.ijstr.org`.

[4] Azo Materials. *Stainless Steel - Grade 302 (UNS S30200)*. Feb. 2013.

[5] Andrea Bagno and Carlo Di Bello. "Surface treatments and roughness properties of Ti-based biomaterials". In: *JOURNAL OF MATERIALS SCIENCE: MATERIALS IN MEDICINE* 15 (2004).

[6] Nick J. van de Berg et al. "Steerable needles for radio-frequency ablation in cirrhotic livers". In: *Scientific Reports* 11.1 (Dec. 2021). ISSN: 20452322. DOI: `10.1038/s41598-020-77869-3`.

[7] Joanna Deaton Bertram et al. *Tutorial: Nitinol and Tungsten Tendon Attachment Techniques for Steerable Continuum Robots*. 2025. DOI: `10.1007/s41745-024-00455-3`.

[8] Patrizia Bocchetta et al. *Passive layers and corrosion resistance of biomedical ti-6al-4v and β-ti alloys*. May 2021. DOI: `10.3390/coatings11050487`.

[9] F X Bosch et al. *The causal relation between human papillomavirus and cervical cancer*. Tech. rep. 2002, pp. 244–265. URL: `http://www.ipvsoc.org`.

[10] Cleveland Clinic. *Cervical cancer*. 2024. URL: `https://my.clevelandclinic.org/health/diseases/12216-cervical-cancer`.

[11] D. Jinghong Yu et al. *FRICTION CONTROLLED BALL JOINT*. June 2014.

[12] M De Vries. "Steerable needles in prostate brachytherapy From sketch to MDR-compliant batch". In: (2023). DOI: `10.4233/uuid:93dee070-5e4b-42b1-97e4-c598bcf27084`. URL: `https://doi.org/10.4233/uuid:93dee070-5e4b-42b1-`.

[13] Nancy J. Deaton et al. "Towards Steering a High-Dose Rate Brachytherapy Needle With a Robotic Steerable Stylet". In: *IEEE Transactions on Medical Robotics and Bionics* 5.1 (Feb. 2023), pp. 54–65. ISSN: 25763202. DOI: `10.1109/TMRB.2023.3237861`.

[14] Yuzhou Duan et al. *A Survey of Needle Steering Approaches in Minimally Invasive Surgery*. June 2024. DOI: `10.1007/s10439-024-03494-0`.

[15] T Duerig, A Pelton, and D Stö. *An overview of nitinol medical applications*. Tech. rep. 1999, pp. 149–160. URL: `www.elsevier.com/locate/msea`.

[16] Elekta. *Advanced Gynecological Applicator Instructions for Use for: 3905TH*. VEENENDAAL, 2019. URL: `www.elekta.com`.

[17] Elekta. *Applicator Guide Brachytherapy Applicator Guide 2020 Brachytherapy Applicator and Accessory Guide 2017*. Tech. rep. 2020.

[18] Elekta. *Venezia advanced gynecological applicator*. 2025. URL: `https://www.elekta.com/products/brachytherapy/venezia/`.

[19] Elias C.N. et al. "Biomedical applications of titanium and its alloys". In: *Biological Materials Science* 60 (Mar. 2008), pp. 46–49. URL: `www.tms.org/jom.html`.

[20] Enrico Franco and Alejandro Donaire. "Energy shaping nonlinear control of underactuated needle insertion". In: *Control Engineering Practice* 128 (Nov. 2022). ISSN: 09670661. DOI: `10.1016/j.conengprac.2022.105326`.

[21] M. Geetha et al. *Ti based biomaterials, the ultimate choice for orthopaedic implants - A review*. May 2009. DOI: `10.1016/j.pmatsci.2008.06.004`.

[22] Christina Gruell et al. "Development of a sterile Interaction Device during Image guided minimal-invasive Interventions". In: *Proceedings of the Annual International Conference of the IEEE Engineering in Medicine and Biology Society, EMBS*. Vol. 2022-July. Institute of Electrical and Electronics Engineers Inc., 2022, pp. 2506–2509. ISBN: 9781728127828. DOI: `10.1109/EMBC48229.2022.9871053`.

[23] Jon Hansen et al. "Comparison of catheter reconstruction techniques for the lunar ovoid channels of the VeneziaTM applicator". In: *Journal of Contemporary Brachytherapy* 12.4 (2020), pp. 383–392. ISSN: 20812841. DOI: `10.5114/jcb.2020.98119`.

[24] Antti Järvenpää, L. Pentti Karjalainen, and Matias Jaskari. "Effect of grain size on fatigue behavior of Type 301LN stainless steel". In: *International Journal of Fatigue* 65 (2014), pp. 93–98. ISSN: 01421123. DOI: `10.1016/j.ijfatigue.2013.05.012`.

[25] Zorana Jeli. "Analysis of a Four-Bar Linkage Mechanism in Its Classical and Compliant Form - A Comparison". In: 2023, pp. 80–95. DOI: `10.2991/978-94-6463-152-4{\_}10`.

[26] Yuji Kamio et al. "The Montreal split ring applicator: Towards highly adaptive gynecological brachytherapy using 3D-printed biocompatible patient-specific interstitial caps". In: *Journal of Contemporary Brachytherapy* 15.6 (2023), pp. 453–464. ISSN: 20812841. DOI: `10.5114/jcb.2023.133676`.

[27] Kanhai S.D.S. "Design of a Detailed Female Pelvis Model for Gynaecological Brachytherapy Applications". PhD thesis. Delft: University of Technology Delft, 2025. URL: `https://resolver.tudelft.nl/uuid:7f2726cf-b8f8-4e38-ae14-5f4b434b2c0a`.

[28] Øyvind Karlsen and Hirpa G. Lemu. "On Modelling Techniques for Mechanical Joints: Literature Study". In: *Lecture Notes in Electrical Engineering*. Vol. 634 LNEE. Springer, 2020, pp. 116–125. ISBN: 9789811523403. DOI: `10.1007/978-981-15-2341-0{\_}15`.

[29] Rohith Karthikeyan, Shivanand Pattanshetti, and Seok Chang Ryu. "Miniature Robotic Tubes with Rotational Tip-Joints as a Medical Delivery Platform". In: *International Conference on Robotics and Automation (ICRA)*. Montreal, 2019. ISBN: 9781538660270.

[30] Mohsen Khadem et al. "Introducing notched flexible needles with increased deflection curvature in soft tissue". In: *IEEE/ASME International Conference on Advanced Intelligent Mechatronics, AIM*. Vol. 2016-September. Institute of Electrical

and Electronics Engineers Inc., Sept. 2016, pp. 1186–1191. ISBN: 9781509020652. DOI: `10.1109/AIM.2016.7576931`.

[31] Young-Ho Kim and Tommaso Mansi. "Shape-adaptive Hysteresis Compensation for Tendon-driven Continuum Manipulators". In: (Sept. 2021). URL: `http://arxiv.org/abs/2109.06907`.

[32] Seong Young Ko and Ferdinando Rodriguez Y Baena. "Toward a miniaturized needle steering system with path planning for obstacle avoidance". In: *IEEE Transactions on Biomedical Engineering* 60.4 (2013), pp. 910–917. ISSN: 00189294. DOI: `10.1109/TBME.2012.2227741`.

[33] Bardia Konh, Naresh V. Datla, and Parsaoran Hutapea. "Feasibility of Shape Memory Alloy Wire Actuation for an Active Steerable Cannula". In: *Journal of Medical Devices, Transactions of the ASME* 9.2 (June 2015). ISSN: 1932619X. DOI: `10.1115/1.4029557`.

[34] Jakub Kowalczyk et al. "Acoustic Properties Comparison of Ti6Al4V Produced by Conventional Method and AM Technology in the Aspect of Ultrasonic Structural Health Monitoring of Adhesive Joints". In: *Applied Sciences (Switzerland)* 13.1 (Jan. 2023). ISSN: 20763417. DOI: `10.3390/app13010371`.

[35] Larry L. Howell. *Compliant Mechanisms*. 1st ed. Wiley, 2002.

[36] Changle Li et al. "A compliant actuator for steering the needle within tissue with feedback of FBG-based shape sensing". In: *Sensors and Actuators A: Physical* 356 (June 2023). ISSN: 09244247. DOI: `10.1016/j.sna.2023.114340`.

[37] Bin Liu et al. *A Review of Nano/Micro/Milli Needles Fabrications for Biomedical Engineering*. Dec. 2022. DOI: `10.1186/s10033-022-00773-6`.

[38] Theodosia Lourdes Thomas et al. *Surgical Applications of Compliant Mechanisms: A Review*. Apr. 2021. DOI: `10.1115/1.4049491`.

[39] M. Abayazid, M. Kemp, and S. Misra. "3D flexible needle steering in soft-tissue phantoms using Fiber Bragg Grating sensors". In: *3D flexible needle steering in soft-tissue phantoms using Fiber Bragg Grating sensors*. Karlsruhe: IEEE, 2013, pp. 5843–5849. ISBN: 9781467356435.

[40] Mohsen Mahvash and Pierre E. Dupont. "Mechanics of dynamic needle insertion into a biological material". In: *IEEE Transactions on Biomedical Engineering* 57.4 (2010), pp. 934–943. ISSN: 00189294. DOI: `10.1109/TBME.2009.2036856`.

[41] Balbina Makurat-Kasprolewicz et al. "Effect of ultrasound on the physicochemical, mechanical and adhesive properties of micro-arc oxidized coatings on Ti13Nb13Zr bio-alloy". In: *Scientific Reports* 14.1 (Dec. 2024). ISSN: 20452322. DOI: `10.1038/s41598-024-75626-4`.

[42] Malka Ronit et al. *Principles of Microscale Flexure Hinge Design for Enhanced Endurance*. IEEE, 2014. ISBN: 9781479969340.

[43] Ruby Mishra. "Mechanisms of flexible four-bar linkages: A brief review". In: *Materials Today: Proceedings*. Vol. 47. Elsevier Ltd, 2021, pp. 5570–5574. DOI: `10.1016/j.matpr.2021.03.457`.

[44] Khadiga E. Mohammed et al. "Dosimetric comparison of high-dose rate cervix brachytherapy with and without interstitial needles and the impact on target volume coverage, and organ at risk constraints". In: *Journal of Medical Imaging and*

Radiation Oncology 66.5 (Aug. 2022), pp. 671–677. ISSN: 17549485. DOI: `10.1111/754-9485.13371`.

[45] Ankur Mourya, Lalit Aggarwal, and Sunil Choudhary. *Evolution of brachytherapy applicators for the treatment of cervical cancer*. Oct. 2021.

[46] T. W. Mukarati, R. J. Mostert, and C. W. Siyasiya. "Development of a mathematical equation describing the strain hardening behaviour of metastable AISI 301 austenitic stainless steel". In: *IOP Conference Series: Materials Science and Engineering*. Vol. 655. 1. Institute of Physics Publishing, Nov. 2019. DOI: `10.1088/1757-899X/655/1/012008`.

[47] Kristin M. Myers et al. "The mechanical role of the cervix in pregnancy". In: *Journal of Biomechanics* 48.9 (June 2015), pp. 1511–1523. ISSN: 18732380. DOI: `10.1016/j.jbiomech.2015.02.065`.

[48] Muhammad Abdun Nafi and Muhammad Pervej Jahan. *Functional Surface Generation by EDM—A Review*. Jan. 2023. DOI: `10.3390/mi14010115`.

[49] Khashayar Nattagh et al. "A training phantom for ultrasound-guided needle insertion and suturing". In: *Brachytherapy* 13.4 (2014), pp. 413–419. ISSN: 18731449. DOI: `10.1016/j.brachy.2014.01.003`.

[50] Mitsuo Niinomi. *Recent research and development in titanium alloys for biomedical applications and healthcare goods*. Sept. 2003. DOI: `10.1016/j.stam.2003.09.002`.

[51] N. T.C. Oliveira and A. C. Guastaldi. "Electrochemical stability and corrosion resistance of Ti-Mo alloys for biomedical applications". In: *Acta Biomaterialia* 5.1 (2009), pp. 399–405. ISSN: 17427061. DOI: `10.1016/j.actbio.2008.07.010`.

[52] Blayton Padasdao and Bardia Konh. "A mechanics-based model for a tendon-driven active needle navigating inside a multiple-layer tissue". In: *Journal of Robotic Surgery* 18.1 (Dec. 2024). ISSN: 18632491. DOI: `10.1007/s11701-024-01900-2`.

[53] Sachin Patil and Ron Alterovitz. "Interactive Motion Planning for Steerable Needles in 3D Environments with Obstacles". In: *IEEE RAS EMBS Int Conf Biomed Robot Biomechatron*. Jan. 2012. DOI: `10.1109/BIOROB`.

[54] Alan R. Pelton, Scott M. Russell, and John DiCello. "The physical metallurgy of Nitinol for medical applications". In: *JOM* 55.5 (2003), pp. 33–37. ISSN: 10474838. DOI: `10.1007/s11837-003-0243-3`.

[55] S. W. Robertson, A. R. Pelton, and R. O. Ritchie. *Mechanical fatigue and fracture of Nitinol*. 2012. DOI: `10.1179/1743280411Y.0000000009`.

[56] William A. Rutala and David J. Weber. "Disinfection and sterilization: An overview". In: *American Journal of Infection Control* 41.5 SUPPL. (May 2013). ISSN: 01966553. DOI: `10.1016/j.ajic.2012.11.005`.

[57] J. Ryhanen et al. "Biocompatibility of nickel-titanium shape memory metal and its corrosion behavior in human cell cultures". In: *Journal of Biomedical Materials Research* 35.4 (June 1997), pp. 451–457. ISSN: 0021-9304.

[58] Dieter Stoeckel, Alan Pelton, and Tom Duerig. "Self-expanding Nitinol stents: Material and design considerations". In: *European Radiology* 14.2 (Feb. 2004), pp. 292–301. ISSN: 09387994. DOI: `10.1007/s00330-003-2022-5`.

[59] Hyuna Sung et al. "Global Cancer Statistics 2020: GLOBOCAN Estimates of Incidence and Mortality Worldwide for

36 Cancers in 185 Countries". In: *CA: A Cancer Journal for Clinicians* 71.3 (May 2021), pp. 209–249. ISSN: 0007-9235. DOI: `10.3322/caac.21660`.

[60] Kari Tanderup et al. *Curative radiation therapy for locally advanced cervical cancer: Brachytherapy is NOT optional*. Mar. 2014. DOI: `10.1016/j.ijrobp.2013.11.011`.

[61] U.S. Department of Health and Human Services Food and Drug Administration. *Use of International Standard ISO 10993-1, "Biological evaluation of medical devices-Part 1: Evaluation and testing within a risk management process"*. Tech. rep. Center for Devices, Radiological Health Center for Biologics Evaluation, and Research, Sept. 2023. URL: `https://www.fda.gov/vaccines-blood-biologics/guidance-compliance-regulatory-information-`.

[62] Mayu Uka et al. "Magnetic Resonance Imaging Guidance for Percutaneous Needle Intervention". In: *Interventional Radiology* (Nov. 2023). DOI: `10.22575/interventionalradiology.2023-0033`.

[63] Ulbrich. *Evaluating 301 Stainless Steel Strip for Spring Applications*. Oct. 2023.

[64] V. Zhao et al. *Nitinol Based Flexible Smart Needle Design*. IEEE, 2015. ISBN: 9781479983605.

[65] Akila N. Viswanathan and Beth A. Erickson. "Three-Dimensional Imaging in Gynecologic Brachytherapy: A Survey of the American Brachytherapy Society". In: *International Journal of Radiation Oncology Biology Physics* 76.1 (Jan. 2010), pp. 104–109. ISSN: 03603016. DOI: `10.1016/j.ijrobp.2009.01.043`.

[66] Akila N. Viswanathan and Bruce Thomadsen. "American Brachytherapy Society consensus guidelines for locally advanced carcinoma of the cervix. Part I: General principles". In: *Brachytherapy* 11.1 (Jan. 2012), pp. 33–46. ISSN: 15384721. DOI: `10.1016/j.brachy.2011.07.003`.

[67] Akila N. Viswanathan et al. "American Brachytherapy Society consensus guidelines for locally advanced carcinoma of the cervix. Part II: High-dose-rate brachytherapy". In: *Brachytherapy* 11.1 (Jan. 2012), pp. 47–52. ISSN: 15384721. DOI: `10.1016/j.brachy.2011.07.002`.

[68] M. de Vries et al. "Axially rigid steerable needle with compliant active tip control". In: *PLoS ONE* 16.12 December (Dec. 2021). ISSN: 19326203. DOI: `10.1371/journal.pone.0261089`.

[69] M. de Vries et al. "Dosimetric benefits and preclinical performance of steerable needles in HDR prostate brachytherapy". In: *Medical Engineering and Physics* 128 (June 2024). ISSN: 18734030. DOI: `10.1016/j.medengphy.2024.104177`.

[70] Ngoc Bich Vu et al. "In vitro and in vivo biocompatibility of Ti-6Al-4V titanium alloy and UHMWPE polymer for total hip replacement". In: *Biomedical Research and Therapy* 3.3 (Feb. 2016). DOI: `10.7603/s40730-016-0014-8`.

[71] Robert J. Webster et al. "Nonholonomic modeling of needle steering". In: *International Journal of Robotics Research*. Vol. 25. 5-6. May 2006, pp. 509–525. DOI: `10.1177/0278364906065388`.

[72] Atsushi Yamada et al. *Bending and extending mechanism based on elastic arm available for endoscopes and needles Active Sheath Mechanism based on Closed Elastica for Endoscope and Steerable Needle*. Japanese. Tech. rep. 2017. URL: `www.DeepL.com/pro`.

[73] Atsushi Yamada et al. "Design and Implementation of Loop Shaped Steering Mechanisms for Flexible

Needles". In: *IFMBE Proceedings*. Vol. 69. Springer Verlag, 2020, pp. 15–19. ISBN: 9789811358586.

[74] Wuxin Yang et al. "Structural optimisation for controlled deflections of additively manufactured single material beams". In: *Scientific Reports* 13.1 (Dec. 2023). ISSN: 20452322. DOI: `10.1038/s41598-023-33946-x`.

[75] Zhiyong Yang et al. "Verification of needle guidance accuracy in pelvic phantom using registered ultrasound and MRI images for intracavitary/interstitial gynecologic brachytherapy". In: *Journal of Contemporary Brachytherapy* 12.2 (2020), pp. 147–159. ISSN: 20812841. DOI: `10.5114/jcb.2020.94583`.

[76] Juhao Zhang et al. "Grain size characterization of Ti-6Al-4V titanium alloy based on laser ultrasonic random forest regression". In: *Applied Optics* 62.3 (Jan. 2023), p. 735. ISSN: 1559-128X. DOI: `10.1364/ao.479323`.

[77] Miaomiao Zhang et al. "Changes of uterocervical angle and cervical length in early and mid-pregnancy and their value in predicting spontaneous preterm birth". In: *Frontiers in Physiology* 15 (2024). ISSN: 1664042X. DOI: `10.3389/fphys.2024.1304513`.

A
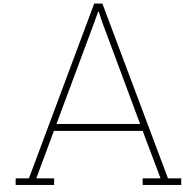
Elekta Geneva and Elekta Venezia gynaecological brachytherapy applicators

The Elekta Geneva and Elekta Venezia applicators are advanced systems designed to deliver precision and flexibility in gynecological brachytherapy procedures. Both applicators are recognized for their adaptability in accommodating various treatment strategies, including intracavitary and interstitial approaches. Their compatibility with imaging modalities such as ultrasound, CT, and MRI makes them integral to modern brachytherapy. However, their integration with steerable needles requires detailed understanding of their specifications and functional requirements. This section provides an in-depth look at the technical aspects of these applicators, along with the requirements they impose on and receive from steerable needle systems. The specifications and descriptions provided in this appendix are based on the official manuals of the Elekta Geneva and Elekta Venezia brachytherapy applicators [16, 17].

Specifications of Elekta Geneva

The Elekta Geneva applicator is designed to provide modularity and precision, catering to diverse patient anatomies and tumor geometries. Its specifications include:

- **Configurations**: Modular configurations for intracavitary-only, interstitial-only, or hybrid setups.
- **Materials**: Constructed from biocompatible materials, primarily stainless steel and medical-grade plastics.
- **Needle Compatibility**: Supports standard 6F (2 mm outer diameter) interstitial needles.
- **Guidance Template**: Includes a needle guidance template ensuring precise alignment and trajectory for interstitial needles.
- **Imaging Compatibility**: Seamless integration with ultrasound, CT, and MRI for precise visualization of the tumor and surrounding anatomy.
- **Sterilization**: Withstands steam sterilization at 134°C.
- **Curvature Limitation**: Optimized for straight or minimally curved needle paths, which can limit flexibility for complex geometries.

Specifications of Elekta Venezia

The Elekta Venezia applicator is designed for advanced and complex gynecological cases, particularly those involving irregular or extended tumor geometries. Its key specifications are as follows:

- **Configurations**: Hybrid treatment approach integrating intracavitary and interstitial therapies.
- **Materials**: High-strength, medical-grade plastics and metals that are biocompatible and sterilizable.
- **Needle Compatibility**: Accommodates standard 6F needles.
- **Guidance Template**: Enhanced needle guidance template for steeper insertion angles compared to Geneva.
- **Imaging Compatibility**: Fully compatible with ultrasound, CT, and MRI imaging modalities.
- **Sterilization**: Supports steam sterilization and gamma irradiation.
- **Curvature Flexibility**: Improved flexibility for curved trajectories, though primarily favors linear paths.

Specifications Comparison Table

Applicator type → Feature ↓	Elekta Geneva	Elekta Venezia
Configurations	Intracavitary, interstitial, or hybrid	Hybrid with greater flexibility
Materials	Stainless steel, medical-grade plastics	High-strength biocompatible materials
Needle Diameter	Standard 6F (2 mm outer diameter)	Standard 6F (2 mm outer diameter)
Guidance Template	Straight or minimally curved trajectories	Steeper angles and improved flexibility
Imaging Compatibility	Ultrasound, CT, MRI	Ultrasound, CT, MRI
Sterilization	Steam sterilization (134°C)	Steam sterilization, gamma irradiation
Curvature Flexibility	Minimal curvature support	Moderate curvature support

Table A.1: Comparison of Elekta Geneva and Venezia Specifications with Emphasized Features

Integration Requirements for Steerable Needles

The integration of steerable needles with the Elekta Geneva and Venezia applicators requires attention to several critical factors. Both applicators impose certain specifications that the steerable needle must meet to function effectively within their systems.

- **Diameter Compatibility**: The steerable needle must not exceed 1.35 mm to ensure compatibility with the applicators' 6F needle guides.
- **Curvature Tolerance**: The curvature must remain within a bending radius of 10 mm to avoid damage or misalignment.
- **Material Selection**: The needle must be biocompatible and sterilizable, capable of withstanding repeated cycles of high-temperature steam sterilization or gamma irradiation.
- **Imaging Visibility**: The steerable needle must be highly visible under ultrasound imaging, which is the primary modality used during insertion and alignment. Compatibility with CT and MRI is beneficial but secondary.
- **Positional Accuracy**: The needle must achieve positional accuracy of to align with the applicators' needle guidance templates and ensure precise targeting.

Applicator Adaptations for Steerable Needles

While the steerable needle must conform to the requirements of the applicators, certain adaptations in the applicators themselves can enhance integration and performance.

- **Low-Friction Channels**: The Geneva and Venezia applicators should include low-friction channels or templates to facilitate smooth navigation of steerable needles.
- **Insertion Angle Flexibility**: Enhanced flexibility in insertion angles can complement the steerable needle's ability to navigate complex trajectories.
- **Imaging Markers**: Applicators should integrate fiducials or markers for improved alignment and visibility under ultrasound or MRI.
- **Stability Mechanisms**: Stability and locking mechanisms are essential to hold the steerable needle in position once it reaches the desired trajectory, preventing drift or deviation.
- **Mechanical Robustness**: Applicators must withstand forces exerted by the needle's steering mechanism, particularly during penetration of dense or fibrous tissues.

By addressing these requirements, the integration of steerable needles with Elekta Geneva and Venezia applicators can significantly improve precision and adaptability in gynecological brachytherapy procedures.

Channel Layout and Numbering in Elekta Venezia Applicator

To support reproducibility and facilitate understanding of needle placement strategies, it is important to visualize the layout and channel numbering of the Elekta Venezia applicator. The applicator includes a ring or ovoid structure with multiple catheter insertion channels that are clearly numbered to assist in precise positioning during brachytherapy procedures.
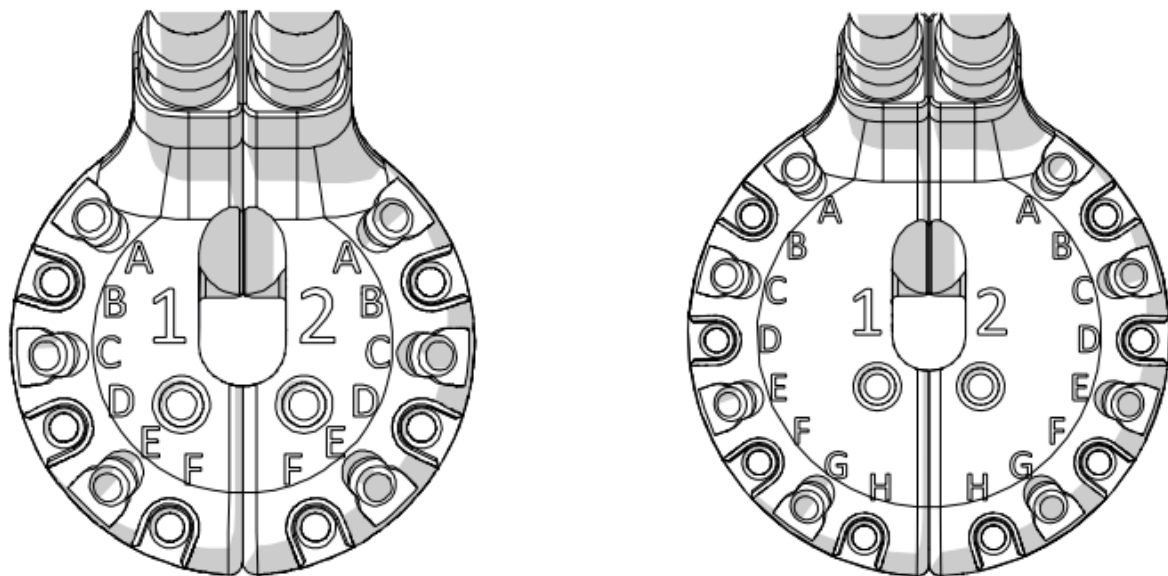
Figure A.1: Top-down view of the Elekta Venezia ring showing the channel layout and numbering system.

The numbered channels are symmetrically arranged and provide fixed paths for inserting interstitial needles. Channels labeled A through F are commonly used, with central channels typically reserved for intracavitary components and peripheral channels used for interstitial needle insertion. Angled slots
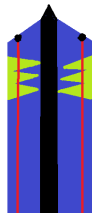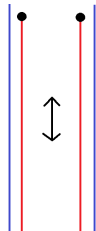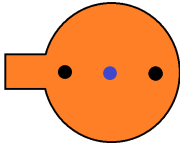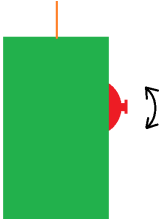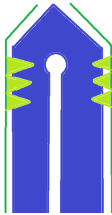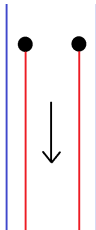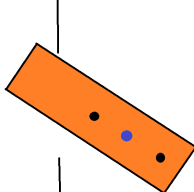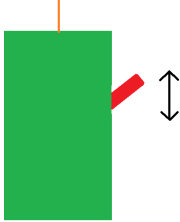
(like channels A and B) allow for steeper insertion trajectories, enabling access to tumor regions that lie lateral or posterior to the applicator.
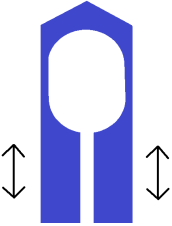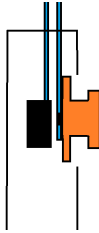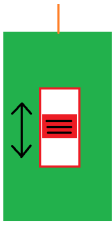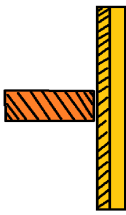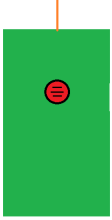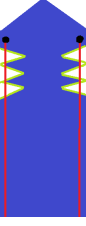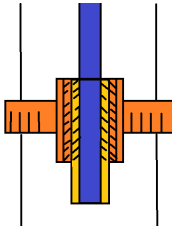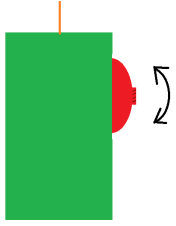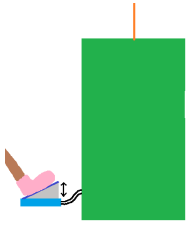
Understanding this layout is essential when integrating steerable needles, as it determines the available working space, insertion angles, and potential steering directions within the clinical geometry.

B

Idea Generation

B.1. Concept development divided in subfunctions

Subfunctions →	1) Convert reciprocating motion into a rotating motion	2) Transfer input from user to steering mechanism	3) Convert input into translation	4) Transfer input from user to steering mechanism
Solutions ↓				
1.	Stylet Design	Tendons	Rotating disk	Joystick
2.	Compliant mechanism with inner and outer needle	Pull wires	Lever transmission	Lever

3.	Ball joint	Compliant mechanism	Slider fixed to needle	Slider
4.	Cylinder joint		Rack and pinion	Push button
5.	Slots cutout		Rotation wheel with screw	Rotation wheel
6.	Multiple segments			Foot pedal
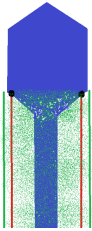
7.	Compliant mechanism with inner and outer needle
8.	Compliant mechanism (active sheet)

Table B.1: Overview of subfunctions and their corresponding solutions

C
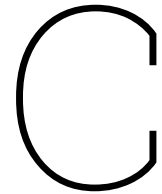
Steering Mechanisms

C.1. Steering Mechanisms

Steering a brachytherapy needle through complex and sensitive regions often demands precise control in a very slender form factor. The subsections below explore four different ways to achieve this steerability: an active sheet approach that uses a deformable strip to introduce curvature under tensile or compressive loading; a ball joint system that creates miniature pivot points for multidirectional angling; a hinge-based arrangement that provides discrete rotation at designated segments; and a compliant mechanism that leverages elastic bending in a single-piece design. Each approach comes with its own advantages and disadvantages, which will be discussed in the following sections

C.1.1. Ball Joint

A ball joint mechanism can be adapted to achieve steerability in needles for HDR brachytherapy, even when the overall outer diameter must remain as small as approximately 1.3–1.35 mm [68]. In this design, one or more miniature spherical joints are placed near the distal tip, creating localized regions where multi-axis rotation is possible. Each joint consists of a small ball nested within a closely matching socket, enabling smooth pivoting when force is transmitted from the proximal handle through a system of slender rods or cables. By carefully pulling or pushing these rods, the distal tip can be angled to traverse curved paths or circumvent anatomical obstacles, allowing fine adjustments at any point during insertion.

Despite its potential to offer a broad range of articulation in a confined space, the ball joint approach raises several engineering challenges. The fabrication of a spherical interface at such a small scale demands tight dimensional tolerances. Any excess clearance may cause the tip to wobble, while an overly tight fit heightens friction and can result in intermittent "stick-slip" movement. Moreover, machining ball-and-socket pairs down to a diameter suitable for a 1.3–1.35 mm needle imposes stringent constraints on material selection and manufacturing methods. Ensuring that the distal segment remains sufficiently rigid for insertion while still allowing free rotation at the joint is similarly complex. In addition, the actuation rods must be routed through or alongside the shaft without dramatically enlarging the overall profile. Even slight friction between these rods and the interior channel can undermine steering precision. Low-friction coatings or polished interfaces can mitigate such issues, although these treatments must remain biocompatible and retain their properties under sterilization conditions [11].

Another point of consideration is how to lock the joint once the desired orientation is achieved. A tension-based clamp near the proximal handle usually suffices to hold the rods in place, thereby fixing the ball's orientation within its socket. However, an overly strong lock may complicate readjustments during the procedure, while an insufficiently secure lock risks unintended drift. Keeping the locking mechanism compact enough to avoid increasing the needle's diameter presents an additional challenge, particularly when multiple ball joints or multiple degrees of freedom are desired [13]. Nevertheless, when appropriately engineered, ball joint mechanisms have been shown to deliver substantial flexibility with minimal bulk. Adapting such designs to the extremely tight geometric constraints required for HDR brachytherapy needles has the potential to reduce multiple insertions and enhance clinical accuracy. By addressing issues of friction control, joint tolerance, and robust locking, a miniaturized ball joint design can facilitate responsive, multi-axis steering within a remarkably small needle footprint.

C.1.2. Classic Hinge

A hinge-based steering mechanism can provide a simple yet effective way to incorporate lateral deflection in an applicator that must remain extremely slender (approximately 1.3–1.35 mm in diameter). In this approach, the needle is segmented into one or more rigid sections joined by a pivot or hinge at the distal end, creating a discrete bending point where the tip can rotate off-axis. A small control linkage, wire, or rod extending from the proximal handle to the hinge enables the operator to induce bending in a controlled manner.

When the hinge is actuated, the distal segment pivots relative to the proximal shaft. A single hinge may be sufficient for minor angular adjustments, whereas multiple hinges, each capable of limited rotation, can be placed in series to achieve a more pronounced overall deflection. Designing these joints at sub-millimeter scale requires careful consideration of several factors [42]. The pivot interface—whether a true pin joint, a living hinge (machined or molded from a single piece of material), or a micro-scale clevis arrangement, must balance robustness and flexibility. A perfectly rigid pivot could risk fracture under repeated loads, while an overly compliant hinge could lead to undesired wobble during insertion. Liu et al. (2021) have shown that using biocompatible alloys or high-strength polymers for such micro-hinges can help maintain sufficient stiffness for tissue penetration while still allowing reliable angular deflection at the joint [37].

Actuating the hinge typically involves routing a narrow rod or cable along or through the main shaft [29]. When tension is applied, the hinged segment rotates to a preset angle or follows a continuous range of motion, depending on the mechanism's geometry. Careful routing is essential to avoid excessive friction, especially given the needle's small internal diameter. Lubricants or low-friction coatings may be used, but must remain compatible with sterilization and not degrade the limited workspace inside the shaft. If friction is not well managed, even a slight mismatch in tolerances can lead to "stick-slip" behavior or require overly large forces to pivot the hinge.

Another challenge lies in ensuring a reliable way to lock the hinge at the desired angle once actuation is complete. A simple tension clamp at the proximal end can suffice for single-hinge designs, holding the control rod in a fixed position so the distal segment remains deflected. Multiple hinges, however, may demand a more sophisticated locking strategy in which each hinge can be individually or collectively secured. Such locks must be small enough to fit within the handle or shaft assembly without increasing overall diameter, yet robust enough to prevent unintended movement during the procedure.

Each additional hinge or pivot introduces potential stress concentrations and points of failure, necessitating iterative testing under simulated insertion forces. Ryu and Nelson (2008) observed that even minor misalignments can significantly increase stress near the joint when pushing the

needle through dense tissue. Material choices—from stainless steel alloys to superelastic nitinol—can help counteract potential buckling or fatigue around these joints, but must be weighed against manufacturability at this miniature scale [42].

Despite these complexities, hinge-based steering remains attractive due to its straightforward mechanical principles. Unlike continuous bending solutions that distribute deformation along the entire shaft, discrete pivots concentrate motion in a well-defined zone. This can simplify modeling and control of the deflection, as well as the manufacturing process, provided the hinges are machined or assembled with sufficient precision. When designed and executed properly, a hinge mechanism offers responsive tip steering within a needle profile that remains suitable for minimally invasive procedures, thereby reducing the need for multiple insertions and improving access to difficult-to-reach areas.

C.1.3. Groove-Based Hinge

A groove-based hinge mechanism offers an alternative method for achieving steerability in brachytherapy needles by incorporating grooves or cut-outs into the needle shaft [12]. In this design, the needle is carefully machined with precise grooves along its length, creating predefined flexion points that facilitate controlled bending when actuated by pull wires. These grooves serve as localized hinges, allowing the distal tip to bend smoothly in response to tension applied through the pull wires. The pull wires are routed alongside the needle and anchored at specific locations, enabling the operator to induce curvature by manually translating the wires from the proximal handle.

When a pull wire is actuated, it generates a differential force that causes the grooved section to flex, steering the needle tip in the desired direction. This method allows for smooth and continuous bending without the need for discrete mechanical joints, maintaining a consistent outer profile that minimizes tissue drag during insertion. The depth, width, and spacing of the grooves are critical parameters that determine the flexibility and range of motion of the needle. Properly engineered grooves ensure precise and repeatable bending behavior, enabling clinicians to navigate complex anatomical pathways with enhanced accuracy.

One significant advantage of the groove-based hinge mechanism is its simplicity and compactness. By eliminating the need for separate mechanical joints, the needle retains a slim profile essential for minimally invasive procedures. Additionally, the absence of discrete moving parts reduces potential points of failure and simplifies the manufacturing process. However, this design also presents challenges. The grooves must be meticulously engineered to ensure consistent bending without compromising the structural integrity of the needle. Excessive grooving can weaken the shaft, increasing the risk of buckling or fracture during insertion [12]. Moreover, the actuation of pull wires requires precise control to achieve smooth and predictable deflection, avoiding abrupt or uneven bends that could lead to tissue damage or misplacement of the radioactive source [43].

Another consideration is the integration of the pull wires within the needle shaft. The routing must be carefully planned to prevent interference with the needle's primary function of delivering the radioactive source. Low-friction coatings or lubricated channels can help minimize resistance and ensure that the pull wires operate efficiently. Additionally, the mechanism for locking the needle's position after bending must be reliable to maintain the desired trajectory during treatment. This often involves tension locks or friction-based clamps that secure the pull wires once the needle is positioned correctly.

Despite these challenges, groove-based hinge mechanisms hold promise for enhancing the steerability of brachytherapy needles. By enabling controlled and repeatable bending in a compact form factor, this approach can improve the accuracy of radioactive source placement and reduce the need for multiple insertions. Future research and development will focus on optimizing groove designs, materials, and

actuation methods to fully realize the potential of this steering strategy in clinical applications [36, 14].

C.1.4. Compliant Mechanism

Compliant mechanisms rely on the elastic deformation of carefully shaped elements rather than using conventional hinges, ball joints, or sliding interfaces to achieve the desired motion [38]. By leveraging localized regions that bend, twist, or flex, a single-piece or monolithic structure can be fabricated to incorporate directional steering without introducing separate mechanical joints. This approach is especially appealing when designing a needle with a maximum diameter of 1.35 mm, as conventional pivots or joints can be challenging to manufacture and may increase overall size.

In a compliant mechanism, the steerable portion of the needle might consist of thin beams or notched flexures arranged in such a way that, when a tensile or compressive force is applied from the proximal end, the distal tip deflects [30]. The geometry of these flexures determines the range of motion and stiffness characteristics. By adjusting beam thickness, width, and length, designers can tailor how much the tip will bend under a given load. A key advantage of this approach is that the structure can often be machined or laser-cut from a single piece of biocompatible material such as nitinol or a specialized stainless steel alloy, eliminating the need for multiple joints or fasteners [54].

One specific type of compliant mechanism is the active sheet. In this design, a thin, deformable strip of material (e.g., superelastic nitinol) is integrated within or alongside the needle shaft [72]. When tension or compression is applied at the needle's proximal end, the distal tip bends in a controlled arc, allowing the operator to adjust the needle's trajectory in real-time. The active sheet mechanism offers a streamlined approach to steerability, as it eliminates the need for multiple joints while still providing precise directional control.

However, ensuring consistent and predictable behavior at such a small scale requires meticulous attention to design parameters. Because the steering motion depends on elastic bending, even minor variations in cross-sectional dimensions or material properties can alter the bending profile. Howell (2001) notes that finite element analysis is frequently employed to evaluate stress distribution and deflection angles in compliant devices, and this method also helps identify potential stress concentrators that could lead to fatigue or fracture [35]. For a needle of just over a millimeter in diameter, any stress risers must be minimized to maintain sufficient structural integrity for insertion into dense tissue.

Another factor to consider is the method of actuation. A thin pull-wire or push-rod can be routed through or alongside the needle shaft, imparting the necessary force to flex the compliant segment [64]. Reducing friction between the actuation wire and surrounding surfaces is crucial for reliable steering response. Using low-friction coatings or employing polished channels can help preserve the fidelity of the deflection, though these solutions must remain compatible with sterilization procedures. Trease et al. (2005) showed that proper selection of flexure geometry in compliant joints can significantly reduce the actuation force required, which becomes an important consideration when attempting to fit an actuator mechanism into a very slender device.

Locking or maintaining the bent position is yet another challenge. Unlike a hinged or ball-joint system, which can be held in place by clamping a rod or pin, a purely elastic mechanism may revert to its neutral (straight) shape as soon as the actuation force is removed. Designers sometimes incorporate a secondary locking feature or a friction-based clamp to hold the pull-wire in tension, preventing the tip from returning to its rest configuration [40]. Integrating such features without increasing device diameter can be particularly demanding at sub-millimeter scales, and it may require novel miniature clamping solutions or friction locks that occupy minimal space.

Additionally, it is important to ensure that the stiffness of the main needle shaft is not compromised

by the inclusion of flexible sections. Excessive compliance along the shaft could lead to unintended bending or buckling during insertion, making the device less predictable [32]. As a result, the flexible region is often isolated to a short distal section, while the remainder of the needle remains relatively rigid. Computational modeling can be used to determine the optimal location, size, and shape of the flexures, balancing the need for controlled tip deflection with the requirement for overall shaft stability [35].

Despite these intricacies, compliant mechanisms, including the active sheet approach, present a compelling option when aiming to achieve steerability in needles of extremely small diameter. Eliminating discrete joints reduces the potential for mechanical wear and backlash, and monolithic construction can simplify assembly and sterilization workflows. With carefully optimized geometry and proper materials, compliant flexures can deliver precise, reliable steering in a miniaturized form factor, opening the door to improved accuracy and fewer insertion attempts in minimally invasive applications.

C.2. Transmission

The transmission system is responsible for transferring force and motion from the proximal handle to the distal steering mechanism of a steerable needle. Its design is intrinsically linked to the type of steering mechanism it supports, as the two must work together seamlessly to ensure precise and reliable motion. While the transmission system plays a crucial role in the needle's performance, the steering mechanism remains the most critical determinant of its overall success. This section explores three common transmission methods—tendons, pull wires, and compliant mechanism-based transmission—discussing their advantages, disadvantages, and compatibility with specific steering mechanisms.

C.2.1. Tendons

Tendons are flexible cables or fibers that transmit pulling forces along the needle shaft. These are often routed through dedicated channels inside or along the needle and are anchored at specific points near the distal tip [52]. Tendons are highly versatile and are particularly effective for steering mechanisms that rely on discrete angular adjustments, such as hinge-based or ball-joint designs [7]. The flexibility of tendons allows them to be routed through complex geometries without significantly increasing the diameter of the needle, making them a practical choice for applications requiring precise directional control.

Tendons work exceptionally well with hinge-based mechanisms, where they provide the force needed to pivot the needle segments at specific points. This setup enables precise and controlled angular adjustments during navigation. Similarly, tendons are compatible with ball-joint mechanisms, as they allow multi-axis movement, enabling the needle to achieve a broad range of motion while maintaining directional accuracy. Tendons are lightweight and can be made from biocompatible materials, such as stainless steel or high-strength polymers, which ensure their compatibility with sterilization processes commonly used in clinical settings.

Despite their versatility, tendons face challenges related to friction within their channels, which can impede smooth motion. Maintaining consistent tension is another critical factor, as slack tendons may result in imprecise motion, while overly tight tendons could restrict flexibility or even damage the needle [31]. To address these issues, careful attention must be given to material selection and channel design, ensuring reliable and efficient performance during clinical procedures.

C.2.2. Pull Wires

Pull wires, a specific type of tendon-based transmission, are often used in applications that prioritize smooth, continuous bending rather than discrete angular adjustments. These wires are routed through

or along the needle shaft and are anchored at the steering mechanism, such as compliant flexures or active sheets, where they generate curvature through applied tension. Pull wires are particularly suited for steering mechanisms that rely on smooth motion, making them ideal for compliant mechanisms or active sheet designs [38].

In compliant mechanisms, pull wires are highly effective in transmitting force to flexible sections, enabling smooth and precise curvature along the needle. This is particularly advantageous in navigating complex anatomical pathways [36]. Similarly, active sheet mechanisms benefit from pull wires, as they allow the deformable sheet to adjust its bending arc in a controlled manner, enhancing the needle's trajectory during insertion. The simplicity and compact nature of pull wires make them well-suited for very slender needles, where space constraints are a concern.

However, pull wires are sensitive to friction, particularly in long or curved routing paths, which can reduce their responsiveness and increase the force required for actuation [14]. Additionally, pull wires typically offer limited tactile feedback, making it more challenging for operators to sense the forces acting on the distal tip. To mitigate these limitations, precise routing and low-friction materials are essential for ensuring reliable performance in clinical settings.

C.2.3. Compliant Mechanism

In some designs, the transmission system is integrated directly into the steering mechanism through compliant mechanisms. This eliminates the need for separate tendons or pull wires, as the elastic deformation of the structure itself transmits motion. Compliant mechanisms are particularly effective for monolithic designs, where the transmission and steering functions are inherently combined into a single structure [38].

This approach is especially suitable for steering mechanisms that rely on elastic deformation, such as integrated compliant flexures. By simplifying the design and removing additional components, compliant mechanism-based transmission reduces the risk of mechanical failure and simplifies sterilization and assembly processes. The streamlined design also makes it an attractive choice for applications that demand compactness and minimal complexity [68].

However, compliant mechanism-based transmission has limitations. Its range of motion is inherently restricted by the material's flexibility and geometry, which can limit its application in scenarios requiring extensive directional adjustments. While it excels in monolithic designs, it may not provide the level of control needed for mechanisms requiring more complex or multidirectional deflection, such as ball joints or hinges [14]. Meticulous attention to material selection and design is required to ensure predictable behavior and sufficient stiffness for effective tissue penetration.

Each of these transmission methods aligns with specific steering mechanisms. Tendons are best suited for hinge-based and ball-joint designs, where precise angular adjustments are required. Pull wires are highly compatible with compliant mechanisms and active sheets, offering smooth, continuous bending that is critical for navigating complex pathways. Compliant mechanism-based transmission integrates seamlessly into monolithic steering designs, providing a simplified and reliable solution for applications where compactness and minimal mechanical complexity are essential.

C.3. Actuation Unit

The actuation unit is the interface through which a clinician controls the steering mechanism of a steerable needle. It translates user input into precise force or motion that is transmitted via the needle's transmission system to adjust its trajectory. The actuation unit is a critical component that must offer

intuitive control, tactile feedback, and ergonomic operation while ensuring compatibility with the specific steering mechanism. Moreover, it is essential that the actuation unit be designed to accommodate both left- and right-handed users, ensuring universal accessibility and ease of use in diverse clinical settings. This aspect of ambidextrous design is especially important in high-stress surgical environments where comfort and precision are paramount [14, 36].

This section discusses common actuation units such as joysticks, sliders, levers, and rotation wheels, as well as their advantages, disadvantages, and compatibility with different steering systems. Additional actuation methods commonly used with steerable needles are also highlighted, emphasizing how their design can be optimized for inclusivity and user adaptability.

C.3.1. Joystick

A joystick is a multidirectional control device that allows clinicians to manipulate the needle's trajectory by tilting or rotating a handle. Joysticks are particularly well-suited for complex steering systems that require precise control in multiple axes, such as ball-joint mechanisms or compliant designs with multidirectional bending capabilities. The motion of the joystick corresponds to the desired curvature of the needle tip, enabling intuitive and continuous adjustments.

The primary advantage of a joystick is its versatility. It provides a high degree of control over complex motions, making it ideal for steering mechanisms requiring multidirectional adjustments. Joysticks also offer real-time tactile feedback, allowing clinicians to gauge resistance and adjust their inputs accordingly. Devices such as the steering joystick proposed by Abayazid et al. (2013) for flexible needles demonstrate the utility of this approach in navigating intricate anatomical structures [39]. However, joysticks can be more challenging to operate in confined surgical environments, as their range of motion requires adequate space for manipulation. Additionally, joysticks may be more mechanically complex compared to simpler actuation units, potentially increasing the overall size and cost of the system.

C.3.2. Slider

A slider is a linear actuation device that enables the user to control needle bending by moving a handle along a track. Sliders are typically used in mechanisms where a unidirectional or bidirectional adjustment is sufficient, such as active sheet or compliant flexure designs. The linear motion of the slider directly correlates to the bending curvature of the needle, offering straightforward and predictable operation.

Sliders are particularly advantageous for their simplicity and compact design. They are intuitive to operate and require minimal mechanical complexity, making them a reliable choice for systems where space constraints are critical. Studies such as those by Li et al. have shown that sliders are effective in guiding compliant mechanisms for brachytherapy needles [36]. However, sliders are less effective for steering mechanisms that require multidirectional adjustments, such as ball joints or multidirectional compliant systems. Additionally, sliders may provide limited tactile feedback, which could make it challenging to detect resistance or obstructions during needle navigation.

C.3.3. Lever

A lever is a pivot-based actuation device that translates rotational input from the user into linear or angular motion at the needle tip. Levers are often used in hinge-based steering systems or designs that require discrete angular adjustments. By applying force to the lever, clinicians can generate controlled motion in the steering mechanism.

The key advantage of levers is their ability to amplify force, making them particularly useful for steering

mechanisms that require high actuation forces, such as those operating in dense or resistant tissues. Levers are also straightforward to operate, offering a combination of simplicity and reliability. For instance, hinge-based mechanisms utilizing levers for precise adjustments have been explored by Zhang et al. (2021) [77]. However, they are less suited for continuous or multidirectional bending, as their operation is inherently discrete and rotational. Levers may also occupy more space than other actuation units, which could limit their use in compact surgical environments.

C.3.4. Rotation Wheel

A rotation wheel is a circular actuation device that allows users to adjust the needle's trajectory by turning a wheel. The rotation wheel is well-suited for compliant mechanisms and active sheets, where continuous bending is required. By rotating the wheel, clinicians can apply tension to pull wires or tendons, achieving precise curvature at the needle tip.

The main advantage of a rotation wheel is its ability to provide smooth and continuous adjustments, making it ideal for mechanisms requiring fine-tuned control. Rotation wheels also offer good tactile feedback, as the resistance felt during rotation correlates to the forces acting on the needle. This approach has been successfully demonstrated in systems such as the flexible needle steering platform described by Webster et al. (2006) [71]. However, the circular motion may be less intuitive for some users compared to linear actuation methods like sliders. Additionally, rotation wheels may require additional space in the proximal assembly, which could be a limitation in highly compact systems.

C.3.5. Other Common Actuation Units

In addition to the methods described above, other actuation units commonly used with steerable needles include push-buttons, knobs, and foot pedals. Push-buttons provide discrete actuation, making them suitable for systems with predefined bending angles or positions. Knobs offer rotational control similar to rotation wheels but are typically smaller and more compact. Foot pedals allow hands-free operation, making them ideal for procedures requiring simultaneous use of multiple instruments. These alternative actuation units can be adapted to various steering mechanisms depending on the specific requirements of the procedure and the ergonomic needs of the clinician.

Each actuation unit is intrinsically linked to the type of steering mechanism and the clinical application of the needle. Joysticks and rotation wheels excel in multidirectional or continuous bending applications, making them ideal for compliant and active sheet mechanisms. Sliders and levers are better suited for unidirectional or discrete angular adjustments, such as those required in hinge-based or ball-joint systems. By aligning the actuation unit with the steering and transmission mechanisms, a steerable needle can achieve optimal performance and usability in advanced brachytherapy procedures.

D
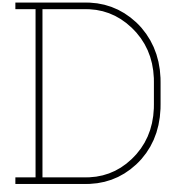
Fused Deposition Modelling (3D printer)

All prototypes presented here were 3D printed in polylactic acid (PLA) using a Creality Ender 3 printer. Fused Deposition Modelling (FDM) was chosen for its rapid turnaround, enabling quick iterations of the steerable needle concept.

In Figures D.1 and D.2, early prototypes of the steerable needle are shown, each featuring a slot near the tip to enable bending. The second prototype features thicker legs intended to increase stiffness; however, this design proved overly rigid, resulting in minimal bending.

Figures D.3 and D.4 illustrate a longer slot and the inclusion of an outer needle for simulating a catheter. Here, a simple steering mechanism is integrated, demonstrating how differential actuation can be introduced. The rotation wheel seen in Figure D.5 was designed to apply a controlled push-pull force on the split needle beams, enabling the tip to bend.

Subsequent designs (Figures D.6 and D.7) introduced a rudimentary handpiece to test single-handed actuation, confirming that both slot dimensions and overall geometry were compatible with the intended clinical motion. An internal view (Figure D.8) shows how the split needle fits within the handpiece. As illustrated in Figure D.9, bending tests confirmed that the prototypes could flex, though the mechanical properties differ substantially from those of a final metal design.

These PLA prototypes were crucial for identifying geometric constraints, refining slot dimensions on a large scale, and validating the feasibility of a differential-actuation approach. While they do not replicate the material properties of medical-grade metals, they provide a rapid, cost-effective method to iterate on the core design principles of the steerable needle.

Figure D.1: 3D printed prototype of needle with slot.

Figure D.2: 3D printed prototype of needle with slot, where the legs are thicker.
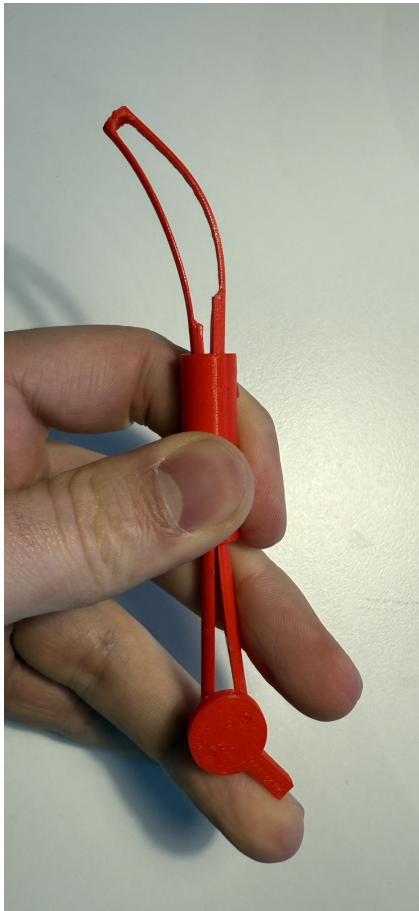
Figure D.3: 3D printed prototype of needle with long sized slot and steering mechanism with outer needle.

Figure D.4: 3D printed prototype of needle with long sized slot and steering mechanism.

Figure D.5: Rotation wheel (for steering).
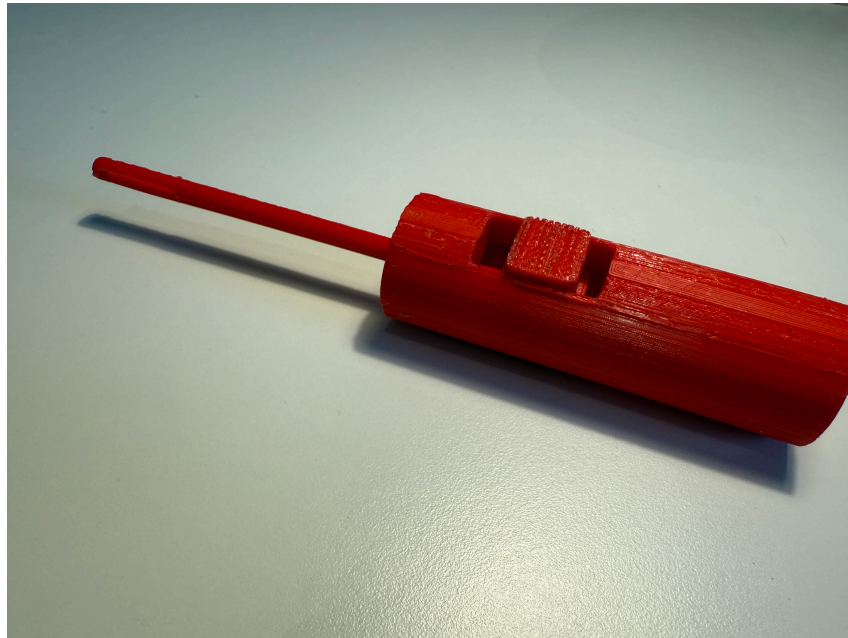
Figure D.6: 3D printed prototype of needle and handpiece
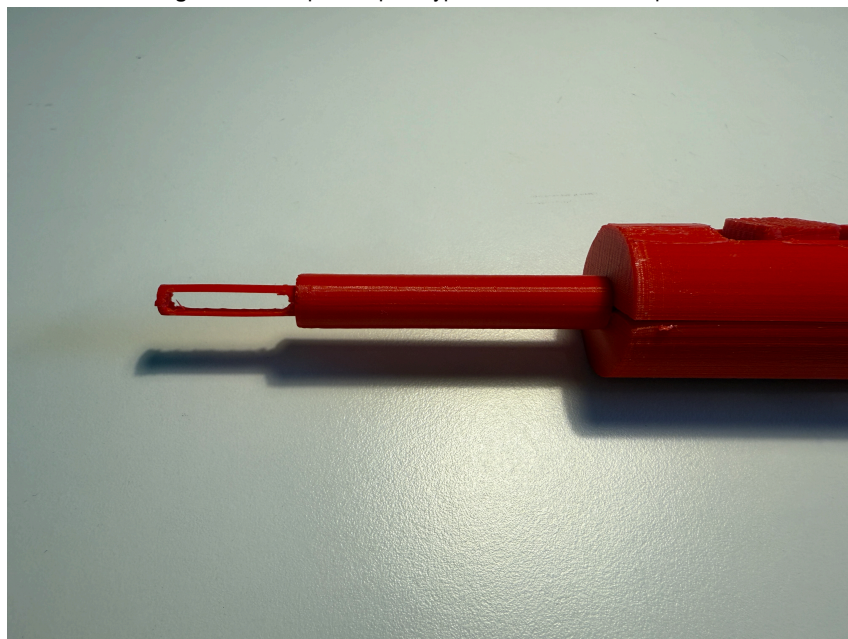
Figure D.7: 3D printed prototype of inner needle with an outer needle and a handpiece
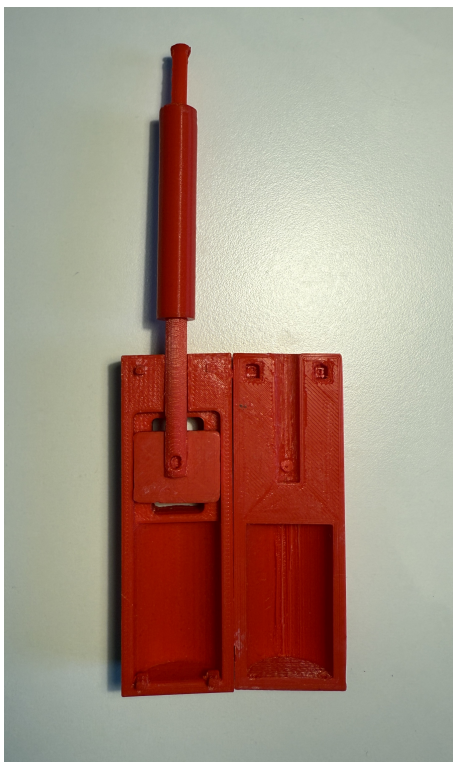
Figure D.8: Inside of the 3D printed prototype
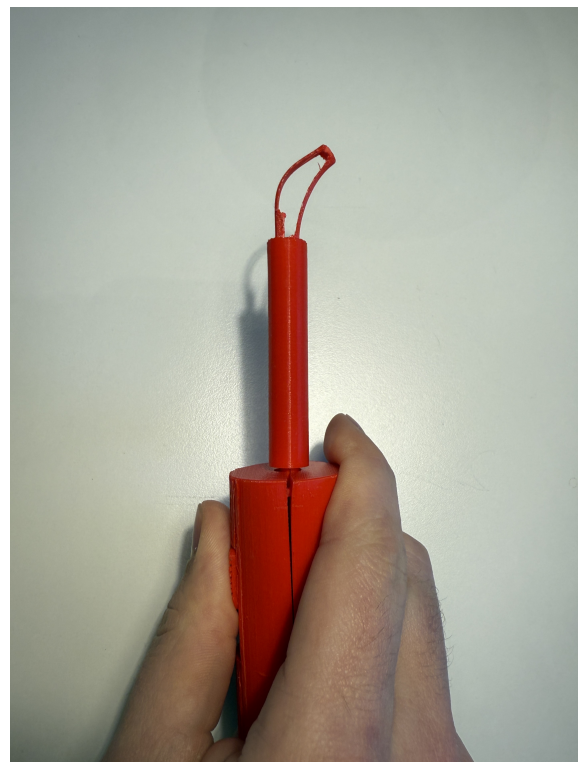
Figure D.9: Needle bending of the 3D printed prototype

E
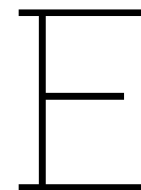
Finite Element Analysis

Finite Element Analysis was performed using COMSOL Multiphysics to evaluate the mechanical performance of the needle catheter assembly under bending conditions. The geometric models of both the steerable needle and the ProGuide 6F catheter were first created in Dassault Systèmes SolidWorks, capturing the precise dimensions of the split-shaft needle, including the slot length and edge thickness. These models were then imported into COMSOL as solid geometry files, where they were meshed with a high-resolution free tetrahedral mesh to capture stress concentrations and localized deformations.

The material properties for AISI 301 stainless steel (needle) and polyoxymethylene (catheter) were assigned in accordance with the values presented in Table 4.1 of Chapter 4. AISI 301 stainless steel was selected for its combination of flexibility and high yield strength, ensuring that it could undergo repeated bending cycles without permanent deformation, while polyoxymethylene was applied to represent the standard ProGuide 6F catheter.

Within COMSOL, static analyses were performed by applying a prescribed displacement of 1.0 mm at the bottom of one beam of the split-shaft needle, with the bottom of the other beam rigidly fixed. The catheter was also fixed at the bottom to represent the boundary conditions encountered during clinical insertion (see Chapter 4 for further details).

In Figure E.2, the assembly with a 5 mm slot is shown. The simulation reports a maximum von Mises stress of 648.054 MPa and a maximum displacement of 157.603 mm. Figure E.1 shows the assembly with a 7.22 mm slot. Here, the maximum von Mises stress decreases to 585.900 MPa, whereas the maximum displacement remains similar at 157.50 mm, indicating a balanced design that lowers stress without sacrificing flexibility. Figure E.3 illustrates a 9 mm slot. Although this slot length increases the maximum displacement to 166.670 mm, the maximum von Mises stress also rises to 702.575 MPa, suggesting that, while more flexibility is gained, the needle experiences elevated stress levels that may compromise structural integrity.

The influence of edge thickness was also investigated by varying the dimension of the metal adjacent to the slot. Figure E.4 displays the results for a 0.28 mm edge thickness, where the simulation reports a maximum von Mises stress of 1048.397 MPa and a maximum displacement of 159.000 mm. Figure E.5 shows that increasing the edge thickness to 0.325 mm reduces the maximum displacement to 139.285 mm but still induces a notable stress of 972.763 MPa. These simulations demonstrate how thinning the edge increases compliance but simultaneously raises stress concentrations, whereas thickening it
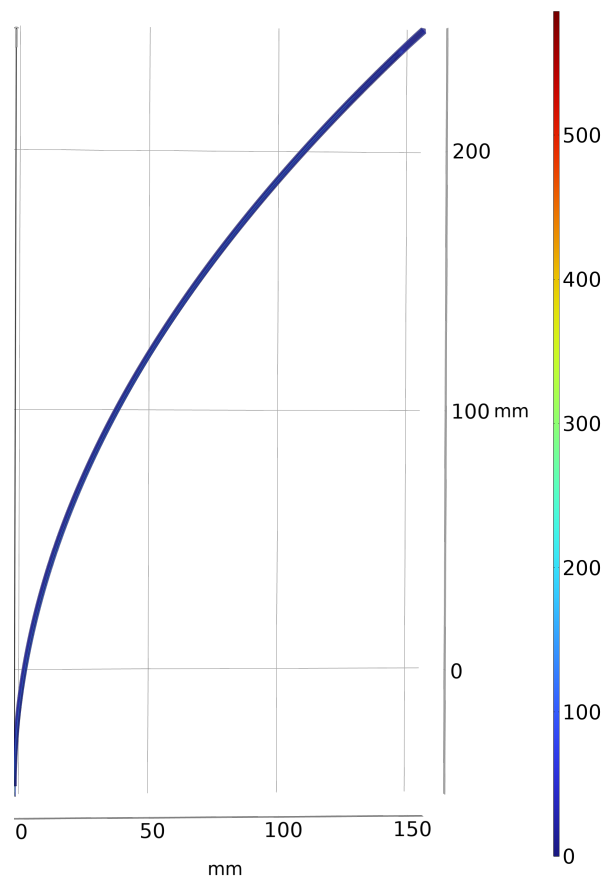
Figure E.1: Needle–catheter assembly with a 7.22 mm slot. The simulation shows a reduced maximum von Mises stress of 585.900 MPa with a maximum displacement of 157.50 mm, indicating a balanced design.

lowers flexibility at the expense of heightened stress in other regions.

These results provide important insights into how slot length and edge thickness affect the mechanical behavior of the needle catheter assembly. The intermediate configuration of a 7.22 mm slot length and 0.3 mm edge thickness appears to balance stress control with adequate bending capacity. Thus, it represents a promising design choice for ensuring both flexibility and structural robustness under clinical loading conditions. Collectively, Figures E.2 through E.5 offer guidance for refining the geometry of the steerable needle. They confirm that small deviations in either slot length or edge thickness can significantly alter stress distributions and overall displacement, shaping the optimal design for achieving controlled deflection in HDR brachytherapy applications.
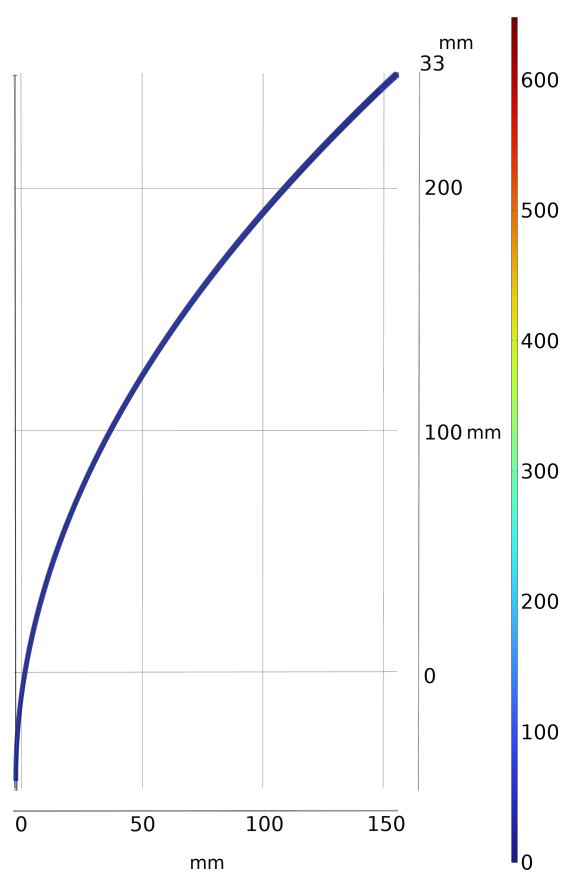
Figure E.2: Needle–catheter assembly with a 5 mm slot. The simulation indicates a maximum von Mises stress of 648.054 MPa and a maximum displacement of 157.603 mm.
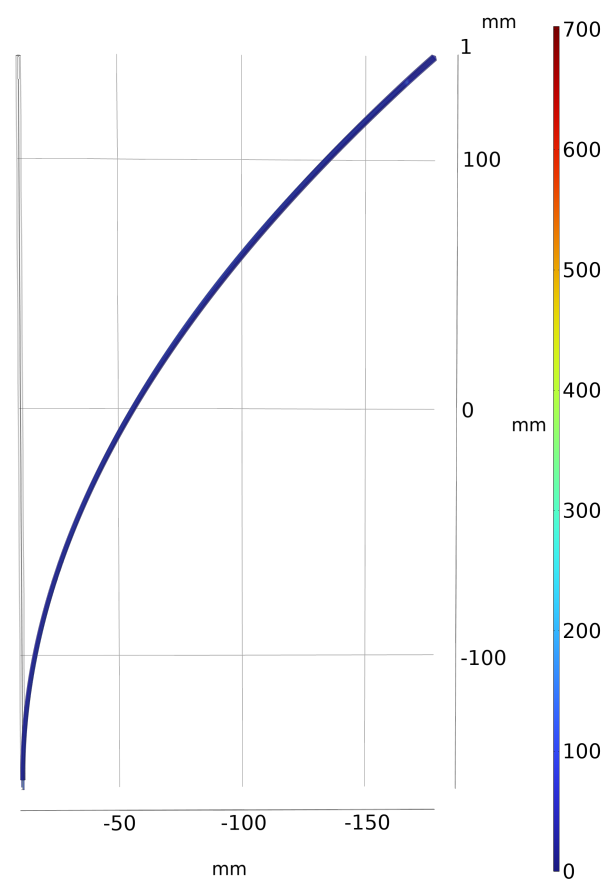
Figure E.3: Needle–catheter assembly with a 9 mm slot. The simulation reveals a maximum von Mises stress of 702.575 MPa and an increased maximum displacement of 166.670 mm, demonstrating enhanced bending accompanied by elevated stress levels.
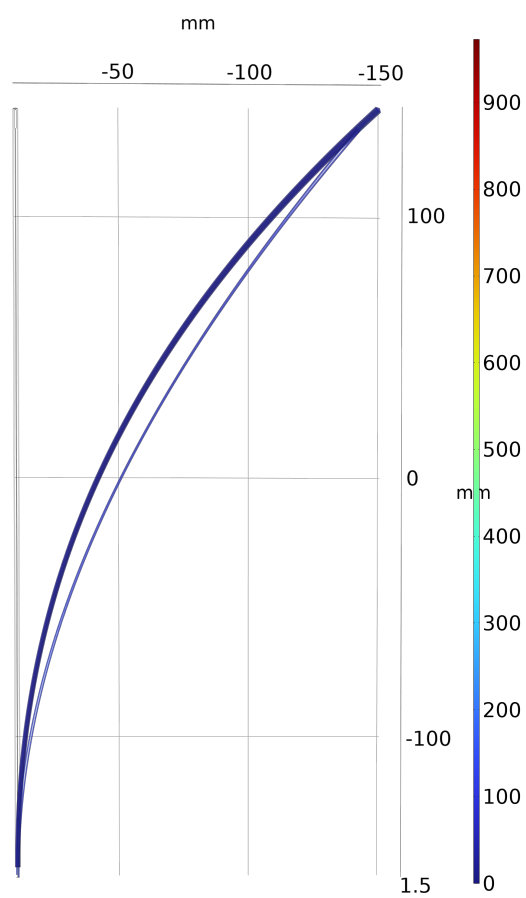
Figure E.4: Needle–catheter assembly with a 0.28 mm edge thickness. The simulation reveals a maximum von Mises stress of 1048.397 MPa and an increased maximum displacement of 159.000 mm.
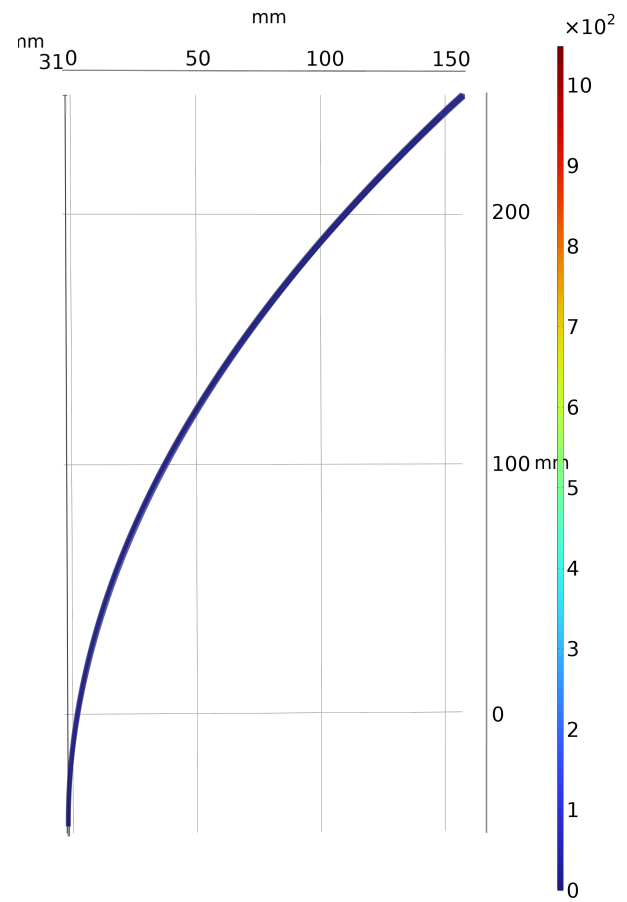
Figure E.5: Needle–catheter assembly with a 0.325 mm edge thickness. The simulation reveals a maximum von Mises stress of 972.763 MPa and an increased maximum displacement of 139.285 mm.

F
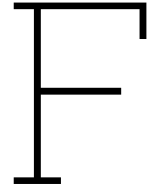
Technical Drawings of the Components

The following technical drawings can be found in this appendix:

- Assembly drawing

  – Assembly handpiece + steerable needle

- Part drawings:

  – Handpiece
  – Needle
  – Rotation disk
  – Holding block
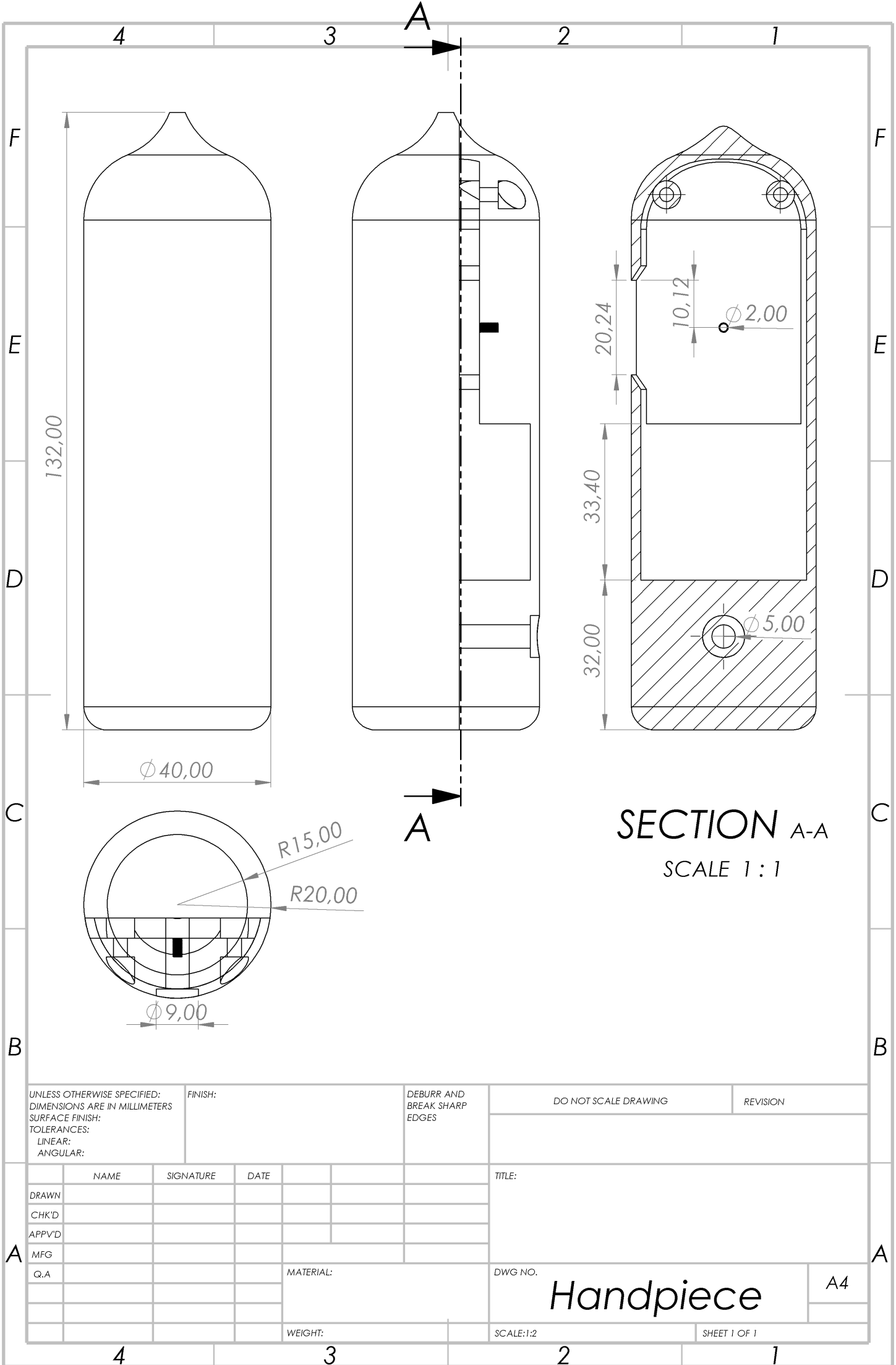
Scale 1:2

339,90

⌀ 39,59

ITEM NO.	PART NUMBER	QTY.
1	Handvat	1
2	Lange naald	1
3	Blokje vasthoudt	2
4	Draaischijf	1
5	Handvat1	1
6	pan cross head_am	2
7	pan cross head_am	2
8	pan cross head_am	1
9	B18.6.7M - M2 x 0.4 x 6 Type I Cross Recessed PHMS -- 6N	1
10	Parallel Pin ISO 2338 - 2.5 h6 x 10 - St	1
11	Parallel Pin ISO 2338 - 2.5 h6 x 6 - St	1

	NAME	SIGNATURE	DATE
DRAWN			
CHK'D			
APPV'D			
MFG			
Q.A			

TITLE:

MATERIAL:

DWG NO.

Steerable needle assembly

A4

WEIGHT:

SCALE:1:5

SHEET 1 OF 1

A

| 4 | 3 | | 2 | 1 |

F

132,00

⌀40,00

⌀2,00

10,12

20,24

33,40

32,00

⌀5,00

E

D

C

SECTION A-A

SCALE 1 : 1

A

R15,00

R20,00

⌀9,00

B

	NAME	SIGNATURE	DATE			TITLE:	
DRAWN							
CHK'D							
APPV'D							
MFG							
Q.A				MATERIAL:		DWG NO.	

WEIGHT:

SCALE:1:2

Handpiece

A4

SHEET 1 OF 1

| 4 | 3 | 2 | 1 |

C

Ø 1,30

0,70

0,30

250,00

0,28

0,51

DETAIL C

SCALE 10 : 1

	NAME	SIGNATURE	DATE				TITLE:
DRAWN							
CHK'D							
APPV'D							
MFG							
Q.A				MATERIAL:			DWG NO.

Needle

A4

WEIGHT:

SCALE:1:2

SHEET 1 OF 1

R21.00

R6.00

R11.00

10.00

Ø2.00

2.50

2.00

R6.00

12,00

4,00

32,80

36,94

Scale 2:1

	NAME	SIGNATURE	DATE			TITLE:		
DRAWN								
CHK'D								
APPV'D								
MFG								
Q.A				MATERIAL:		DWG NO.		

Rotation disk

A4

WEIGHT:

SCALE:1:1

SHEET 1 OF 1

Scale 5:1

| | 4 | 3 | 2 | 1 |

F
E
D
C
B
A

Ø2,00
5,00
15,00
6,00

Ø2,50
3,00
5,00

6,00

6,00
5,00

	NAME	SIGNATURE	DATE			TITLE:
DRAWN						
CHK'D						
APPV'D						
MFG						
Q.A						

MATERIAL:

WEIGHT:

DWG NO.

Holding block

A4

SCALE:5:1   SHEET 1 OF 1
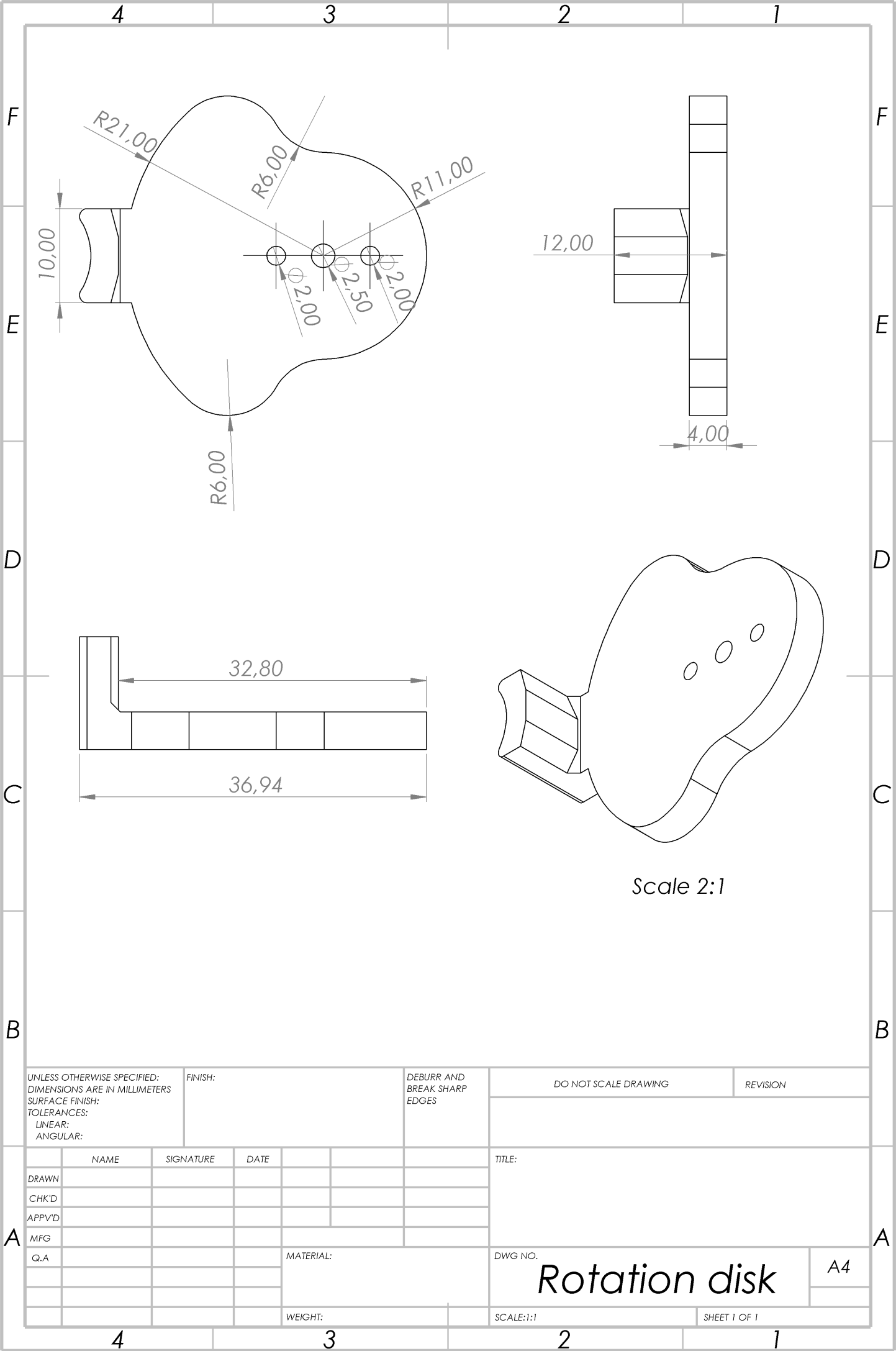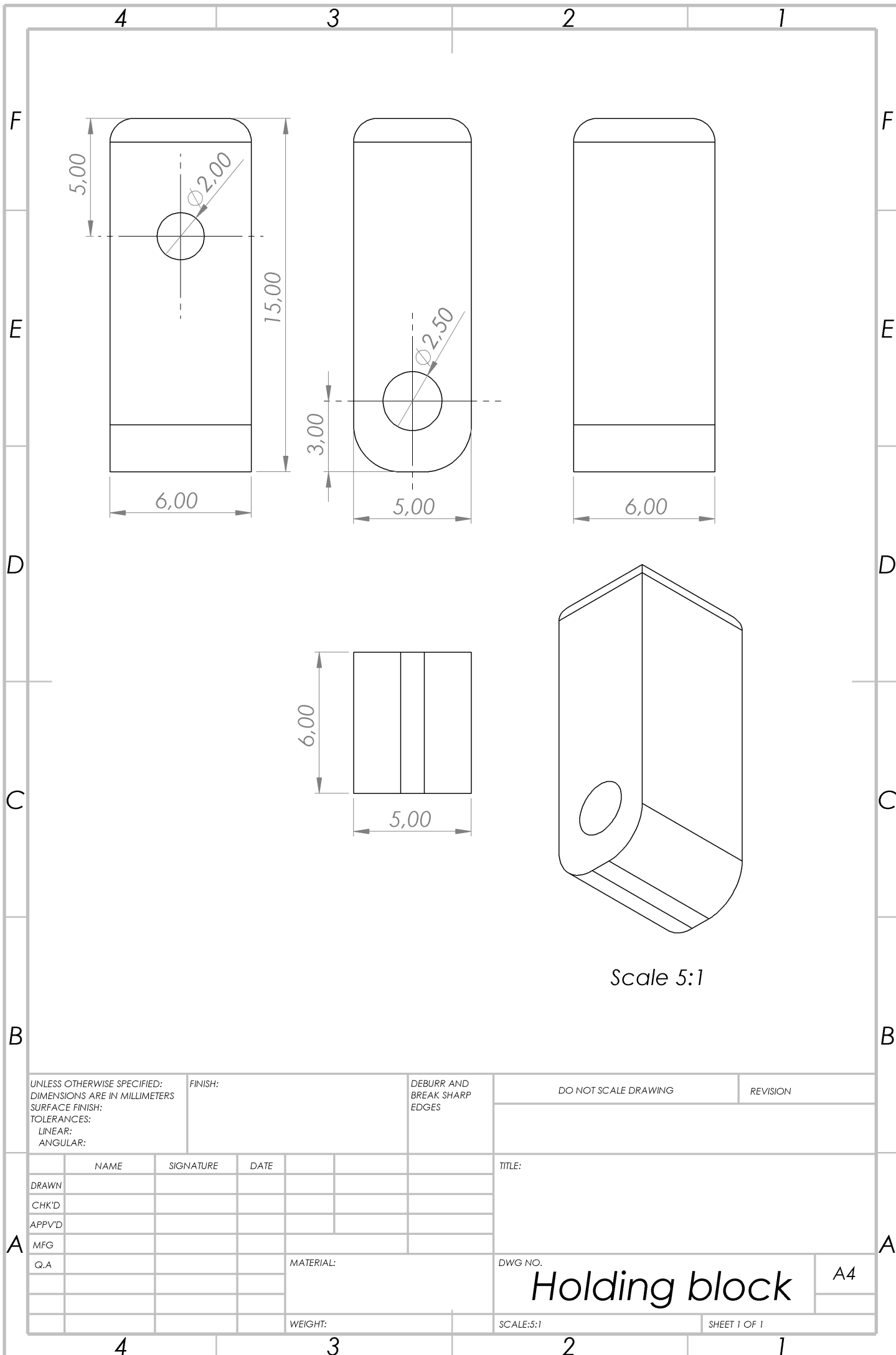
G

SPSS Output - Experiment 1

Descriptives

Notes

Output Created		20-MAR-2025 15:00:44
Comments		
Input	Data	C: \Users\sstre\Documents\Th esis\Testafbeeldingen\Anal yse.sav
	Active Dataset	DataSet1
	Filter	<none>
	Weight	<none>
	Split File	<none>
	N of Rows in Working Data File	28
Missing Value Handling	Definition of Missing	User defined missing values are treated as missing.
	Cases Used	All non-missing data are used.
Syntax		DESCRIPTIVES VARIABLES=Deflectie /STATISTICS=MEAN STDDEV MIN MAX.
Resources	Processor Time	00:00:00,00
	Elapsed Time	00:00:00,00

[DataSet1] C:\Users\sstre\Documents\Thesis\Testafbeeldingen\Analyse.sav

Descriptive Statistics

	N	Minimum	Maximum	Mean	Std. Deviation
Deflectie	28	9,16	33,66	17,7263	6,35634
Valid N (listwise)	28				

Univariate Analysis of Variance

Notes

Output Created		20-MAR-2025 15:03:07
Comments		
Input	Data	C:\Users\sstre\Documents\Thesis\Testafbeeldingen\Analyse.sav
	Active Dataset	DataSet1
	Filter	<none>
	Weight	<none>
	Split File	<none>
	N of Rows in Working Data File	28
Missing Value Handling	Definition of Missing	User-defined missing values are treated as missing.
	Cases Used	Statistics are based on all cases with valid data for all variables in the model.
Syntax		UNIANOVA Deflectie BY Katheter Procedure /METHOD=SSTYPE(3) /INTERCEPT=INCLUDE /PRINT ETASQ DESCRIPTIVE /CRITERIA=ALPHA(.05) /DESIGN=Katheter Procedure Katheter*Procedure.
Resources	Processor Time	00:00:00,00
	Elapsed Time	00:00:00,01

Between-Subjects Factors

		Value Label	N
Katheter	1,00	Klassiek	14
	2,00	Dun	14
Procedure	1,00	10cm	14
	2,00	5cm	14

Descriptive Statistics

Dependent Variable: Deflectie

Katheter	Procedure	Mean	Std. Deviation	N
Klassiek	10cm	15,2993	3,24432	7
	5cm	10,9057	1,87493	7
	Total	13,1025	3,41724	14
Dun	10cm	26,6143	3,47066	7
	5cm	18,0857	1,50602	7
	Total	22,3500	5,11754	14
Total	10cm	20,9568	6,69976	14
	5cm	14,4957	4,06802	14
	Total	17,7263	6,35634	28

Tests of Between-Subjects Effects

Dependent Variable: Deflectie

Source	Type III Sum of Squares	df	Mean Square	F	Sig.
Corrected Model	920,754[a]	3	306,918	43,297	<,001
Intercept	8798,158	1	8798,158	1241,163	<,001
Katheter	598,614	1	598,614	84,447	<,001
Procedure	292,218	1	292,218	41,223	<,001
Katheter * Procedure	29,922	1	29,922	4,221	,051
Error	170,127	24	7,089		
Total	9889,039	28			
Corrected Total	1090,881	27			

Tests of Between-Subjects Effects

Dependent Variable: Deflectie

Source	Partial Eta Squared
Corrected Model	,844
Intercept	,981
Katheter	,779
Procedure	,632
Katheter * Procedure	,150
Error	
Total	
Corrected Total	

a. R Squared = ,844 (Adjusted R Squared = ,825)

Explore

Notes

Output Created		20-MAR-2025 15:59:26
Comments		
Input	Data	C:\Users\sstre\Documents\Thesis\Testafbeeldingen\Analyse.sav
	Active Dataset	DataSet1
	Filter	<none>
	Weight	<none>
	Split File	<none>
	N of Rows in Working Data File	28
Missing Value Handling	Definition of Missing	User-defined missing values for dependent variables are treated as missing.
	Cases Used	Statistics are based on cases with no missing values for any dependent variable or factor used.
Syntax		EXAMINE VARIABLES=Deflectie BY Procedure Katheter /PLOT BOXPLOT STEMLEAF NPPLOT /COMPARE GROUPS /STATISTICS DESCRIPTIVES /CINTERVAL 95 /MISSING LISTWISE /NOTOTAL.
Resources	Processor Time	00:00:05,00
	Elapsed Time	00:00:01,50

Procedure

Case Processing Summary

		Cases					
		Valid		Missing		Total	
	Procedure	N	Percent	N	Percent	N	Percent
Deflectie	10cm	14	100,0%	0	0,0%	14	100,0%
	5cm	14	100,0%	0	0,0%	14	100,0%

Descriptives

Procedure				Statistic	Std. Error
Deflectie	10cm	Mean		20,9568	1,79059
		95% Confidence Interval for Mean	Lower Bound	17,0885	
			Upper Bound	24,8251	
		5% Trimmed Mean		20,8159	
		Median		20,9020	
		Variance		44,887	
		Std. Deviation		6,69976	
		Minimum		10,79	
		Maximum		33,66	
		Range		22,87	
		Interquartile Range		9,86	
		Skewness		,107	,597
		Kurtosis		-,672	1,154
	5cm	Mean		14,4957	1,08722
		95% Confidence Interval for Mean	Lower Bound	12,1469	
			Upper Bound	16,8445	
		5% Trimmed Mean		14,4908	
		Median		15,2200	
		Variance		16,549	
		Std. Deviation		4,06802	
		Minimum		9,16	
		Maximum		19,92	
		Range		10,76	
		Interquartile Range		8,21	
		Skewness		-,066	,597
		Kurtosis		-1,781	1,154

Tests of Normality

		Kolmogorov-Smirnov[a]			Shapiro-Wilk		
	Procedure	Statistic	df	Sig.	Statistic	df	Sig.
Deflectie	10cm	,133	14	,200[*]	,960	14	,723
	5cm	,162	14	,200[*]	,887	14	,073

*. This is a lower bound of the true significance.

a. Lilliefors Significance Correction

Deflectie

Stem-and-Leaf Plots

```
Deflectie Stem-and-Leaf Plot for
Procedure= 10cm

 Frequency    Stem & Leaf
```

Page 5

```
   3,00      1 .  014
   4,00      1 .  6779
   2,00      2 .  24
   4,00      2 .  5667
   1,00      3 .  3

 Stem width:      10,00
 Each leaf:       1 case(s)
```

```
Deflectie Stem-and-Leaf Plot for
Procedure= 5cm

 Frequency    Stem &  Leaf

   3,00      0 .  999
   4,00      1 .  0124
   7,00      1 .  5678899

 Stem width:      10,00
 Each leaf:       1 case(s)
```

Normal Q-Q Plots

Normal Q-Q Plot of Deflectie

for Procedure= 10cm

Normal Q-Q Plot of Deflectie

for Procedure= 5cm

Detrended Normal Q-Q Plots

Detrended Normal Q-Q Plot of Deflectie

for Procedure= 10cm

Detrended Normal Q-Q Plot of Deflectie

for Procedure= 5cm
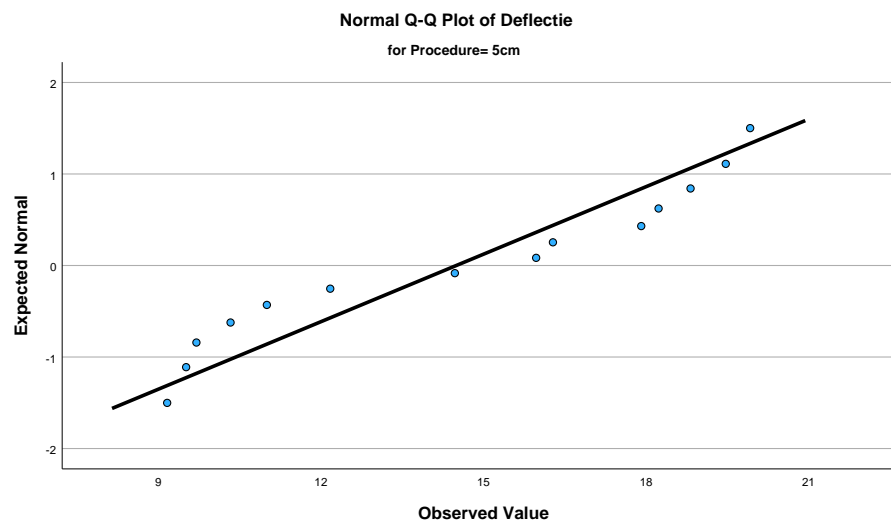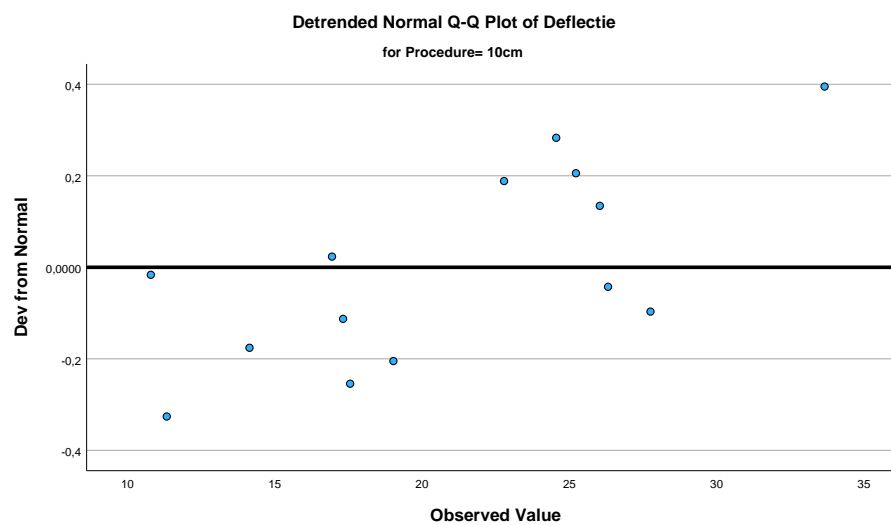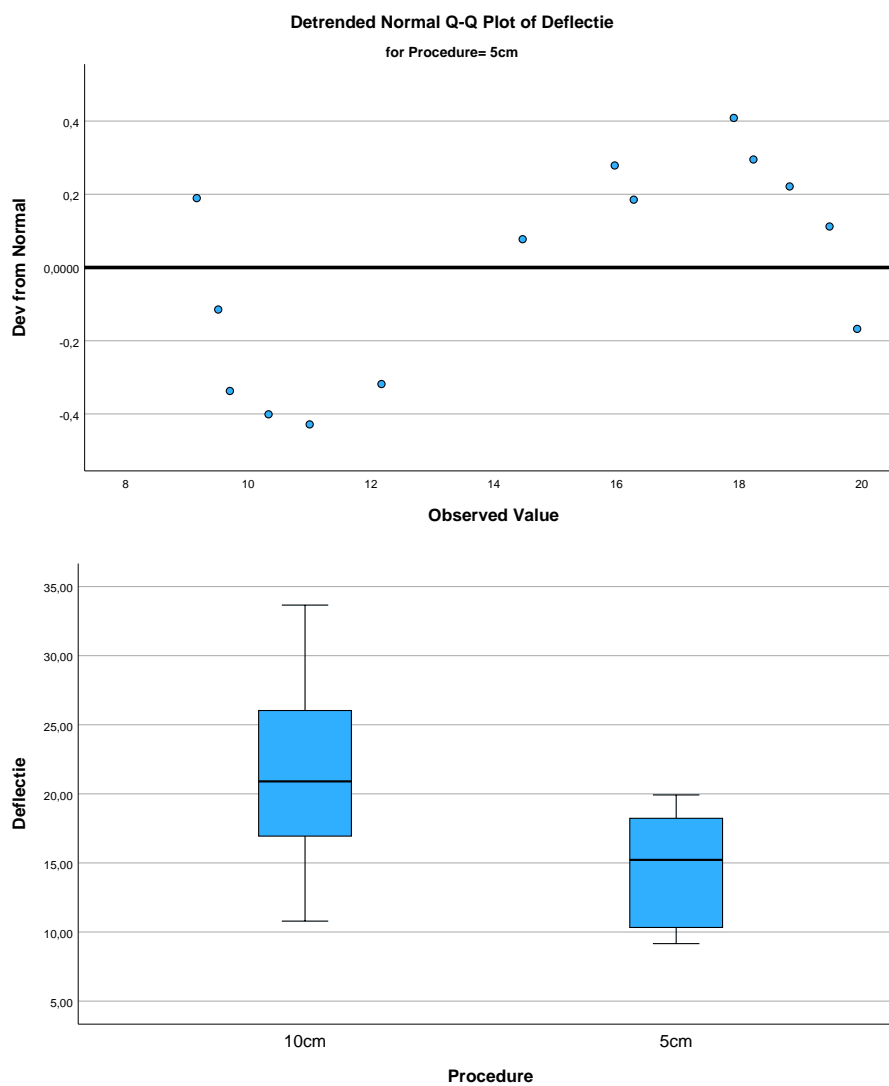
Katheter

Case Processing Summary

| | | Cases | | | | | |
| | | Valid | | Missing | | Total | |
	Katheter	N	Percent	N	Percent	N	Percent
Deflectie	Klassiek	14	100,0%	0	0,0%	14	100,0%
	Dun	14	100,0%	0	0,0%	14	100,0%

Page 8

Descriptives

Katheter				Statistic	Std. Error
Deflectie	Klassiek	Mean		13,1025	,91330
		95% Confidence Interval for Mean	Lower Bound	11,1294	
			Upper Bound	15,0756	
		5% Trimmed Mean		12,9926	
		Median		11,7500	
		Variance		11,678	
		Std. Deviation		3,41724	
		Minimum		9,16	
		Maximum		19,02	
		Range		9,86	
		Interquartile Range		6,86	
		Skewness		,527	,597
		Kurtosis		-1,311	1,154
	Dun	Mean		22,3500	1,36772
		95% Confidence Interval for Mean	Lower Bound	19,3952	
			Upper Bound	25,3048	
		5% Trimmed Mean		22,0761	
		Median		21,3500	
		Variance		26,189	
		Std. Deviation		5,11754	
		Minimum		15,97	
		Maximum		33,66	
		Range		17,69	
		Interquartile Range		7,95	
		Skewness		,688	,597
		Kurtosis		,028	1,154

Tests of Normality

	Katheter	Kolmogorov-Smirnov[a]			Shapiro-Wilk		
		Statistic	df	Sig.	Statistic	df	Sig.
Deflectie	Klassiek	,198	14	,142	,889	14	,079
	Dun	,183	14	,200[*]	,930	14	,310

*. This is a lower bound of the true significance.

a. Lilliefors Significance Correction

Deflectie

Stem-and-Leaf Plots

```
Deflectie Stem-and-Leaf Plot for
Katheter= Klassiek

 Frequency    Stem &  Leaf
```

```
   3,00      0 . 999
   7,00      1 . 0011244
   4,00      1 . 6779

 Stem width:      10,00
 Each leaf:       1 case(s)
```

```
Deflectie Stem-and-Leaf Plot for
Katheter= Dun

 Frequency    Stem &  Leaf

    7,00      1 . 5678899
    2,00      2 . 24
    4,00      2 . 5667
    1,00      3 . 3

 Stem width:      10,00
 Each leaf:       1 case(s)
```
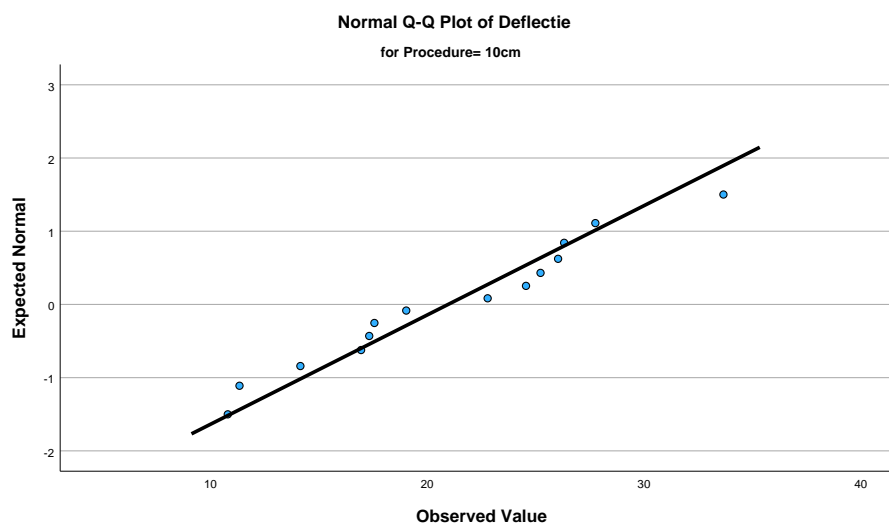
Normal Q-Q Plots

Normal Q-Q Plot of Deflectie

for Katheter= Klassiek

Normal Q-Q Plot of Deflectie

for Katheter= Dun

Detrended Normal Q-Q Plots

Detrended Normal Q-Q Plot of Deflectie

for Katheter= Klassiek

Detrended Normal Q-Q Plot of Deflectie

for Katheter= Dun
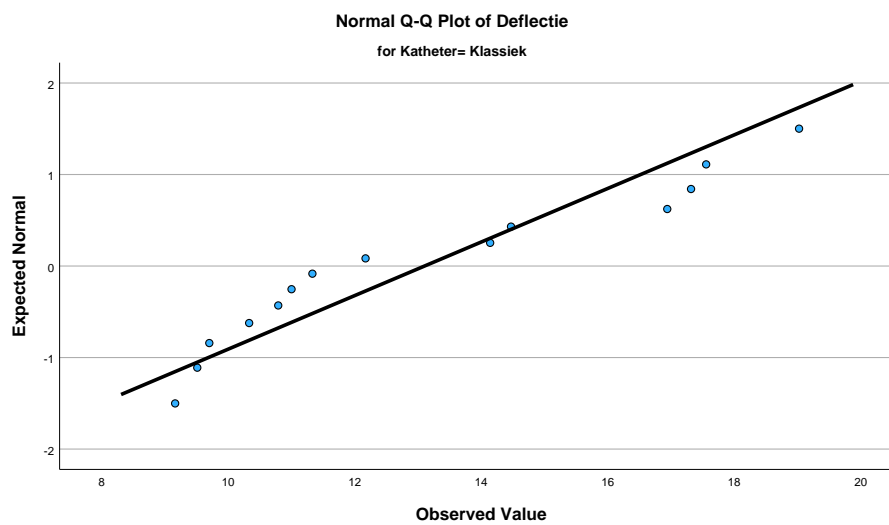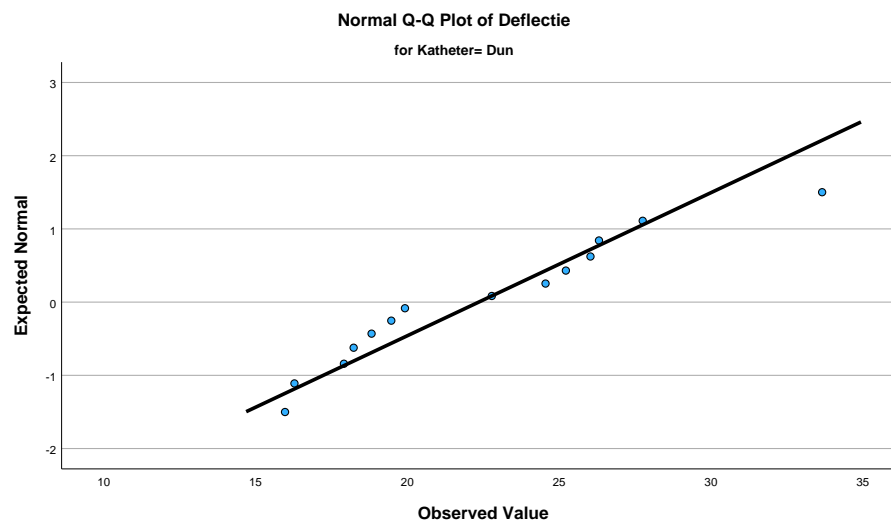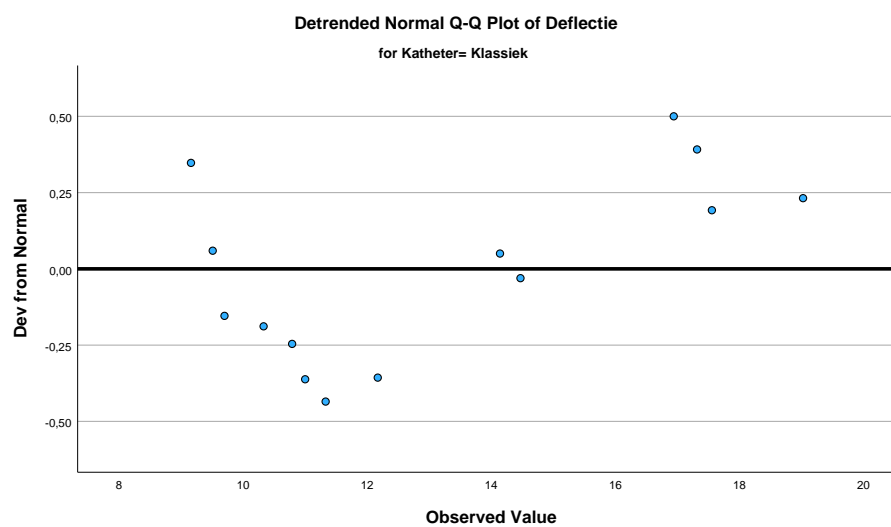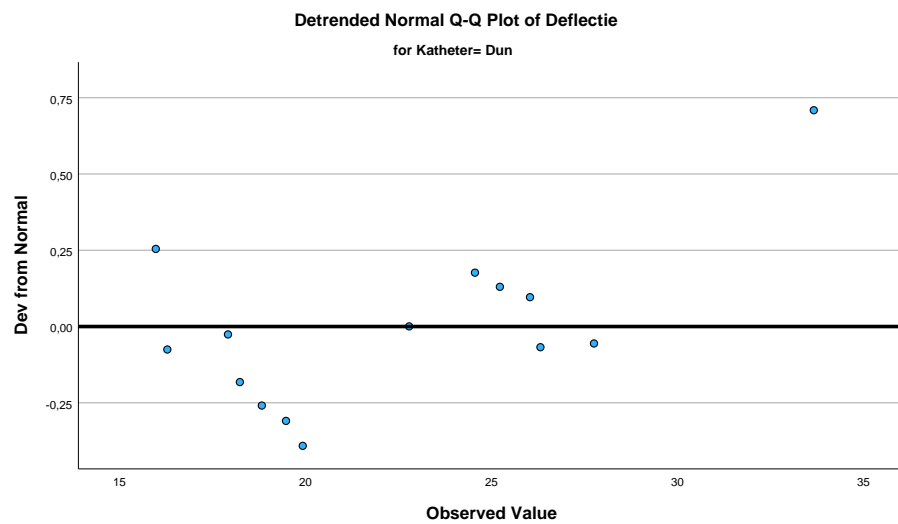
Boxplots
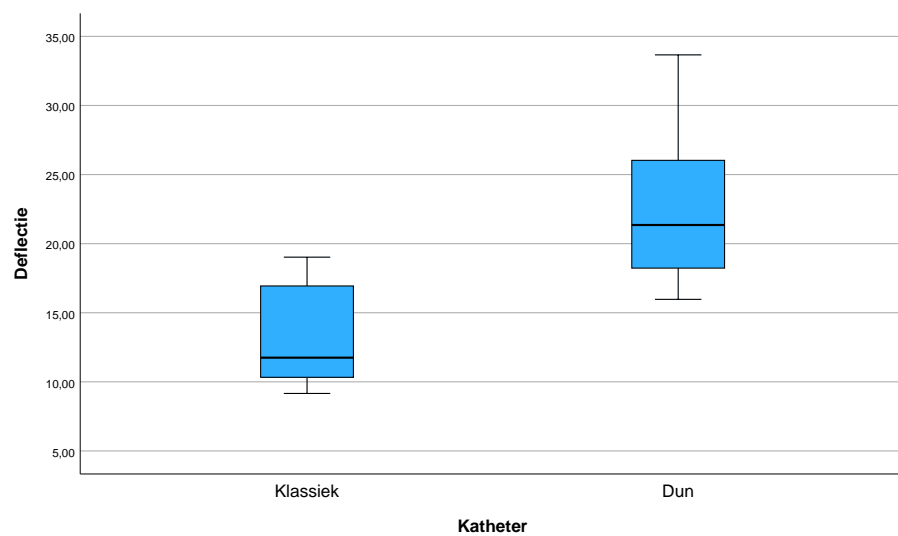
H

SPSS Output - Experiment 2

Univariate Analysis of Variance

Notes

Output Created		02-APR-2025 16:24:11
Comments		
Input	Data	C:\Users\sstre\Documents\Thesis\SPSS\CT scan analyse gelatine.sav
	Active Dataset	DataSet1
	Filter	<none>
	Weight	<none>
	Split File	<none>
	N of Rows in Working Data File	18
Missing Value Handling	Definition of Missing	User-defined missing values are treated as missing.
	Cases Used	Statistics are based on all cases with valid data for all variables in the model.
Syntax		UNIANOVA Deflection BY Needle_type Catheter_type Depth /METHOD=SSTYPE(3) /INTERCEPT=INCLUDE /CRITERIA=ALPHA(0.05) /DESIGN=Needle_type Catheter_type Depth Needle_type*Catheter_type Needle_type*Depth Catheter_type*Depth Needle_type*Catheter_type*Depth.
Resources	Processor Time	00:00:00,03
	Elapsed Time	00:00:00,01

Between-Subjects Factors

		Value Label	N
Needle_type	1	Steerable	12
	2	Straight	6
Catheter_type	1	ProGuide 6F	12
	2	Flexible Implant Tube	6
Inbrengdiepte in cm	5,00		9
	8,00		9

Tests of Between-Subjects Effects

Dependent Variable: Deflection

Source	Type III Sum of Squares	df	Mean Square	F	Sig.
Corrected Model	1757,598[a]	5	351,520	37,710	<,001
Intercept	3894,261	1	3894,261	417,765	<,001
Needle_type	382,505	1	382,505	41,034	<,001
Catheter_type	319,683	1	319,683	34,295	<,001
Depth	264,210	1	264,210	28,344	<,001
Needle_type * Catheter_type	,000	0	.	.	.
Needle_type * Depth	4,526	1	4,526	,486	,499
Catheter_type * Depth	53,101	1	53,101	5,696	,034
Needle_type * Catheter_type * Depth	,000	0	.	.	.
Error	111,860	12	9,322		
Total	6110,878	18			
Corrected Total	1869,458	17			

a. R Squared = ,940 (Adjusted R Squared = ,915)

Univariate Analysis of Variance

Notes

Output Created		02-APR-2025 16:33:04
Comments		
Input	Data	C:\Users\sstre\Documents\Thesis\SPSS\CT scan analyse gelatine.sav
	Active Dataset	DataSet1
	Filter	<none>
	Weight	<none>
	Split File	<none>
	N of Rows in Working Data File	18
Missing Value Handling	Definition of Missing	User-defined missing values are treated as missing.
	Cases Used	Statistics are based on all cases with valid data for all variables in the model.

Page 2

Notes

Syntax		UNIANOVA Deflection BY Needle_type Catheter_type Depth /METHOD=SSTYPE(3) /INTERCEPT=INCLUDE /EMMEANS=TABLES (Needle_type) /EMMEANS=TABLES (Catheter_type) /EMMEANS=TABLES (Depth) /EMMEANS=TABLES (Needle_type*Catheter_type) /EMMEANS=TABLES (Needle_type*Depth) /EMMEANS=TABLES (Catheter_type*Depth) /EMMEANS=TABLES (Needle_type*Catheter_type*Depth) /PRINT ETASQ DESCRIPTIVE HOMOGENEITY /CRITERIA=ALPHA(.05) /DESIGN=Needle_type Catheter_type Depth Needle_type*Catheter_type Needle_type*Depth Catheter_type*Depth Needle_type*Catheter_type *Depth.
Resources	Processor Time	00:00:00,02
	Elapsed Time	00:00:00,02

Between-Subjects Factors

		Value Label	N
Needle_type	1	Steerable	12
	2	Straight	6
Catheter_type	1	ProGuide 6F	12
	2	Flexible Implant Tube	6
Inbrengdiepte in cm	5,00		9
	8,00		9

Page 3

Descriptive Statistics

Dependent Variable: Deflection

Needle_type	Catheter_type	Inbrengdiepte in cm	Mean	Std. Deviation	N
Steerable	ProGuide 6F	5,00	12,8833	,75036	3
		8,00	18,4633	3,50058	3
		Total	15,6733	3,80365	6
	Flexible Implant Tube	5,00	18,9990	2,11432	3
		8,00	32,9933	6,15536	3
		Total	25,9962	8,70034	6
	Total	5,00	15,9412	3,63782	6
		8,00	25,7283	9,13199	6
		Total	20,8348	8,36932	12
Straight	ProGuide 6F	5,00	2,8200	,49427	3
		8,00	5,9433	,71396	3
		Total	4,3817	1,79671	6
	Total	5,00	2,8200	,49427	3
		8,00	5,9433	,71396	3
		Total	4,3817	1,79671	6
Total	ProGuide 6F	5,00	7,8517	5,54113	6
		8,00	12,2033	7,22015	6
		Total	10,0275	6,54345	12
	Flexible Implant Tube	5,00	18,9990	2,11432	3
		8,00	32,9933	6,15536	3
		Total	25,9962	8,70034	6
	Total	5,00	11,5674	7,16753	9
		8,00	19,1333	12,25193	9
		Total	15,3504	10,48657	18

Levene's Test of Equality of Error Variances[a,b]

		Levene Statistic	df1	df2	Sig.
Deflection	Based on Mean	4,785	5	12	,012
	Based on Median	1,082	5	12	,418
	Based on Median and with adjusted df	1,082	5	3,030	,506
	Based on trimmed mean	4,385	5	12	,017

Tests the null hypothesis that the error variance of the dependent variable is equal across groups.

a. Dependent variable: Deflection

b. Design: Intercept + Needle_type + Catheter_type + Depth + Needle_type * Catheter_type + Needle_type * Depth + Catheter_type * Depth + Needle_type * Catheter_type * Depth

Tests of Between-Subjects Effects

Dependent Variable: Deflection

Source	Type III Sum of Squares	df	Mean Square	F	Sig.
Corrected Model	1757,598[a]	5	351,520	37,710	<,001
Intercept	3894,261	1	3894,261	417,765	<,001
Needle_type	382,505	1	382,505	41,034	<,001
Catheter_type	319,683	1	319,683	34,295	<,001
Depth	264,210	1	264,210	28,344	<,001
Needle_type * Catheter_type	,000	0	.	.	.
Needle_type * Depth	4,526	1	4,526	,486	,499
Catheter_type * Depth	53,101	1	53,101	5,696	,034
Needle_type * Catheter_type * Depth	,000	0	.	.	.
Error	111,860	12	9,322		
Total	6110,878	18			
Corrected Total	1869,458	17			

Tests of Between-Subjects Effects

Dependent Variable: Deflection

Source	Partial Eta Squared
Corrected Model	,940
Intercept	,972
Needle_type	,774
Catheter_type	,741
Depth	,703
Needle_type * Catheter_type	,000
Needle_type * Depth	,039
Catheter_type * Depth	,322
Needle_type * Catheter_type * Depth	,000
Error	
Total	
Corrected Total	

a. R Squared = ,940 (Adjusted R Squared = ,915)

Estimated Marginal Means

1. Needle_type

Dependent Variable: Deflection

Needle_type	Mean	Std. Error	95% Confidence Interval Lower Bound	95% Confidence Interval Upper Bound
Steerable	20,835	,881	18,914	22,755
Straight	4,382[a]	1,246	1,666	7,097

a. Based on modified population marginal mean.

2. Catheter_type

Dependent Variable: Deflection

Catheter_type	Mean	Std. Error	95% Confidence Interval Lower Bound	95% Confidence Interval Upper Bound
ProGuide 6F	10,028	,881	8,107	11,948
Flexible Implant Tube	25,996[a]	1,246	23,280	28,712

a. Based on modified population marginal mean.

3. Inbrengdiepte in cm

Dependent Variable: Deflection

Inbrengdiepte in cm	Mean	Std. Error	95% Confidence Interval Lower Bound	95% Confidence Interval Upper Bound
5,00	11,567[a]	1,018	9,350	13,785
8,00	19,133[a]	1,018	16,916	21,351

a. Based on modified population marginal mean.

4. Needle_type * Catheter_type

Dependent Variable: Deflection

Needle_type	Catheter_type	Mean	Std. Error	95% Confidence Interval Lower Bound	95% Confidence Interval Upper Bound
Steerable	ProGuide 6F	15,673	1,246	12,958	18,389
	Flexible Implant Tube	25,996	1,246	23,280	28,712
Straight	ProGuide 6F	4,382	1,246	1,666	7,097
	Flexible Implant Tube	.[a]	.	.	.

a. This level combination of factors is not observed, thus the corresponding population marginal mean is not estimable.

5. Needle_type * Inbrengdiepte in cm

Dependent Variable: Deflection

Needle_type	Inbrengdiepte in cm	Mean	Std. Error	95% Confidence Interval	
				Lower Bound	Upper Bound
Steerable	5,00	15,941	1,246	13,225	18,657
	8,00	25,728	1,246	23,013	28,444
Straight	5,00	2,820[a]	1,763	-1,021	6,661
	8,00	5,943[a]	1,763	2,103	9,784

a. Based on modified population marginal mean.

6. Catheter_type * Inbrengdiepte in cm

Dependent Variable: Deflection

Catheter_type	Inbrengdiepte in cm	Mean	Std. Error	95% Confidence Interval	
				Lower Bound	Upper Bound
ProGuide 6F	5,00	7,852	1,246	5,136	10,567
	8,00	12,203	1,246	9,488	14,919
Flexible Implant Tube	5,00	18,999[a]	1,763	15,158	22,840
	8,00	32,993[a]	1,763	29,153	36,834

a. Based on modified population marginal mean.

7. Needle_type * Catheter_type * Inbrengdiepte in cm

Dependent Variable: Deflection

Needle_type	Catheter_type	Inbrengdiepte in cm	Mean	Std. Error	95% ... Lower Bound
Steerable	ProGuide 6F	5,00	12,883	1,763	9,043
		8,00	18,463	1,763	14,623
	Flexible Implant Tube	5,00	18,999	1,763	15,158
		8,00	32,993	1,763	29,153
Straight	ProGuide 6F	5,00	2,820	1,763	-1,021
		8,00	5,943	1,763	2,103
	Flexible Implant Tube	5,00	.[a]	.	.
		8,00	.[a]	.	.

7. Needle_type * Catheter_type * Inbrengdiepte in cm

Dependent Variable: Deflection

Needle_type	Catheter_type	Inbrengdiepte in cm	95% ... Upper Bound
Steerable	ProGuide 6F	5,00	16,724
		8,00	22,304
	Flexible Implant Tube	5,00	22,840
		8,00	36,834
Straight	ProGuide 6F	5,00	6,661
		8,00	9,784
	Flexible Implant Tube	5,00	.
		8,00	.

a. This level combination of factors is not observed, thus the corresponding population marginal mean is not estimable.